1-1-2003

Characterization of activated sludge flocs by confocal laser scanning microscopy and image analysis

Eva Nowak
Ryerson University

In compliance with the
Canadian Privacy Legislation
some supporting forms
may have been removed from
this dissertation.

While these forms may be included
in the document page count,
their removal does not represent
any loss of content from the dissertation.

CHARACTERIZATION OF ACTIVATED SLUDGE FLOCS BY CONFOCAL LASER SCANNING MICROSCOPY AND IMAGE ANALYSIS

by

Eva Nowak, B.Sc. (Toronto, 2001)

A thesis presented to Ryerson University in partial fulfillment of
the requirement for the degree of Master of Applied Science
Environmental Applied Science and Management

Toronto, Ontario, Canada, 2003

Your file Votre référence
ISBN: 0-612-87164-9
Our file Notre référence
ISBN: 0-612-87164-9

Author's Declaration

I hereby declare that I am the sole author of this thesis.

I authorize National Library of Canada to lend this thesis to other institutions or individuals for the purpose of scholarly research.

Eva Nowak

I further authorize National Library of Canada to reproduce this thesis by photocopying or by other means, in total or in part, at the request of other institutions or individuals for the purpose of scholarly research.

Eva Nowak

Ryerson University requires the signatures of all persons using or photocopying this thesis. Please sign below and give address and date.

Signature of Borrower	Address	Date

ABSTRACT

Characterization of Activated Sludge Flocs By Confocal Laser Scanning Microscopy and Image Analysis

Eva Nowak, M.A.Sc.
Environmental Applied Science and Management
Ryerson University

September 2003

The purpose of this study was to characterize microbial floc structure and properties under phosphorus (P) limiting and non-limiting regimes. The P-limitation applied to the biomass did not significantly impact on reactor performance in terms of COD removal and MLSS. The composition of EPS was affected by the P-limitation with significantly increased accumulation of carbohydrates, uronic acids and proteins. CLSM and glycoconjugate mapping revealed that the relative abundance of α and β-*N*-acetylgalactosaminyl / galactopyranosyl and *N*-acetylglucosaminyl residues was affected by P-limitation, suggesting changes in microbial populations within the floc structure, which in turn could cause the compositional changes of EPS. The image analysis performed on CLSM images indicated that under non-limiting conditions the cell clumps within the floc were significantly smaller as compared to P-limiting conditions. The fractal dimension and porosity under limiting conditions were either significantly higher or lower than under P-rich conditions.

ACKNOWLEDGEMENTS

I would like to express my appreciation to my supervisor, Dr. Steven Liss, for his patience, encouragement and continuous coaching throughout the term of my thesis. I would like to thank Dr. Steven Liss for supporting me financially for this project through the Natural Sciences and Engineering Research Council of Canada Strategic Grant, and for giving me the opportunity to participate at the International Water Association (IWA) Specialised Conference in Rome, and the American Society for Microbiology Conference in Washington. I am also grateful to Dr. Steven Liss for opening the doors to the research world during my undergraduate years, and for being my mentor and friend ever since.

I extend my appreciation to my friend Heather Scozzaro, for her time and patience while giving me training on the confocal laser scanning microscope, and for her expertise and advice during the technical reviews of this study.

Many thanks to Moses Akingbade, for his day to day help with the SBR system, and for his hard work at assisting me with the EPS extraction and EPS analysis. Appreciation is also due to Brenda Hum, for joining and contributing her technical assistance in the laboratory as part of her co-operative education program.

Acknowledgement is due to Haluk Beyenal, of Montana State University, for his support and advice on technical aspects of ISA3d software.

Sincere thanks to all my colleagues in the Environmental Biotechnology Laboratory at Ryerson University, for their friendship, advice and continuous support: Dean Whitaker, Margaret de Jesus, Penny Petropoulos, Joe Bautisa, Heather Scott and Jamie McBean.

I would like to sincerely thank my soul mate, Wojtek Widnicki, for his untiring understanding and patience, and for his everyday caring, kindness and love.

Finally, I would like to express my gratitude to my Mom and Dad, for their unconditional love, confidence, and their financial assistance. I also give the warmest appreciation to my sister Dorotka, whose presence was always a great support.

TABLE OF CONTENTS

LIST OF FIGURES

LIST OF TABLES

NOMENCLATURE

AF	Alexa Fluor
BOD	biochemical oxygen demand
BOD_5	biochemical oxygen demand in 5 days
C	carbon
CLSM	confocal laser scanning microscopy
COD	chemical oxygen demand
COM	conventional optical microscopy
ConA	concanavalin A
DNA	deoxyribonucleic acid
EPS	Extracellular Polymeric Substances
MATH	microbial adherence to hydrocarbons
MLSS	mixed liquor suspended solids
N	nitrogen
P	phosphorus
PBS	phosphate buffered saline
PolyP	polyphosphate
SBA	soybean agglutinin
SBR	sequencing batch reactor
SEM	scanning electron microscopy
SRT	sludge retention time
SS	suspended solids
TEM	transmission electron microscopy
tmr	tetramethylrhodamine
UASB	upflow anaerobic sludge bed
WGA	wheat germ agglutinin

CHAPTER 1: INTRODUCTION

1.1 Background

Flocculated particles are essential to a number of environmental processes within engineered and natural systems. Flocs can be viewed as individual microecosystems that continuously interact with their surroundings to obtain building material, energy, nutrients and chemicals for biological growth, chemical reactions and morphological development (Droppo et al., 1997). While flocs can regulate their own environment, they also have the ability to regulate surrounding water or wastewater quality by their physical, chemical and biological activity (Liss et al., 1996). Considerable attention has been given to study of activated sludge flocs since the performance of this secondary wastewater treatment process depends on the microbial floc formation and physical separation of the resulting microbial mass from the treated effluent. Many major principles of the activated sludge process are related to or dependent on the morphology and surface properties of the floc. Consequently many major operating problems in the process, such as those which occur in solid-liquid separation, can be attributed to the properties of floc. It is therefore important to understand the physical characteristics of activated sludge flocs in order to ensure long-term operation free from sludge settling problems.

The three factors known to affect flocculation of microorganisms are genetic/physiological factors, environmental and nutritional factors. Natural waters are often phosphorus limited (Ozkanca and Flint, 1996). In many of the industrial activated sludge systems, phosphorus is often limited in wastewater and has to be added to achieve maximum treatment efficiency (Saunamaki, 1994; Ericsson and Eriksson, 1988; Alphenaar et al., 1993). However, researchers have suggested that lower phosphorus concentrations may improve treatment efficiency, while saving chemical costs to the plants (Wu and Casey, 1978; Lee, 1997; Whittaker, 2002). Lee (1997) has also suggested limiting phosphorus in the treatment process may result in better sludge characteristics. Thus, the understanding of nutritional requirements and their effect on flocculation of microorganisms has important implications for the operation and performance of activated sludge.

Past research on nutrient effects in activated sludge process has focused mostly on the growth of filamentous microorganisms and bulking. Little attention has been paid to the floc structure and floc physicochemical characteristics which are the basic and underlying factors

ultimately affecting the control and overall treatment efficiency of activated sludge processes. Thus, the primary goal of this study was to gain an understanding of floc structure under two phosphorus (P) regimes. Specific objectives of this study were:

i, to study the physicochemical properties of sludge flocs (EPS composition, surface charge, hydrophobicity) in P-rich and P-limited environments

ii, to study the structure properties of sludge flocs (EPS distribution, diffusional distance, fractal dimension and porosity) in P-rich and P-limited environments

iii, to study the effect of P-limitation on the physicochemical properties and structure of microbial floc

The approach taken in this study involved a laboratory sequencing batch reactor (SBR) system and glucose based synthetic feed. Nutrient variations, including the P-rich (COD:N:P = 100/5/1) and P-limited conditions (COD:N:P = 100/5/0.1), were examined. The effects of these conditions on the floc properties were then studied, with the emphasis on the SBR system performance, floc physicochemical properties and floc structure. The floc structure was analyzed using confocal laser scanning microscopy (CLSM) coupled with image analysis.

1.2 Thesis Outline

The next section of this report is a review of the literature relevant to this study. The information provides background on activated sludge wastewater process, nutrient requirements and P-limitation, microbial floc structure and EPS, physicochemical properties of microbial aggregates. Additionally, microscopic techniques are reviewed with the emphasis on confocal laser scanning microscopy and glycoconjugate analysis since it was used extensively in this study.

Chapter 3 outlines the experimental conditions, chemicals used, equipment set up, analytical assays used in the experimentation, microscopy and image analysis. Chapter 4 presents summarized result of analytical and microscopic analysis. Detailed discussion of the results is provided in Chapter 5. Conclusions and recommendations are given in Chapter 6. Experimental data and detailed protocols are included in the appendices.

CHAPTER 2: LITERATURE REVIEW

2.1 Activated Sludge Process

Activated sludge is one of the most common processes used for wastewater treatment. The activated sludge process always consists of two liquid stream processing units - the aeration basin (biological reactor) and the secondary clarifier. The aeration basin provides an environment for the removal and transformation of organic mater into carbon dioxide and cell materials through biological oxidation. The secondary clarifier allows the incorporation of colloidal matter into settleable solids by flocculation and gravity sedimentation and subsequent separation from the treated wastewater. The purpose of the secondary clarifier is to provide low suspended solids (SS) and low turbidity overflow (secondary effluent) and a thickened underflow (return activated sludge).

For efficient treatment both the aeration basin and the secondary clarifier must function satisfactorily. Many major principles of the activated sludge process are related to or dependent on the physical characteristics of the floc. These include substrate transfer and utilization, bioflocculation (floc aggregation and breakup), solid-liquid separation, sludge thickening and sludge dewatering (Li and Ganczarczyk, 1989). Consequently many major operating problems in the process are more or less directly related to the morphological and surface characteristics of the floc. These problems include poor clarification and turbid effluents, either due to the inability of small clumps of bacteria to flocculate (dispersed growth) or due to break up of larger flocs and formation of small compact flocs which do not settle well (pinpoint floc). Furthermore, poor sludge settleability due to non-filamentous or viscous bulking is most probably related to the morphological characteristics of the floc and the presence of large amounts of exocellular slime (Andreadakis, 1993). In the case of filamentous bulking, the connection between floc characteristics and the settlement problem is more complex (Section 2.3). Therefore, a more careful consideration of critical floc characteristics may ensure long-term operation free from sludge settling problems.

2.2 Role of Nutrients

Some of the factors affecting microbial flocculation include pH and temperature, substrate loading intensity, mixing intensity, and nutrients. Nutrients are all elements utilized by microorganisms to carry out biosynthesis and cell metabolism. Nutrients are classified

into three general categories: macronutrients (C, O, H, N, P, S), micronutrients (e.g. Fe, S, Na, Ca, K, Mg) and trace elements (e.g. Zn, Cu, Mn, Mo). Microorganisms require appropriate amounts of these nutrients to synthesize cell mass and carry out specific enzymatic reaction. Therefore nutrient requirements play an important role in the operation and performance of activated sludge systems.

In addition to carbon, the principal nutrients are nitrogen (N) and phosphorus (P). N is needed for the synthesis of proteins, nucleic acids and other substances. P is present in nucleic acids, phospholipids, and other cell components. In activated sludge, nutrient deficiency almost always means deficiency of nitrogen and/or phosphorus (Jenkins et al., 1993). The lack of these nutrients may significantly affect microbial growth in activated sludge systems and can favour undesirable filamentous growth (P-deficient bulking). The growth of filamentous bacteria can result from a combination of environmental stresses, including low dissolved oxygen in the aeration basin, treatment of wastes with high carbon to nitrogen (C:N) ratios and phosphorus limitation (Jenkins et al., 1993; Contreras et al., 2000).

For conventional activated sludge systems, the nutritional requirements of the microorganisms are the major factor controlling the efficiency of carbon oxidation and removal of nutrients. The impact of nutritional requirements is assessed in terms of a carbon: nitrogen: phosphorus (C: N: P) ratio. If this ratio is too high as compared to microbial requirements, energy and biosynthesis might not be fully coupled, resulting in lower biochemical oxygen demand (BOD) removal efficiency. If the ratio is too low, limited N or P removal is observed. Usually the BOD_5/N/P ratio of 100/5/1 is used for adequate BOD removal (Jenkins *et al*, 1993). This ratio is regarded as the minimum nutrient requirement of activated sludge systems designed for carbon removal. This ratio of nitrogen and phosphorus is only a rough index. The ratio of nitrogen and phosphorus in the cell varies with age of the biomass, given operational conditions, a type of waste to be treated, as well as the capacity of the biomass to store and recycle sources of N and P.

2.2.1 Nutrient Deficiency

Availability of nutrients is an important factor in activated sludge processes since it is related to microbial growth. Nitrogen and phosphorus are among the macronutrients needed in biological wastewater treatment, and both are essential for successful results. Phosphorus

is present in wastewaters as orthophosphate (PO_4-P), condensed phosphates and organic phosphorus. Condensed phosphates may break down to yield ortho-phosphate. Total phosphorus is the sum of all these constituents.

A typical problem resulting from phosphorus or nitrogen deficiency in activated sludge treatment is sludge bulking, which is often caused by proliferation of filamentous bacteria. Activated sludge bulking is a condition in which sludge settling rates decrease and thickening of the settled sludge is poor. In a treatment plant, bulking can lead to the production of dilute return and waste-activated sludge streams, hydraulic overloading of solids handling processes, high effluent SS and BOD as a result of sludge blanket overflow from the secondary clarifier, and in severe cases, washout of the activated sludge culture (Lau et al., 1984). Although bulking is also caused by numerous other factors, among them oxygen deficiency, its prevention demands sufficient nutrient levels.

While wastewaters in general contain sufficient amounts of micronutrients, waste waters from pulp and paper mills require additional nitrogen and/or phosphorus in amounts depending on the conditions at the plant in question (Saunamaki, 1994). Also for the fermentation of some solid wastes, phosphorus dosage is required (Alphenaar et al. 1993). The required phosphorus concentration in the wastewater is based on its biological availability. The requirement is also dependent on the chemical oxygen demand (COD) loading and type of the organic substrate. In the wastewater treatment literature, various phosphorus levels needed for viable bacterial biomass are mentioned: Stanier et al. (1977) referred to a C: N: P ratio of 100:28:6 (% wt/wt) for bacterial matter in general; Scherer et al. (1983) reported C: P ratios for methanogens varying from 16:1 to 75:1 (w/w); Alphenaar et al. (1993) mentioned the 2 to more than 50 mgP l^{-1} phosphate additions to the wastewater. The old "textbook rule" of BOD: P =100:1 usually provides excessive phosphorus loading in relation to BOD (Jenkins et al., 1993; Saunamaki, 1994).

Ericsson and Eriksson (1988) studied the effect of low concentrations of BOD and easily assimilated phosphates. Their investigations showed that depletion of easily assimilated phosphate favoured filamentous organisms and deterioration of activated sludge sedimentation characteristics (a significant increase in the sludge volume index).

Alphenaar et al. (1993) studied the effect of phosphate limitation on upflow anaerobic sludge bed (UASB) reactor performance and on methanogenic activity. Phosphorus

deficiency (influent 0 μg P l^{-1}) reduced methanogenic activity in UASB. The increase of methanogenic activity was observed when less than 0.1mg PO_4-P l^{-1} was added. This indicated that supplementary free available phosphorus may have been required for maximal methanogenic activity. The study concluded that a phosphorus limitation does not significantly reduce the treatment efficiency for sludge loading rates below the methanogenic activity of the sludge under P-limiting conditions. As long as moderate loading rates were applied, the performance of phosphorus-limited reactors was satisfactory.

Saunamaki (1994) tested the need for the addition of phosphorus during the treatment of pulp and paper wastewaters using activated sludge method. The study found that when wastewater treatment was operated at low or normal loading, a small amount of phosphorus (BOD:P=100:0.3-0.5) had to be added or otherwise the reduction of the water's oxygen demand failed and the plant drifted into disequilibrium. The optimum BOD:P ratio was about 100: 0.4, in which case the treated effluent had a total phosphorus content of 0.5mg/l, a soluble phosphorus content of 0.3mg/l and a phosphate phosphorus well below 0.1 mg/l. Larger phosphorus additions produced no further improvement in treatment results.

Lee (1997) studied the effects of nutrients on the physicochemical properties of activated sludge flocs by using sequencing batch reactors (SBRs) and glucose synthetic feed. This study demonstrated that an excess P concentration did not improve treatment efficiency and a lower-than-traditional P loading did not negatively affect reactor performance. However, the components of the extracellular polymeric substances (EPS) were affected by the nutrient loading in this study. When the biomass in SBRs was P-starved (0 μg P l^{-1}), an increase in the concentrations of carbohydrates, protein and deoxyribonucleic acids (DNA) in the EPS matrix was observed. A similar trend was observed under P-limited conditions, except that there was also a significant increase in the acid polysaccharide concentration. The increase in DNA concentration in the EPS and the accumulation of P within the EPS under the P-starved condition suggested a possible mechanism for recycling P within the biomass during transitional nutrient deficient conditions. Such potential for using extracellular P as a nutrient source has been suggested by Lee to be a survival mechanism.

Whittaker (2002) demonstrated that the activated sludge process could be run at alternative COD/N/P rations other than the traditional 100/5/1 ratio, by altering the quantity of P in the simulated photographic chemical manufacturing wastewater, in the laboratory

SBR systems. Whittaker observed that decreasing the amount of P in the simulated wastewater had no significant impact on the COD removal efficiency, MLSS and ESS concentrations, as well as SVI. However there was a minor decrease in treatment efficiency (COD) observed under a COD/N/P loading of 100/5/0.05 versus the traditional loading of 100/5/1. In P-rich environments, some microorganisms were capable of accumulating intracellular pools of polyphosphate. In response to P-limited or P-starved conditions, many microorganisms have evolved enzymes, which can release inorganic phosphatases. Traditionally it was thought that bacterial populations could accumulate and store quantities of P only intracellularly as polyphosphate (polyP) granules. However, Whittaker (2002) demonstrated that when phosphorus was supplied in excess, the biomass was capable of accumulating P both intracellularly, as well as extracellularly in the EPS. Furthermore, it was observed that when biomass was fed excess P (traditional ratio of 100/5/1) the biomass was able to accumulate P reserves. During the periods of P-limitation, the P reserves declined significantly both intracellularly and extracellularly, indicating that the biomass has the capacity to utilize P reserves. When quantifying DNA present in the EPS in this study, no significant difference between the levels of DNA present in the EPS under P-rich or P-limited conditions was observed. Whittaker suggested that the biomass grown under P-limited conditions may maintain a potential capacity to undergo further P-limitations in which the biomass may recycle extracellular DNA as an additional source of P.

In summary, lower additions of phosphorus to wastewater treatment systems can not only reduce maintenance costs for wastewater treatment plants, but also can result in much lower, or eliminate, potentially harmful phosphorus discharges to the environment. Most of previous studies only examined the effects of P-limitations on the performance of activated sludge systems. The actual effect of P-limitation on the floc structure, and how this in turn affects microbial flocculation and system treatment efficiency are not known. Therefore the relationship between P-limitation, floc structure and floc physicochemical properties have yet to be fully established.

2.3 Microbial Floc Model

One of the most difficult problems when analyzing biological flocs is the complexity of the floc constituents and their chaotic structure. The internal organization of the floc is a

heterogeneous composition of biological components (bacteria, fungi, protozoa and metazoans) and non-biological components (organic and inorganic exocellular polymeric substances (EPS) and metabolic excretions). Depending on the species involved, the floc may be composed of 50-90 % EPS matrix and only 10-25% cell biomass (Costerton, 1999; Wilen et al., 2003). The cell biomass in activated sludge can be divided into two main groups: the floc formers and those growing as filaments. In the typical activated sludge the size of the flocs ranges from 20-200μm (Urbain et al., 1993) but Parker et al. (1971) showed a bimodal size distribution from 0.5-5μm (single bacteria) and up to 25-3000μm. When an activated sludge culture contains filamentous organisms, the flocs are usually large and irregularly shaped (Jenkins et al., 1993; Lau et al., 1984). On the other hand, when filamentous organisms are absent, or present only in small numbers, the flocs are usually small (up to about 75 μm in dimension), spherical and compact (Jenkins et al., 1993)

On the basis of visual observation and physical measurements, it has been suggested that there are two levels of structure in the activated sludge flocs, only floc forming bacteria, and floc forming bacteria bridged by filamentous bacteria. It is probable that the filamentous organisms' network provides a "backbone" for the buildup of the floc which is subsequently formed by various polymer bridges between primary particles and smaller flocs. Some filamentous microorganisms can grow within the floc and others extend from the confines of the floc into the bulk solution (Figure 2.1). Many settling, compaction, and separation properties of activated sludge are related to the relative numbers of filamentous and floc-forming microorganisms in the activated sludge floc. It is well established that the extent of the filamentous organisms' growth is a reflection of the comparative physiological properties of filamentous and floc-forming organisms (Andreadakis, 1993). Outgrowth of excessive quantities of filamentous organisms (more than approximately 10^7 μm filaments/mg activated sludge dry solids) was correlated with bulking (sludge volume index 150 mL/g) (Lau et al., 1984). The excessive growth of filamentous bacteria can result from a variety and/or combination of environmental stresses, including low dissolved oxygen in the aeration basin, high carbon-to-nitrogen ratios and phosphorus limitation (Jenkins et al., 1993; Contreras et al., 2000). On the other hand, the absence of filamentous organisms or their presence in very low numbers was postulated to lead to the production of weak, small flocs, where the larger flocs settled rapidly but small bacterial aggregates remained and contributed to effluent

turbidity (pin-point floc) (Jenkins et al., 1993). An ideal activated sludge floc would exist when there was a balance between filamentous and floc-forming organisms (Figure 2.1).

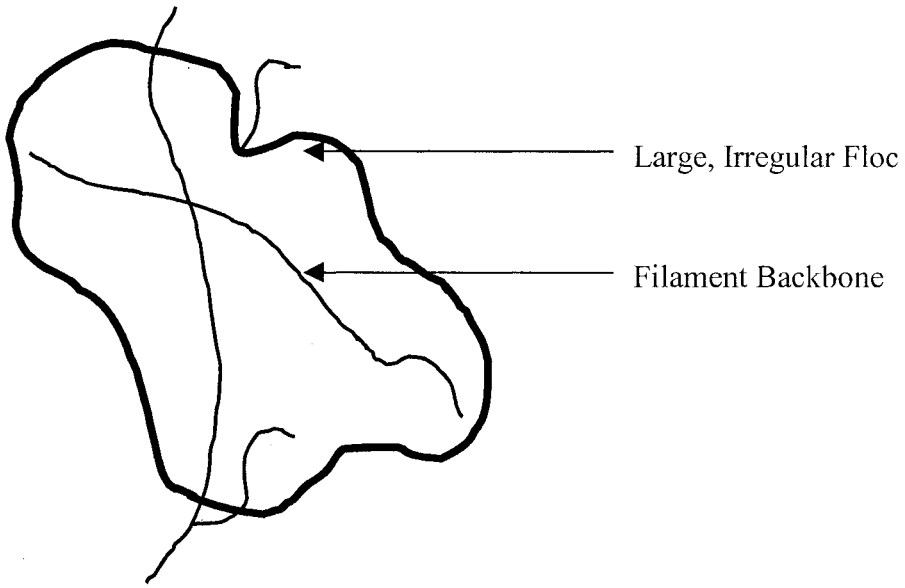

Figure 2. 1: Schematic representation of an ideal non-bulking activated sludge floc on an arbitrary scale of size, when filamentous organisms and floc forming organisms are in balance (adapted from Jenkins et al., 1993)

The structure of activated sludge floc is imparted by processes of microbial adhesion, aggregation and bioflocculation. While the mechanism of bioflocculation in activated sludge is complex, it has been shown that EPS are an important structural component of the floc matrix as they are often a dominant entity within the large voids of the flocs as well as being associated with the surfaces of many bacteria (Liss et al., 1996; Li and Ganczarczyk, 1990; Jorand et al., 1998). At present, polymer bridging is an accepted mechanism in describing activated sludge floc formation. Floc growth through attachment of single cells or smaller flocs may occur through EPS (Figure 2.2). The binding and cross-linking of the polymers may be by mechanical entanglement or by electrostatic bridging between polyvalent metal ions and humic types of substances (Eriksson et al., 1992). The EPS, which contain different negatively charged groups, provides an adsorption site for inorganic ions such as divalent cations (e.g. Ca^{2+} and Mg^{2+}). EPS-metal complexes form large polymeric networks in which the different floc constituents (e.g. single bacteria, bacterial colonies and/or inorganic particles) are embedded. This model is supported by several studies where it has been shown that the removal of divalent and trivalent cations from the sludge flocs

leads to deflocculation and disintegration of microbial floc (Wilen et al., 2003; Urbain et al., 1993). In addition, it has been proposed that hydrophobic and hydrophilic regions within EPS interact with the surfaces of cells thereby reinforcing the stability of the aggregate (Jorand et al., 1998)

The activated sludge floc often appears to be most dense in the area closest to the core of the floc (Figure 2.3). Furthermore, it is believed that the interior layer of sludge flocs has a growth rate lower than that of the outer layer, due to the limitation of diffusion of oxygen and nutrients to the core from the bulk solution (Eriksson et al., 1992; Costerton, 1999; Liao et al., 2002). The outer part of the floc is usually less hydrophobic and more negatively charged in addition to having a more loose arrangement of EPS (Liao et al., 2002). In the central part of the floc which is generally seen as a collection of compact clumps, the cells are embedded in a strong EPS matrix. Liao et al., (2002) observed that the sludge retention time (SRT) played an important role in the heterogeneity in the packing of and the type of EPS. At a low SRT, the inner EPS region, although more compact than the outer region of the floc, consists of a more open matrix and is less compact than what is observed for a high SRT floc. At a high SRT floc, the outer region of the EPS appears to condense to form a smooth skin layer. The relative importance of inter-particle interactions changes with respect to the SRT, with ionic interactions and hydrogen bonds being most important at a low SRT. Other mechanisms related to the composition and arrangement of EPS and the more hydrophobic nature of flocs may be more important in maintaining the stability of sludge flocs at a higher SRT.

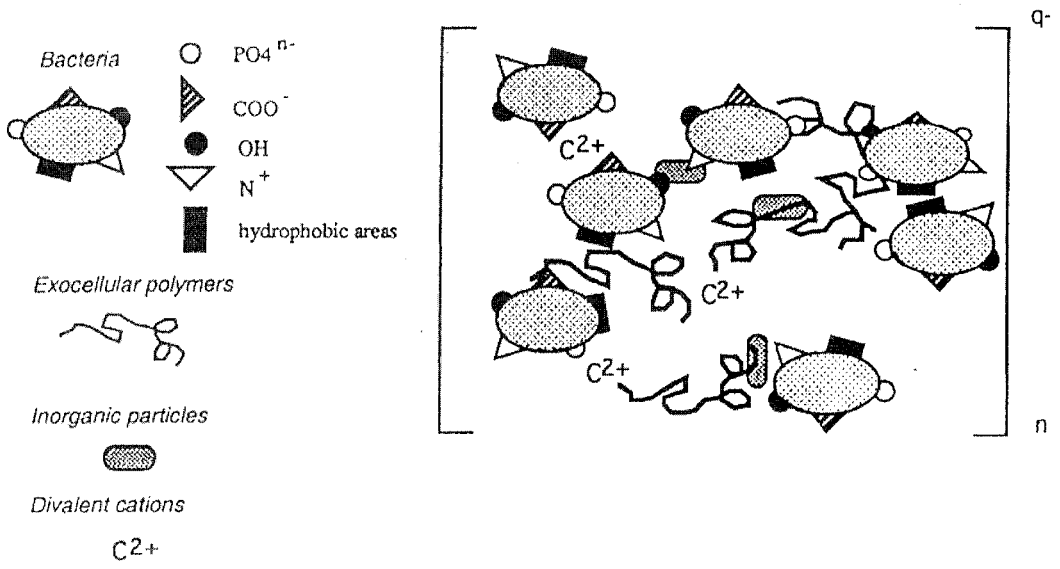

Figure 2. 2: Schematic representation of the activated sludge floc on an arbitrary scale of size with microorganisms connected together by EPS matrix (reproduced from Urbain et al., 1993)

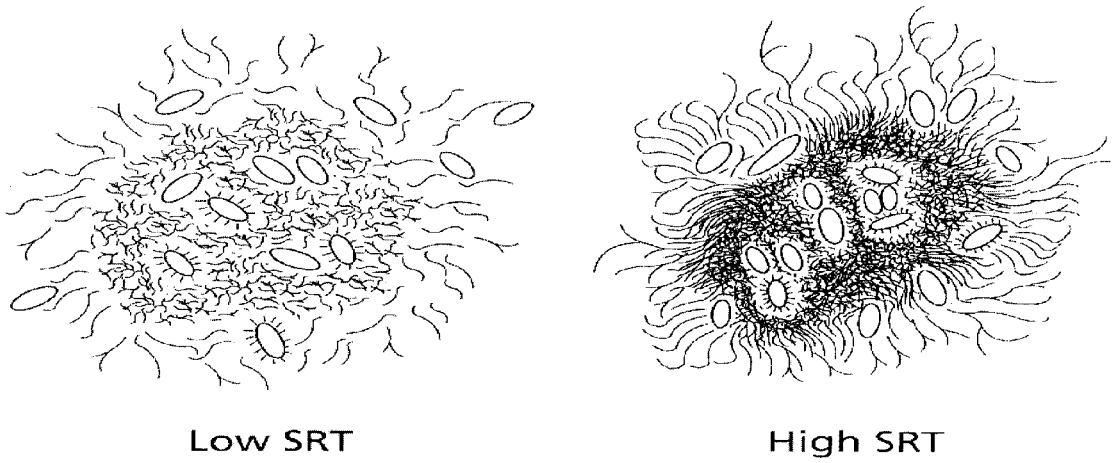

Figure 2. 3: Schematic model of the activated sludge floc (reproduced from Liao et al., 2002). At the low SRT the EPS is more diffuse. At high SRT localized association of EPS appear to condense to form a smooth interface between the floc surface and the bulk water.

2.4 Microbial Floc Surface Properties

The cell surface properties of bacteria are important in terms of flocculation, adhesion, and biofilm formation (Palmgren et al., 1998). Surface properties, such as hydrophobicity, surface charge and the composition of the EPS are invariably linked to microbial floc formation and structure, and floc properties including settling, water-binding ability and dewatering (Bura et al, 1998). A number of mechanisms, such as charge neutralization, hydrophobic interactions, hydrogen bonds, ionic interactions, and physical enmeshment, have been suggested to be important in controlling the formation of sludge floc and its stability (Liao et al., 2002).

2.4.1 Extracellular Polymeric Substances (EPS)

Researchers have only recently begun to acknowledge the important role of EPS in microbial communities, which may include cell adhesion and aggregation, granulation, organic chemical degradation, metal accumulation, biofouling, cell-to-cell communication, biofilm structure, and resistance to heavy metal toxicity (Wolfaardt et al., 1998). In wastewater activated sludge processes, EPS are major components of the activated sludge floc matrix and thus has a great influence on the floc structure. It was found that depending on the species involved, the microbiological aggregates may be composed of 10-25% cells and 75-90% EPS matrix (Costerton, 1999). Furthermore, EPS seem to be crucial to the settleability, filament dominancy, bioflocculation and dewatering of activated sludge (Dignac et al., 1998, Urbain et al., 1993, Bura et al, 1998; Liao et al, 2000). There is increasing evidence that the composition and properties (hydrophobicity and surface charge) of EPS is more important with respect to settleability (Bura et al, 1998; Andreadakis, 1993) and bioflocculation (Liao et al, 2000) than the amount of EPS produced.

EPS are high molecular weight compounds (more than 10 000 amu) produced by microorganisms under certain environmental conditions (Morgan et al., 1990). EPS originate from metabolism or lysis of microorganisms (proteins, DNA, polysaccharides and lipids) and from the wastewater itself (e.g. cellulose, humic acids, etc.) Most bacteria are able to produce EPS, either as capsules attached to the cell wall or as mucoid secretions in the extracellular environment (Wolfaardt et al., 1998). EPS play an important role in several cellular processes that relate to microbial competitiveness and reproductive success, such as

the formation of microcolonies, attachment to surfaces, and increased resistance to antimicrobial agents (Wolfaardt et al., 1998). EPS also plays an important role in the concentration of nutrients (Wolfaardt et al,. 1998) and itself can serve as carbon and energy reserves during starvation (Liu and Fang, 2002).

The chemical composition of the EPS matrix is reported to be very heterogeneous. A variety of polymeric materials have been found to occur in the EPS. These include neutral and acidic polysaccharides, lipopolysaccharides, proteins, nucleic acids and humic acids (Frølund et al., 1995). Carbohydrates and proteins are usually found as the major EPS components with a protein to carbohydrate ratio between 0.2-5(w/w) (Frølund et al., 1995). Carbohydrates were considered the main constituent of EPS in pure cultures (Morgan et al., 1990). However, recent studies of mixed cultures in wastewater treatment systems found that protein was the predominant constituent in EPS.

Frølund et al. (1995) showed that activated sludge mainly consisted of protein (46-52% of volatile suspended solids (VSS)), humic compounds (18-23% of VSS) and carbohydrate (17% of VSS). Andreadakis (1993) found that the carbohydrate content varied between 6-18%. Nielsen et al. (1996) found that proteins comprised approximately 55%, while carbohydrate and humic compounds made up 16-19% of the sludge organic content. Dignac et al. (1998) found that proteins accounted for more than 65% of the total organic carbon content (TOC). Liu and Fang (2002) found that 41.3% of EPS were protein and 18.7% were carbohydrate. The ratio of carbohydrate and protein for this study was 0.45. Whittaker (2002) observed protein/total polysaccharides ratio of 2.32 for P-rich conditions and 1.43 for P-limited conditions. Predominance of proteins in activated sludge EPS could be due to the presence of large quantities of exoenzymes entrapped in the floc (Frølund et al., 1995; Dignac et al, 1998). The complexity of the substrate present in wastewater could explain the presence of exoenzymes around bacteria in activated sludge, while the synthetic substrate added to pure cultures is much simpler. The extracellular proteins could also originate from wastewater compounds or from either cell lysis or from excretion (exoenzymes and structural proteins) (Dignac et al., 1998).

Since 70-80% of the extracellular organic carbon can be attributed to proteins and sugars, the remaining 20-30% of organic carbon in EPS can be composed of humic substances, uronic acid or amino acids, lipids and DNA. Humic and fulvic acids or lignins

found in the flocs are supposed to come from wastewater (Urbain et al., 1993). Uronic acids are specific components of extracellular and cell wall material and amino acids are the primary units of bacterial cell walls. Extracellular nucleic acids, originating from cell lysis, were shown to account for 1-2% of VSS of the sludge (Urbain et al., 1993; Frølund et al., 1996). Lipids have been identified in EPS by Goodwin and Forster (1985). Dignac et al. (1998) showed that fatty acids, coming from mono-di- and tri-glycerides or phospholipids, and sterols represented less than 1% of the TOC.

Since the EPS is a major component of flocs, and has charged functional groups and hydrophilic/hydrophobic regions, it is reasonable to assume that they contribute to the net surface properties of the flocs, and thus the flocculation properties. It has been shown that nutrients have significant effect on EPS production and surface properties (Lee, 1997; Bura et al., 1998). To date, there is only limited knowledge on the precise function of EPS in relation to bioflocculation, and very little is known about the relationship between the EPS constituents and the surface properties of activated sludge floc. The surface properties are affected by the chemical composition of the EPS, but little information is available in the literature. Therefore, the relationship between nutrients and EPS composition, and resulting surface properties, would be important in understanding flocculation.

2.4.2 Hydrophobicity

Biological flocs are highly hydrated structures. Bacterial cell surface hydrophobicity is an important factor that governs bacterial adhesion to various surfaces such as activated sludge (Zita and Hermansson, 1997b; Zita and Hermansson, 1997a). Therefore, hydrophobic interactions may play an important role in bioflocculation (Urbain et al., 1993; Liao et al., 2001). Cell surfaces exhibit hydrophobic areas due to side chains of amino acids, methyl groups in polysaccharides, and long-chain carbon groups in lipids (Urbain et al., 1993). Hydrophobic interactions result from the behaviour of entities (particles or molecules), which are incapable of interacting electrostatically or establishing hydrogen bonds with water and are therefore drawn together when plunged in an aqueous phase (Jorand et al., 1998). In the case of microbial cells in aqueous media, the bound water layer near the cell surface accounts for the hydrophobic or hydrophilic interactions (Urbain et al., 1993; Zita and Hermansson, 1997). When two hydrophobic surfaces approach each other, the bound water layers overlap,

displacing the intervening layers of water to the bulk solution. This displacement reaction causes a decrease in entropy resulting in an energetically favourable condition for aggregation. In the case of hydrophilic surfaces, the opposite is true in that entropy increases resulting in repulsion of cells. Therefore, any alternation to cell surface that increases its hydrophobicity will favour flocculation.

Several factors influencing the measured cell surface hydrophobicity have been suggested: temperature, pH, ionic strength, growth phase, growth conditions, and the addition of polycations to the cell suspension. Jorand et al. (1994) observed the presence of hydrophobic cells in activated sludge and the dependence of hydrophobic cell surface variations on the cell's physiological state. Palmgren et al. (1998) studied the influence of oxygen on the cell surface hydrophobicity of bacteria isolated from activated sludge. They found that oxygen limitation generally caused a lowering of the cell surface hydrophobicity especially in the exponential phase of growth. Zita and Hermansson (1997a) shown that adhesion of bacteria to activated sludge flocs was related to a high cell surface hydrophobicity. In the later study (Zita and Hermansson, 1997b) measured cell surface hydrophobicity of single cells by enumerating hydrophobic fluorescent microspheres that were associated with the wastewater treatment plant bacterial surface. Bacteria had a broad distribution of cells with different cell surface hydrophobicities, even though most of the cells were generally hydrophilic. The samples showed no differences in cell surface hydrophobicity between morphological groups. However, bacterial filaments extending out from sludge flocs were sometimes covered by microspheres indicating a strong hydrophobic character.

Lastly, EPS possess both hydrophobic and hydrophilic properties (Jorand et al., 1998). A significant proportion of the EPS fraction in the Jorand et al. (1998) study was hydrophobic. The hydrophobic fraction was made up of proteins and not of carbohydrates. Their findings indicate that amino acids with hydrophobic side groups contribute significantly to the hydrophobicity of a microbial floc. Liao et al. (2000) found that hydrophobicity and surface charges of sludge surfaces were affected by the SRT. The core of the floc was more hydrophobic than the outer layer. First because hydrophobic surfaces have natural tendencies to avoid hydrate environments. Second a lower growth rate (due to diffusional restrictions) can result in a more hydrophobic surface.

It is likely that hydrophobic interactions (and/or van der Waals) play an important role in the initial stage of bioflocculation by overcoming the repulsive interactions and bringing the sludge microorganisms close enough to form specific interactions. Therefore, the relationship between EPS composition and its effect on floc hydrophobic properties, would be important in understanding flocculation.

2.4.3 Surface charge

The surface charge has been investigated with regard to its role in controlling the stability of fine particle suspensions and its role in settleability (Liao et al., 2001; Liao et al., 2002) as well as in activated sludge floc formation and stability (Zita and Hermansson, 1994). The overall floc structure is negatively charged and is the result of physico-chemical interactions between microorganisms (mainly bacteria), inorganic particles (silicates, calcium phosphate and iron oxides, and multivalent cations) and EPS. The surface charge for activated sludge is usually negative having values between -10 mV to -20mV (Morgan et al., 1990)

The concentration and nature of EPS present at sludge surfaces may influence the sludge surface charge. The higher yields of extracted EPS correlated with the greater values of the overall electronegativity of the sludge surface in the Morgan et al., 1990 study. They have also reported that the proportion of EPS components (proteins/total carbohydrates) was more important than the quantities of individual EPS components in determining the surface charge of both anaerobic and aerobic sludge flocs. High concentrations of anionic surface biopolymers can consequently be correlated with deteriorating sludge settling characteristics because of the influence of floc- repulsion.

Whittaker (2002) found that the surface charge was influenced by P-limited conditions. He observed a significantly greater negative surface charge for floc grown under COD:N:P ration of 100/5/0.05 as compared to a conventional COD:N:P ratio of 100/5/1. He suggested that the increase in surface charge may have been attributed to the increase in concentration of the acid polysaccharides present in the EPS. Liao et al. (2000) found that the surface charge was not influenced by the total EPS content of the sludge but by variation in the protein, total carbohydrate, and DNA content in the EPS. The importance of the ratio of proteins to carbohydrates in determining the surface charge could be related to the unique

charge properties of proteins. The amino groups in proteins carry positive charges, and can neutralize some of the negative charge from carboxyl and phosphate groups and therefore decrease the net negative surface charge of the sludge flocs. The study also found that surface charge and hydrophobicity of sludge surfaces were affected by the SRT. Sludge surfaces at higher SRT were less negatively charged and more hydrophobic than those at lower SRTs. Lastly it was found that the presence of a large amount of EPS had a negative effect on the compressibility of the sludges.

It has been found that the chemical composition of EPS affects the overall negative surface charge of the sludge floc. Since these electrostatic bridges are in most cases necessary for bioflocculation to occur (Eriksson et al., 1992), the relationship between EPS composition, and resulting surface charge properties, would be important in understanding flocculation.

2.5 Microbial Floc Structural Properties

2.5.1 Microbial Floc Porosity

The porosity of flocculated microorganisms usually is calculated from the density of floc. The density of floc is calculated from the settling velocity measurements using a modified Stokes' law and taking into account the shape factor of floc (Li and Ganczarczyk, 1987). Porosity is expressed as a percentage which is used mathematically for the prediction or inference of floc hydrodynamics or substrate uptake by natural or wastewater flocs through advective flow and diffusional gradients (Li and Ganczarczyk, 1987, 1992).

Andreadakis (1993) observed floc structures with porosities in the range 85-97%. Li and Ganczarczyk (1987) showed that the porosity of activated sludge flocs increased as the floc size increased. It has also been shown that the porosity increases at a higher rate when floc sizes were smaller than 200μm (longest dimension) as compared with that of the flocs larger than 200μm. Li and Logan (2001) found that for fractal aggregates, porosity increases with size. The increase in the aggregate porosity with size becomes larger as the fractal dimension decreases in magnitude.

Porosity is a complicated issue as the definition or identification of pores is highly dependent on the resolving power used for the observation. Pores observed with COM appear to be devoid of materials and appear to be significantly open channels for the

movement of water and nutrients through the floc. TEM observations often reveal that many of these macro-pores are in fact filled with a complex network of cells and EPS. As such, calculations of porosity that do not consider the internal structure of the pores may be erroneous (Droppo et al., 1997).

2.5.2 Diffusion Distance

Bacteria in the floc interior are not in contact with the bulk concentration of substrates and must depend on diffusional transport of nutrients into the floc particle. Thus the nutrient availability varies from a maximum at the floc surface to a minimum in the floc center (Lau et al., 1984). The substrates to be transferred have to overcome not only the diffusional resistance of water but that of the EPS in the flocs before they reach the majority of microbial cells, especially those encapsulated in the microcolonies that are completely surrounded by the polymers (Li and Ganczarczyk, 1990). The EPS matrix material often appears to be most dense in the area closest to the core of the floc (Costerton, 1999). Furthermore, it is believed that the interior layer of sludge flocs has a growth rate lower than that of the outer layer, due to the limitation of diffusion of oxygen and nutrients from the bulk solution (Eriksson et al., 1992; Liao et al., 2002).

The diffusion distance for a cluster is a measure of the distance from the cells in the cluster to the interstitial space. A larger diffusion distance indicates a higher distance that substrate has to diffuse in the cell cluster. Diffusion distance is related to both the sizes of the clusters and their general shape (Yang et al., 2000). The average diffusion distance reflects the length a substrate needs to travel to get to the middle of the floc. If the diffusion distance increases, chances are that the substrate will be exhausted before it reaches the middle section of the floc. It is then reasonable to expect that the middle of the floc will be occupied by different microorganisms than the outer boundary of the microcolony (Yang et al., 2000).

2.5.3 Fractal dimension

It is difficult to describe floc structures and characterize flocs in terms of size, shape and/or density because of their irregular form. However, it was noted that activated sludge flocs generally possess a self-similar property and thus can be characterized as fractal. A

fractal is an object in which similar structural patterns are repeated at different length scales, with the result that small sections of the object, upon magnification, appear very similar to the original object. Fractal geometry quantifies the degree of roughness (raggedness) of cell cluster perimeters, where the higher the fractal dimension value, the more irregular (ragged) the floc boundary (surface) (Yang et al., 2000). The fractal dimension ranges in value between 3 for space filling objects (or flocs whose density does not drop with mass) to 1 in the case of extremely tenuous (rod-like) structures. The fractal dimensions of the flocs produced in water treatment plants are in the range of 1.4-2.8; whereas the flocs and biofilms generated in wastewater treatment have fractal dimension values that range from 1 to 3.

Fractal dimensions can be used to describe the spatial structure of flocs, i.e. how the particles occupy space in the flocs. Additionally, physical properties such as aggregate permeability, packing density, and porosity can be calculated from the fractal dimension and have important implications for the aggregation kinetics, floc break-up, and settling velocities of these aggregates as a function of their fractal structure (Thill et al. 1998).

2.6 Microscopic Techniques

Microscopy is an important analytical technique for many investigations of floc size and structure. Studies of floc structure generally require techniques such as conventional optical microscopy or more advanced microscopy such as confocal laser scanning microscopy or electron microscopy. Microscopy examination of biofilms and flocs enables an understanding to be gained of the spatial organizations that occur within them and on the surface supporting their development in which the individual microorganisms interact. The information that may be gained from various microscopy techniques includes labeling of cell surface components (EPS), identification of specific species within the consortia, distinction between viable and non-viable cells, measurements of depth and size of biological aggregates (Surman et al., 1996).

2.6.1 Conventional Optical Microscopy (COM)

Historically, and presently, conventional optical light microscopy (COM) is the most common method of analysis for studying the gross morphology (> 1 μm) and has focused primarily on size, shape, density, porosity, and settling velocity (Barbusinski and

Koscielniak, 1994; Li and Ganczarczyk, 1989). Also for the observation, measurement and modeling of biological structure and behaviour (i.e. transport and settling), COM is often the technique of choice.

Light microscopy depends on the ability of an object to absorb (color) and refract (density) light rays (Brown et al., 1998). Typical total magnification used is generally around 100× (10× objective) and will yield a lower resolution of approximately 1-2 μm when interfaced with image analysis software (Liss et al., 1996). This scale (> 1 μm) however is used because the outward behaviour of flocs can be observed at this resolution. Furthermore, from an engineering stand point, flocs greater than 1.0 μm will represent the majority of the biomass for settling studies (Droppo et al., 1997).

2.6.3 Scanning Confocal Laser Microscopy

The introduction of scanning confocal laser microscopy (CLSM) has increased the analytical precision of light microscopy. Since the illumination source for CLSM is reflected instead of transmitted, the thickness of the sample has a lesser effect on the ability to obtain high-resolution image (DeLeo et al. 1997). The high-resolution capability (200 nm) makes individual cells situated in each CLSM scan plane clearly visible, without any defocused interference from overlying or underlying cell or noncellular material (Lawrence et al., 1991). This technique creates an optical thin plane-of-focus in which out-of-focus light has been blocked, traditionally by optical barriers (pinhole) and by the physics of light absorption (photon microscopy) (Palmer and Sternberg, 1999). Furthermore, CLSM allows one to scan thin-sections to relatively great depths (tens of microns) in order to characterize microbial growth throughout a sample (DeLeo et al., 1997). Fully hydrated samples, undisturbed by complex and destructive preparation methods, can be examined by CLSM (Silyn-Roberts and Lewis, 1997). The output of CLSM can provide a series of 2D digital images at regular depths within a specimen (a z-stack series of digital xy optical sections) by computer-controllable alteration of the microscope's stage in z dimension. Sections in the xz plane (saggital sections) can also be acquired. Additionally, CLSM allows a three dimensional analysis of the xy axis compared with the xz axis, since the intense and deeply penetrating excitation energy enables the examination of both internal and external structures obtained by

optical sectioning (Silyn-Roberts and Lewis, 1997) . A collected z-stack can be computer-processed to represent serial optical sections, including 3D rendering and reconstruction.

The earliest applications of the CLSM to biological research were descriptive. Arrangements of single cells and of microcolonies within living hydrated biofilms were described. Most of these early studies were carried out with monoculture biofilms and established important models of biofilm growth or architecture. Costerton et al., 1994 studied a freshwater system biofilm and noted significant differences from then-established monoculture models. They clearly demonstrated a lower biomass density at the substratum than at locations closer to the bulk-liquid interface and many cells were positively stained.

Accurate measurement of thickness and biofilm coverage is difficult, in that it may vary considerably because of the morphological features of the biological aggregate. The total depth of biofilm and exact coverage of the biofilm was determined using CLSM by Silyn-Roberts and Lewis (1997) and DeLeo et al. (1997.

The development of species-selective fluorescently-labeled oligonucleotide probes has enabled distinctions to be drawn between morphologically similar cells within a biofilm. Although this hybridization-based method is destructive to the specimen, it is a powerful tool for sorting out spatial relationships between microorganisms. Hybridization can be combined with other techniques to show physiological interactions. Schramm et al. (1996) showed how the spatial relationship at the single-cell level of physiologically important microcolonies within wastewater-treatment biofilms can be correlated with microelectrode profiles of depth-dependent changes in concentration of soluble chemical species (nitrate/nitrite, oxygen).

Furthermore, CLSMs can be used to determine a biofilm's reflective material, auto fluorescence, cell distribution, EPS distribution, viability, cell identity, cell activity, enzyme activity and various parameters of the microenvironment. These imaging parameters can be used in combination with digital imaging analysis to quantify and compare the effects of different treatment, for example different nutrient loading or contaminant exposure (Neu et al. 2002).

2.6.3.1 Sample preparation and stabilization

The structural analysis of microbial flocs has depended upon the sequestering of the microbial aggregates onto a surface such as microscope slides or filters for microscopic observation. Such a method is potentially destructive to the floc structure because of sample manipulation (e.g. pipetting and poring, suction pressure). In order to stabilize and preserve the spatial arrangement of floc material, the immediate stabilization in agarose or Nanoplast (a hydrophilic resin) was employed in the past. Both embedding techniques allow for an extended period of observation and sample storage.

Decho and Kawaguchi (1999) embedded microbial cells and EPS in Nanoplast. The stabilization method used in their study resulted in a relatively simple imaging technique to visualize the EPA matrix in hydrated biofilms. Ganczarcyk et al. (1992) stabilized microbial aggregates in solidified agar for light microscopy studies. They were able to rapidly measure the size of individual cells as well as evaluate some morphologic properties of the activated sludge flocs.

Droppo et al. (1996) compared compositional differences in the flocs stabilized in low melting point agarose and non-stabilized flocs. Their observations revealed that no obvious structural or compositional differences in the flocs were evident. Since the agarose did not appear to generate erroneous results, they concluded that flocs stabilized in agarose minimized the limitations of handling, preparing and examining floc structures that were not stabilized. Furthermore, the embedded flocs can be easily stained. Penetration of the stains and washes is rapid and complete due to the large pentagonal pores formed during the bridging of the linear polysaccharide chains by hydrogen bonding. The diffusion rate within agarose is close to the rate of water (Droppo et al., 1996). The use of the plankton chambers and agarose embedding eliminates the problem of particle morphological changes due to particle-particle interactions upon resuspension during staining and washing that would be associated with the use of filters. Also, both washing and staining can be accomplished directly within the chamber reservoir eliminating handling of the agarose gel (Droppo et al., 1996).

2.6.3.2 Glycoconjugate Mapping by Lectin Binding Assay

It is important to recognize that confocal microscopy (or any epifluorescence technique) cannot generally be used to visualize unstained (non-fluorescent) material, such as the exopolymer matrix in which biofilm cells are embedded. However, extracellular matrix presence/absence/changes and their relationship to biofilm structure/function can be explored using appropriate techniques such as fluorescent lectin staining. Lectins are proteins of plant and animal origin that recognize and bind to specific configurations of carbohydrate residues (Johnsen et al. 2000). Assessment of the positions of specific carbohydrates at the ultra-structural level is possible by conjugation of lectins to fluorescent markers, thus making lectins useful for the study of polysaccharides and cell surfaces (Wolfaardt et al., 1998).

Epifluorescence microscopy and lectin binding have been used to study plant – bacterial interactions and to characterize marine biofilms during the early stages of developments. Del Gallo et al. (1989) studied extracellular polysaccharides synthesized by bacteria of the genus *Azospirillum* where fluorescein isothiocyanate (FITC)-labeled wheat germ agglutinin (WGA) and FITC-labeled soybean lectin (SBA) were used as lectins. In a study of mixed species biofilm, Michael and Smith (1995) used lectins (*Canavalis ensiformis* (ConA) *and Limulus polyphemus*) to characterize the chemical nature and physical distribution of glycoconjugates (e.g., glycolipids, glycoproteins, and polysaccharides) in 1- and 3-day-old marine biofilms. They found that each lectin had localized, discrete domains of binding on the biofilm surface.

Since epifluorescence microscopy does not allow analytical measurements with depth, due to out-of-focus haze and limited working distance CLSM was used in recent studies on lectin binding. Wolfaardt et al. (1998) studied the chemical nature and spatial arrangements of exopolymers in a degradative biofilm community using CLSM and a total of nine of FITC and tetramethyl rhodamine isothiocyanate- conjugated probes (including *Canavalia ensiformis* and *Glycine*). The lectin analysis in this study demonstrated a high degree of horizontal and vertical heterogeneity in the distribution of glycoconjugates in the biofilms. They found both discrete regions and considerable overlap in lectin binding within the biofilm.

Neu and Lawrence (1997) used lectin binding analyses (*Arachis hypogaea, Canavalia ensiformis, Erythrina cristagalli,* and *Ulex europaeu*) to examine the dominance of certain

bacteria and their extracellular polymeric products. The conjugated lectins showed the complex chemical composition of the biofilms and highly heterogeneous spatial distribution. Later, Lawrence et al. (1998) used conjugated lectins (*Triticum vulgaris* and *Canavalia ensiformis*) to identify and allow quantification of EPS in biofilm communities.

Decho and Kawaguchi (1999) used Con A-FITC to image EPS using CLSM. The result showed that EPS was observed well in interstitial spaces and between the substrates. However, they found inhomogeneous fluorescence throughout the EPS matrix suggesting that EPS may consist of varying compositions and/or distinct channels.

Johnsen et al. (2000) evaluated the use of lectins for the characterization of *Sphingomonas* biofilms by investigating the binding of five fluorescent lectins with known specificities to *sphingomonas* biofilms (*Conavalia ensiformis, Phaseolus vulgaris, Arachis hypogaea, Ulex europaeus* and *Triticum vulgaris).* They demonstrated that fluorescence from WGA and ConA is closely associated with the cells and that the strongest fluorescence emanated from groups of cells and microcolonies. Their results also showed that the binding of lectins to a biofilm does not necessarily prove the presence of specific target sugars in the EPS in biofilms since the lectins may bind to non-EPS targets or adhere nonspecifically to components of the biofilm matrix.

2.6.4 Advanced Microscopy

While the outward floc structure and behaviour may be derived from COM, the internal architecture of the floc cannot be resolved at this scale. Additionally, while CLSM has imaging advantages over COM, its resolving power is not sufficient for ultrastructural observations of individual EPS fibrils within flocculated material. Such analysis can only be obtained by high-resolution electron microscopy (Liss et al., 1996).

Electron microscopy can be used in both the scanning (SEM) and transmission (TEM) modes. SEM depends on the ability of the specimen to emit secondary electrons when it is "excited" by a powerful electron beam, whereas TEM depends on the ability of the mass of the specimen to scatter the electrons of a powerful electron beam as the electron pass through it. SEM gives better resolution than light or confocal laser scanning microscopy and allows good resolution for magnifications up to 30 000 ×. Conventional SEM is operated in a high vacuum, which requires the specimen to be dried and coated with gold, to both

disperse surface chard and to optimize secondary electron emission (Brown et al., 1998). Thus the analysis of hydrous flocs is difficult since the dehydration process seriously damages the floc and leads to shrinkage and loss of EPS matrix (Stewart et al., 1994; Cornelissen et al., 1997) SEM has proved to be useful to view the details of the initial bacterial attachment to the mineral surface before the biofilm EPS becomes established. However, when EPS was produced, it hid the bacteria from view and SEM lost its discriminative power. Thus SEM does not allow observations of the biofilm or floc interior (Stewart et al., 1994; Brown et al., 1998). In addition, quantitative analysis of SEM images is difficult because the three dimensional information is condensed into two dimensions (Stewart et al., 1994)

TEM is able to produce images of floc with even higher magnification and resolution than the SEM. TEM has resolving power of 1nm and magnification of up to 200 000 ×. The system, however, does not operate under cryo conditions and samples need to be transparent to electrons. This means that the TEM can only be used on thin samples (Liss et al., 1996; Brown et al., 1998; Cornelissen et al., 1997). Additionally, for very large flocs, the examination of too many sections in sequence (1 nm apart) can be very costly and impractical if one wishes to examine the entire floc. In this regard, COM and SCLM images can be very useful as an indication of the number of TEM sections required for a collection of representative images of a floc (Liss et al., 1996). The use of high resolution allows for detailed observation of the internal structure and composition of flocs otherwise not seen with COM and CLSM techniques. At this fine scale it was found that the large pores within the floc are not necessarily open channels devoid of structural matter (as appeared to be when observed with COM), but contain a complex matrix of EPS fibrils (Liss et al., 1996). On the other hand, TEM really can not be used for comparison of floc component distributions because of the expense, the time required for analysis and the extremely small fields of view. Often a complete floc can not be observed in one field of view. In addition, the floc is physically sectioned into sequential slices and thus the whole floc is not viewed and the true size of the floc is difficult and expensive to determine (Droppo et al., 1996)

In summary, the internal structure of flocs and their potential impact on floc behaviour should really be examined with correlative microscopy. Correlative microscopy is a strategy that uses different microscope types to derive multiple levels of information from a

given specimen. By analyzing one sample over a full range of magnifications (>1.0 mm to <1.0 μm) with COM, SCLM and electron microscopy, it is possible to bridge the resolution gaps which exist with single microscopic interpretations and provide more information for floc structural and behavioral investigation (Droppo et al., 1997)

CHAPTER 3 EXPERIMENTAL METHOD

3.1 General Description

This chapter describes in detail the equipment, chemicals used in the study, and experimental conditions. A laboratory scale sequencing batch reactor (SBR) system fed with a synthetic feed was used in the experiments. Similar SBR systems have been used in other wastewater research and found to perform well in chemical oxygen demand (Lee, 1997). The SBR is a fill-and-draw type reactor system involving a single complete-mix reactor in which all steps of the activated sludge process occur. Mixed liquor remains in the reactor during all cycles, thereby eliminating the need for a separate secondary sedimentation tank and sludge return system (Davis and Cornwell, 1998). The SBR system is designed to operate under non-steady state conditions and has been previously shown to be excellent in filamentous bulking control. Norcross (1992) also reported excellent removal efficiency for biochemical oxygen demand (BOD), total suspended solids (TSS), and nitrogen and phosphorus in full scale industrial and municipal wastewater treatment plants. A SBR system offers several advantages including a smaller reactor volume requirement than a conventional reactor, its resemblance to a plug flow reactor, minimal feed requirements, and good foaming and bulking control. A glucose-based synthetic feed was used in this study. Using industrial wastewater, which usually fluctuates daily, weekly, and seasonally, makes the control of nutrient levels and concentrations of toxic substances entering the reactor nearly impossible. In contrast, the use of the synthetic feed allows the easy manipulation of nutrient levels and the concentrations of the chemical components and thus it allows a well-controlled environment in the reactor.

An inoculum was obtained from a municipal wastewater plant. Two reactors were set up for P-excess conditions and the other two reactors were set up for P-limited conditions by using different COD:N:P ratios in the synthetic feed for the two sets of conditions. For P-excess and P-limited conditions, experimental COD: N: P ratios in the synthetic feed were 100/5/1 0and 100/5/0.1 respectively. Samples of mixed liquor and effluent from each reactor were collected throughout the experimental period for standard wastewater analysis, and chemical and microscopical floc analysis.

3.2 Experimental System

3.2.1 Laboratory Sequencing Batch Reactors

The SBR system consisted of four parallel sequencing batch reactors (see Figure 3.1), a refrigerated feed storage, a feed preheater unit, four pH controllers with a pH buffer, a constantly circulating water bath, and four individual times for each reactors controlling feeding, mixing and settling phase.

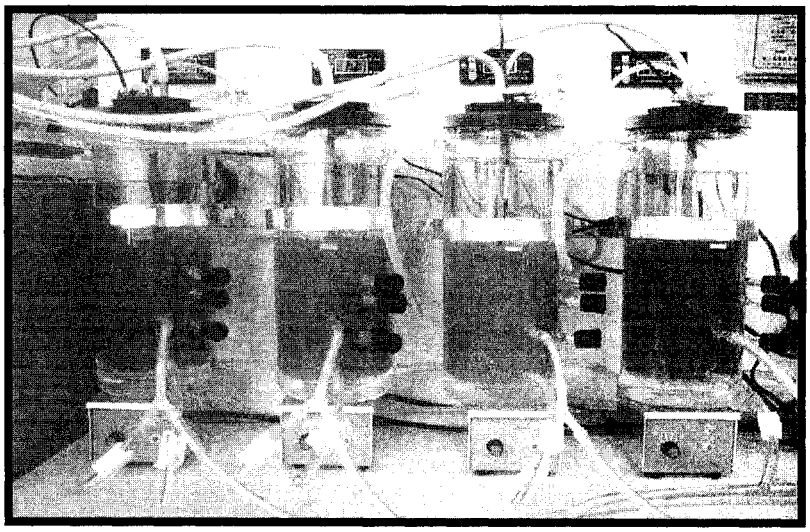

Figure 3.1 Four parallel sequencing batch reactors (SBR) used in this study.

The feed was stored in four 9 L autoclavable rectangular polypropylene carboys (Nalgene Company, Rochester, NY), which were kept in refrigerator maintained at 4°C. The feed was cooled to prevent premature degradation of COD and other nutrients. The pre-heater unit kept a water bath at a constant 45°C. The tubes, which carry the 4°C feed from refrigerator to the SBRs, pass through the water bath. This process warms up the feed to 27°C before it is pumped into the reactors. The feed was transferred from the fridge to the SBRs using four individual peristaltic pumps driving 1 pump head each (Masterflex Standard Pump Drive and master flex L/S size 18 Pump head and Masterflex silicone tubing, Cole-Parmer Instrument, Co., Niles, Illinois, USA). The pumps were operated at maximum speed.

The four sequencing batch reactors were jacketed glass reactors of 2 L capacity. Five outlet ports were positioned at reactor volumes of 0, 0.4, 0.5, 0.8, and 1 L. The 0.4 L port was used to decant treated effluent. The 0.5 L port was used to collect mixed liquor samples. The rest of the unused ports were plugged with rubber septa (Suba-Seal white rubber septa, Aldrich Chemical Company Inc., Milwaukee, WI). A rubber stopper with a hollow ring

made of Lucite was used to hold the aeration tube, the feed tube, the pH probe and the pH buffer tube in each of the four reactors. Aeration in each reactor was achieved using an aquarium type air pump and plastic air diffuser positioned at a level of approximately 0.5 L reactor volume. Mixing in each reactor was achieved using a magnetic stirrer (VWR-Canlab, Toronto, ON) with a magnetic spin bar.

The on-line pH controllers were used to maintain pH in reactors using NaOH solution. The pH electrode was immersed at the 0.4 L reactor volume level in each SBR and the electrode was connected to an on-line pH controlled (LED pH/OPR controlled, Coel-Parmet Instrument Co., Niles, Illinois, US). A 20 nM NaOH solution was used as the pH buffer and was introduced to the SBRs by on-line pH controllers to maintain the pH at a neutral level (7.0+/-0.2). The operation temperature of the SBRs was maintained at a constant 27°C by constantly circulating 28°C water through the jackets of the reactors (1°C above the operating temperature due to heat losses along the tubes). The 28°C water was passed through the 28°C water bath (VWR Scientific Canada Ltd., London, On) then it was circulated through the reactor jackets and passed back into the 28°C water bath. The water was circulated by using a peristaltic pump driving 4 pump heads (Masterflex Standard Pump Drive and masterflex L/S size 18 Pump head and Masterflex silicone tubing, Cole-Parmer Instrument, Co., Niles, Illinois, USA). The pumps were operating at low speed to minimize tubing damage.

The cyclic operations of the SBR were controlled by the use of 4 on-and-off programmable timers (Sper Scientific Model 810030, Sper Scientific Ltd., Scottsdale, Arizona, USA). The programmable timers controlled the transfer of the refrigerated feed to the pre-heater unit, the transfer of the heated feed to the SBRs, the aeration and mixing time, and the discharge of the treated effluent. The control was achieved by turning the electric equipment on and off at predetermined times. The operation conditions of the SBR system are shown in Table 3.1. The Peristaltic pumps (Masterflex Standard Pump Drive and masterflex L/S size 18 Pump head and Masterflex silicone tubing, Cole-Parmer Instrument, Co., Niles, Illinois, USA) were used in all fluid transfer steps. Fluid transfer steps included the transfer of the refrigerated feed to the preheater unit, the transfer of the heated feed to the SBRs, the discharge of the treated effluent and the constant circulation through SBRs jackets 27°C water bath.

3.3 Experimental Approach

3.3.1 Preparation of Feed

The composition of the standard synthetic feed is shown in Table 3.2. The standard feed contained a COD level of 300 mg/L and a COD: N: P ratio of 100:5:1 for reactors 1 and 2 and a COD: N: P ratio of 100:5:0.1 for reactor 3 and 4. Stock solutions of glucose, KH_2PO_4, NH_4Cl, and inorganic salts were prepared separately every week and kept at 4°C before use. The synthetic feed was prepared fresh every two days and kept at 4°C in the feed storage. All chemicals used were of analytical grade. All dilution was done using deionized distilled water (Milli-Q Water Systems, Millipore Corporation, MA).

3.3.2 Inoculum

The inoculum used in this study was a mixed liquor sample obtained from the Toronto Main Treatment Plant (ON, Canada). The inoculum was collected and transported to the laboratory and added into the reactors immediately upon return to the laboratory (less than 2 hours).

3.3.3 Cyclic Operation of the Sequencing Batch Reactors

The SBR is a fill-and-draw activated sludge system. The reactors operated on an n hours per cycle, and N cycles per day basis (see table 3.1). In each cycle, there were four discrete stages: fill, aeration (reaction), settling (clarification) and withdraw. The synthetic feed was pumped from the preheater unit to the reactors in fill mode. When the reactor volume reached approximately 0.8 L, the filling step would stop and the aeration mode, with mixing, would start. At the end of the aeration mode, the stirrers and air diffusers were turned off, and the mixed liquors were allowed to settle down to the bottom of the reactor. A volume of 0.6 L of the treated effluent, which is 60 % of the total operating volume of 1 L, was withdrawn from the reactors during the withdrawal mode. The cyclic operation continued. The length of each operating mode is shown in Table 3.1. Sludge samples were collected for characterization at the end of the aeration phase.

Table 3. 1 The SBR cycles for the experimental run

Cyclic Operation of SBR	**Duration**
Length of cycle, n (hours)	6 hours
Number of cycles per day, N	4 times a day
Length of operation mode:	
Fill	10 min
React	5 hours
Settle	40 min
Withdraw	10 min

Table 3. 2 Constituents of standard synthetic feed (COD=300mg, COD: N: P=1000:5:1)

Nutrients	**Compounds**	**Concentrations (mg/L)**	**Sources**
C-source	Glucose	281.25 (112.5 mg C)	
N-source	NH_4Cl	57.32 (15 mg N)	Sigma, Mississauga, Canada
P-source	KH_2PO_4	13.17 (3 mg P)	Sigma, Mississauga, Canada
Others	$MgSO_4$	2.48 (0.5 mg Mg)	Fisher, Mississauga, Canada
	$FeSO_4 \cdot 7H_2O$	2.49 (0.5 mg Fe)	Fisher, Mississauga, Canada
	$Na_2MoO_4 \cdot 2H_2O$	1.26 (0.5 mg Mo)	Fisher, Mississauga, Canada
	$MnSO_4 \cdot 4H_2O$	0.308 (0.1 mg Mn)	Allied, Mississauga, Canada
	$CuSO_4 \cdot 5H_2O$	0.393 (0.1 mg Cu)	Fisher, Mississauga, Canada
	$ZnSO_4 \cdot 7H_2O$	0.440 (0.1 mg Zn)	BDH, Mississauga, Canada
	NaCl	0.254 (0.1 mg Na)	
	$CaSO_4 \cdot 2H_2O$	0.430 (0.1 mg Ca)	
	$CoCl_2 \cdot 6H_2O$	0.404 (0.1 mg Co)	Fisher, Mississauga, Canada

3.3.4 Experimental Procedures

Stable operation of the SBRs was determined by monitoring MLSS, ESS and soluble chemical oxygen demand (COD) removal. Only when all the monitored parameters showed relatively constant levels, the SBR was considered to be at stable operation conditions. This study was conducted over a six-week period. Three stable SRTs were observed before the experimental procedures began.

3.4 Standard Wastewater Analysis

3.4.1 Mixed Liquor Suspended Solids (MLSS)

MLSS were measured at the end of the reaction phase in accordance with Standard Methods (APHA, 1980).

3.4.2 Effluent Suspended solids

The ability of the sludge to flocculate in the SBR system was evaluated by the effluent suspended solids (ESS) measurement as described in Standard Methods (APHA, 1980). The level of the ESS was determined after a 40-minute settling period of the mixed liquor.

3.4.3 Chemical Oxygen Demand

The COD from each reactor was measured on a weekly basis. The closed reflux colourimetric method (APHA, 1980) was used to determine the chemical oxygen demand (COD) of the feed and the treated effluent. The treated effluent was filtered through a 0.45 μm pore size disposable glass fibre filter (Schleicher & Schuell Glass Fiber Filters, diameter 25 mm) before the digestion solution and reagents were added. Culture tubes with desired feed and effluent (2.5 mL), digestion solution ($K_2Cr_2O_7$ + $HgSO_4$ + H_2SO_4), and reagents (Ag_2SO_4 + H_2SO_4) were heated in a Hach COD reactor (Model 45600-00, Hach Co., Loveland, CO, USA) for 2 hours at 150°C. The samples were then cooled to room temperature and measured spectrophotometrically (Spectronic Instruments –Spectronic 20^+) at 600 nm. Potassium hydrogen phthalate (KHP) was used as a COD standard. All chemical reagents were from Sigma-Aldrich Canada Ltd., and were of analytical grade.

3.5 Extraction and Chemical Analyses of EPS

3.5.1 Extraction

The EPS was extracted from sludge flocs using the cation exchange resin (CER) method (Frølund et al., 1996; Bura et al., 1998; Liao et al., 2001). The duplicate sludge samples collected from the SBR system were concentrated via gravity sedimentation to approximately 1.5-3.0 g/L. The sludge samples were then washed twice with the extraction buffer solution (Frølund et al., 1996) at pH = 7, and centrifuged at 2000 g at +4°C for 5 minutes each time. The recommended extraction buffer solution contains the following in 1L ddH_2O (pH=7): 2mN Na_3PO_4; 4mN NaH_2PO_4; 9 mN NaCl; 1 mN KCl. The MLSS of the washed sample were measured, and the amount of CER (DOWEX® HCR-W2 Cation Exchange Resin) in the sodium form was determined and added to each washed sample, based on 80g of resin per g of MLSS. The CER was washed with the buffer solution until the liquid was clear, before mixing with the sample. The mixture of each sample and CER was added to the extractor assembly. The extraction assembly was kept at a constant temperature of 4 °C by placing it in an ice-water bath, and stirring it at 247 rpm for 2 hours (Liao, 2000; Whittaker, 2002; Kraemer, 2002). The sample was then decanted into high-speed centrifugal tubes and centrifuged at 9, 500 g at + 4°C for 20 min. The supernatant was decanted into a new centrifuge tube, and stored at - 20°C for future analysis of carbohydrates, proteins, acidic polysaccharides, and DNA. When each sample was thawed for analysis, the samples were centrifuged if required, at 3500 g at +4°C in order to remove any remaining floc particles.

3.5.2 Chemical Analyses

3.5.2.1 Total Polysaccharides

Total polysaccharide concentration was performed by the Anthrone method (Gaudy, 1962). A standard solution of D-glucose was used to prepare a standard calibration curve in the range of 5-100 mg/L. A standard stock solution of glucose was stored in the refrigerator at 4°C for no more than a week. The anthrone solution was prepared weekly by dissolving 0.2 g of anthrone reagent in 100 mL of 95% H_2SO_4.

A triplicate of 2.0 mL aliquot of the extracted EPS and standards was pipetted into the HACH test tubes. This was followed by an addition of 5 mL cold Anthrone reagent to each

HACH test tube at 60 seconds intervals. The tube contents were then mixed with a vortex mixer for 30 seconds and placed in a boiling water bath for 15 min to completely digest the polysaccharides. After digesting, each sample was sequentially cooled to room temperature in an ice bath. The colour intensity of the developed solution was measured as absorbance at 625 nm (Spectronic 20^+, Spectronic Instruments, Rochester, NY, USA).

The total polysaccharide concentration (glucose equivalent) present in the extracted EPS was then calculated from the standard curve (mg/L), then expressed as mg/g MLSS, based on the biomass concentration for the EPS extraction.

3.5.2.2 Proteins

The protein concentration within the EPS was quantified by colorimetry using the Folin reaction (Lowry et al., 1951; Liao et., 2001; Whittaker 2002; Kreamer 2002). Bovine serum albumin (BSA) was used as the standard solution (20-100 mg/L) to prepare a standard calibration curve. A 1 mL aliquot of blank, standard and sample solution (triplicate) was added to separate HACH test tube. At 30 seconds interval, 5.0 mL of prepared reagent (20 g Na_2CO_3 in 1 L of 0.1 N NaOH, mixed with 0.25 g $CuSO_4 \cdot 5H_2O$ dissolve in 50 mL of 1%(w/v) aqueous solution of sodium tartrate, in a ratio of 25:1) was added to each test tube, mixed with a vortex mixer for 15 seconds, and allowed to stand for 10 minutes at room temperature. A 0.5 mL aliquot of diluted Folin reagent (Folin-Ciocalteu's phenol reagent diluted to a ration of 1:1 with ddH_2O) was added to the solution and immediately mixed with a vortex mixer for 15 seconds. The mixture was allowed to stand for 30 minutes at room temperature for colour development. The absorbances of the solutions were measured at 750 nm using a spectrophotometer (Spectronic 20^+, Spectronic Instruments, Rochester, NY, USA). The protein concentration was calculated from the standard curve and converted into mg (BSA equivalent) per g MLSS.

3.5.2.3 Acidic Polysaccharides

The uronic acid determination within the EPS was quantified using the Filisetti-Cozzi and Carpita (1991) method. A standard solution of D-glucuronic acid was used to prepare a standard calibration curve (range 5-20 mg/L). 0.8 mL aliquots of blank, standard, and sample solution (triplicate) were pipetted into HACH test tubes. 80 μL of 4 M sulfamic

acid-potassium sulfamate (pH 1.6, adjusted with saturated KOH at +4°C) were added to each test tube and mixed with a vortex mixer for 20 seconds. At 60 seconds intervals a 4.8 mL aliquot of ice cold analytical grade (96.4%) H_2SO_4 containing 75 mM sodium tetraborate, was added to each test tube, mixed again using a vortex mixer for 30 seconds, and then placed in a boiling water bath for 20 min. Each sample was sequentially chilled for several minutes in an ice-water bath to cool the solution to room temperature. A 160 μL aliquot of 0.15% (w/v) m-hydroxydiphenyl in 0.5% (w/v) NaOH was added and mixed with the vortex mixer for 15 seconds. 10 minutes after the addition of the final reagent, a pink/red colour developer and the absorbance were measured at 525 nm. The acid polysaccharide concentration was calculated from the standard curve and expressed as mg (glucuronic acid equivalent) per g MLSS.

3.5.2.4 DNA

DNA was quantified by using a standard fluorescent DNA quantitation kit (BIO-RAD Laboratories, Hercule, CA). Calf thymus DNA was used to prepare a standard calibration curve. The Hoest dye was added to each sample in triplicate, and the measurements were taken using a 360 nm excitation filter and a 460 nm emission filter.

3.6 Physical Analysis of Biomass

3.6.1 Surface Charge

The surface charge of microbial flocs was determined by colloidal titration (Morgan et al., 1990). The surface charge of a sample biomass was measured by mixing a known amount of sludge with a known amount of positively charged polymer, polybrene, and titrating the solution with a negatively charged polymer polyanetholsulfonic acid. This experiment was modified in that the polyvinyl sulphate was replaced by the polyanetholsulfonic acid. The endpoint volume of the titration was compared with the endpoint volume of a blank sample.

A mixed liquor sample of sludge was collected from each reactor. Each sample of sludge was washed once with ddH_2O water and centrifuged at 3000 g for 5 minutes at +4°C. Each sample was washed again with ddH_2O water at pH 7.0 and centrifuged at 3000 g for 5 minutes at +4°C. In 40.0 mL of pH-balanced ddH_2O, 2.0 mL of washed sludge was mixed

with 4.0 mL of excess polybrene. A standard solution of polyanetholsulfonic acid was used to titrate with the excess polybrene, using toluidine blue as an indicator. A blank was also titrated where the 2.0 mL washed sludge sample was replaced by 2.0 mL of pH-balanced ddH_2O. The surface charge of each sample was calculated using the formula:

$$\text{Surface charge} = \frac{-(V_o - V) \times N \times 10^9}{2 \times \text{MLSS}} \quad [1]$$

where N =0.001 eq/L, V= volume of polyanetholsulfonic acid (L) required to reach the endpoint, and V_o=volume of polyanetholsulfonic acid (L) to reach the endpoint for a blank solution. MLSS was measured in mg/L.

3.6.2 Hydrophobicity Determination

The Microbial Adherence to Hydrocarbons (MATH) method was employed for determination of the relative % of hydrophobicities of microbial flocs (Rosenberg et al., 1980). The method relies on the principle that upon mixing, hydrophobics in the microbial sludge suspension adhere to hydrocarbon at the hydrocarbon-aqueous interface. The absorbance of the aqueous phase was subsequently measured to estimate the relative hydrophobicity of the sample.

A mixed liquor sample of sludge was collected from each reactor and immediately analyzed. Each sludge sample was washed twice with ddH_2O and centrifuged at 3000 g for 5 minutes at + 4°C after each washing. Samples were shaken gently to resuspend the pellet, and then homogenized using a blender. The initial absorbance of the dispersed suspension (I_o) was adjusted to 1.3±0.30 at 400nm, using ddH_2O for dilution. 10 mL of the adjusted sludge suspension was mixed with 1.0 mL of hexadecane using a vortex mixer for 2 minutes. The hydrophobic and hydrophilic phases were left to separate for 10 minutes in a separatory funnel. The aqueous phase was collected and absorbance (I) was measured at 400 nm Spectronic 20^+ (Spectronic Instruments, Rochester, NY, USA). Relative hydrophobicity was calculated using the formula:

$$\%\text{Hydrophobicity} = \frac{(I_o - I)}{I_o} \times 100 \quad [2]$$

3.7 Confocal Laser Scanning Microscopy

The CLSM analysis was performed using a Zeiss Axioplan LSM 510 (Carl Zeiss Inc., Toronto, Ontario) equipped with an argon laser (excitation line 488nm), and helium-neon lasers (excitation lines 543nm and 633nm). The microbial floc samples were embedded in low melting point agarose (Droppo et al., 1996) for stabilization. Lectins conjugated with fluorescent dyes were used to identify specific polysaccharides within the floc matrix (Kraemer, 2002).

3.7.1 Polysaccharide specific lectins conjugated with fluorescent dyes

Lectins are proteins that selectively bind to specific carbohydrate components to form a glycoconjugate. Each lectin is conjugated with a fluorescent dye in order to allow visualization when excited by a laser source, such as an argon or helium-neon laser. Lectins were selected on the basis of observation from other studies that have shown EPS to contain mannose, glucose, galactose, N-acetylglucosamine, N-acetylgalactosamine, and other residues. The chosen lectins included: *Conavalia ensiformis* (concanavalin A, ConA), *Triticum vulgaris* (wheat germ agglutinin, WGA), *Glycine max* (soybean agglutinin, SBA). The lectin-conjugate stains used for analysis, as well as their approximate absorption and fluorescence emission and their carbohydrate specificity, are given in Table 3.3.

Table 3. 3 Lectin-conjugates used for CLSM analysis

Lectin-conjugate	Abs/Em	Carbohydrate Specificity
Concanavalin A –Fluorescein; Alexa Fluor 633	494/518; 632/647	α-mannopyranosyl and α-glucopyranosyl residues
Wheat Germ Agglutinin-Texas Red; Tetramethylrhodamine	595/615; 555/580	N-acetylglucosaminyl Residues
Soybean Agglutinin -Alexa Fluor 488	554/576	α and β-N-acetylgalactosaminyl and galactopyranosyl residues

* Approximate absorption (Abs) and fluorescence emission (EM) maxima in nm

[1] Supplied by Molecular Probes, Inc., Eugene, Oregon, USA

A stock solution for each lectin-conjugate is prepared at selected concentrations as in Kreamer (2002), and stored at –20° C. The solution used for each lectin-conjugate stain and their working concentrations are given in Table 3.4. Prior to use, the stains are thawed and centrifuged for 1 minute at 14, 000 x g to remove any aggregates (see Appendix G for a detailed protocol).

Table 3. 4 Required solutions and working concentrations for lectin-conjugate analysis

Lectin-conjugate	**Stock Concentration (µg/mL)**	**Working Concentration**
Wheat germ agglutinin-tetramethylrhodamine	1-2 mg/mL in 0.1 M $NaHCO_3$ containing 1 mM Mn^{2+} and 1 mM Ca^{2+} at pH 8.3	10 µg/mL in 0.1 M NaHCO3 containing 1 mM Mn^{2+} and 1 mM Ca^{2+} at pH 8.3
Concanavalin A-Alexa Fluor 647	2 mg/mL in 0.1 M $NaHCO_3$ containing 1 mM Mn^{2+} and 1 mM Ca^{2+} at pH 8.3	100 µg/mL in 0.1 M NaHCO3 containing 1 mM Mn^{2+} and 1 mM Ca^{2+} at pH 8.3
Soybean agglutinin-Alexa Fluor 488	2 mg/mL in distilled deionized water	10 µg/mL in 0.1 M NaHCO3 containing 1 mM Mn^{2+} and 1 mM Ca^{2+} at pH 8.3

3.7.2 Agarose stabilization and staining for floc samples

To retain moisture and maintain stability, the biological floc samples were embedded in low melting point agarose (Droppo et al., 1996). The floc samples for CLSM analysis were prepared by adding 0.5 mL of MLSS to 1.0 mL low melting point agarose. After mixing, by inversion in a 1.5 mL microcentrifuge tube, the mixture was poured into a plankton chamber and allowed to solidify. A 1.0 mL working solution was made with the appropriate volume of lectin-conjugate in solution and poured over the flocs embedded in the agarose. The sample was incubated at room temperature in the dark for 15 minutes. Then the sample was washed three times with a buffer solution and incubated for 10 minutes after each washing (see Appendix G for a detailed protocol).

3.7.3 Detection and acquisition of images

The CLSM analysis was performed using a Zeiss Axioplan LSM 510 (Carl Zeiss, Toronto, Ontario) equipped with an argon laser (excitation line 488nm), and helium-neon lasers (excitation lines 543nm and 633nm). For each experiment, the argon laser was set at 50% of its total power. When collecting images, the argon laser was operated at 50 % transmission power. The total power of the helium-neon lasers was not adjustable; however, helium-neon laser (excitation lines 543nm) was operated at 10% and helium-neon laser (excitation line 633nm) was operated at 100% transmission power.

Samples were scanned by using three channels at selected z-intervals through the thickness of the flocs embedded in the agarose. For all images collected, channels 1, 2, and 3 represent the fluorescently labeled lectins Con A (blue), SBA (green), and WGA (red) respectively. Scans were captured using Zeiss 63x/0.9 NA water immersion Apochromat objective, a scan speed of 8.96 μs/pixel, and line averaging of 2. The pinhole diameter (for the Achroplan objective) for channels 1, 2, and 3 was set at 191μm, 146 μm and 169 μm respectively.

For comparison purposes, floc samples were imaged in reflectance mode after being scanned in fluorescence mode. The sample was scanned in reflectance mode in the exact same location and at approximately the same depths as the scan in the fluorescence mode. Samples were scanned by using one channel (channel 2) at selected z-intervals through the thickness of the flocs embedded in the agarose. The reflected images were captured by detecting scattered light from the sample, rather than fluorescent light. The argon laser was set at 50% of its total power and 100% of its transmission power. The power of the helium-neon lasers was not adjustable; however, helium-neon laser (excitation line 633nm) was operated at 100% transmission power. The helium-neon laser (excitation line 543nm) was not used to excite the sample. Reflectance mode scans were captured using Zeiss 63x/0.9 NA water immersion Apochromat objective, a scan speed of 8.96 μs/pixel, and line averaging of 2. The pinhole diameter for the one channel (channel 2) was set at 146 μm.

To optimize each image in fluorescence or reflective mode, the brightest and darkest pixels were detected by adjusting the detector gain, amplitude gain, and amplitude offsets for each channel.

LSM 510 Release 2.3 software (Carl Zeiss, Toronto, Ontario) was used to create gallery images, projections and depth-coded images for each z-stacked image. The z-stacks and projections can be displayed using a split channel image. A split channel image represented the three individual lectin-conjugates employed and a combined lectin-conjugate image. In all split channel images presented, the upper left, upper right, lower left, and lower right quadrants represent Con A (channel 1, blue), SBA (channel 2, green), WGA (channel 3, red), and combined lectins respectively. Gallery images were created by displaying sequential z-sections side by side. A projection could be viewed at numerous angles and three-dimensional impressions were generated. The depth of the sequence of z-sections was visualized by depth coding, and a colour scale bar provided information about the various components of the image at varying depths. The digital images were analyzed to determine parameters such as regions at various depths containing EPS, porosity, diffusional distances, and fractal dimensions.

3.8 Image Analysis

3.8.1 Image Structure Analysis Software

Analysis of the digital images was conducted using a program Image Structure Analyzer 3 (ISA3D), a software package developed by the Biofilm Structure-Function research group, Center for Biofilm Engineering, Montana State University, over the past seven years for the purpose of quantifying biofilm structure. It was developed for the UNIX/Motif environment in C++, with all calculations done in double precision arithmetic.

The software calculates both textural parameters and areal parameters. The textural parameters describe the microscale heterogeneity of the image. The areal parameters describe the morphological structure of the floc. Each parameter measures a unique characteristic of either the cell cluster or interstitial space within the floc. These parameters are concerned with the size, orientation and shape of surface features of the constituent parts (Yang et al., 2000). For purpose of this study only areal parameters were considered.

3.8.2 Manipulation of digital image

The digital analysis was performed only on the images captured in a reflectance mode. The microbial flocs were observed using Zeiss 63x/0.9 NA water immersion

Apochromat objective, a scan speed of 8.96 μs/pixel, and line averaging of 2. The pinhole diameter was set at 146 μm. The argon laser (50% of its total power and 100% of its transmission power) and helium-neon lasers (excitation line 633 and operated at 100% transmission power) were used as illumination. Images were captured with a camera connected to Zeiss Axioplan LSM 510 (Carl Zeiss, Toronto, Ontario).

The two-dimensional image size was 146.2μm x 146.2μm and the pixel size was 3.502μm. CLSM stack images of an activated sludge sample were taken at 1 μm distance intervals between the optical sections. The digital analysis was presented in two ways: as the depth profile and as average values for each parameter (fractal dimension, average diffusion distance, and porosity).

For a depth profile, individual sections were removed from an acquired z-stack and exported as a TIF-tagged image file into Adobe Photoshop. When using Adobe Photoshop the image was viewed in grayscale mode and the actual pixel view, with grids. 25 slices were analyzed where the first slice represented the relative top of the floc, and subsequent slices were 1 μm apart and leading toward the center of the floc. Since the flocs did not cover the whole field of view under 630 x magnifications, a portion of each individual image -where the biomass was detected through the 25 slices - was selected for analysis. The size of the cropped area within the digital image was 72x72 (pixels), which corresponds to 20.56μm x 20.56μm (or 422.69μm^2) of the actual area of the observed sample under 630x magnification.

The average value for each parameter was calculated using the values obtained for the depth profile. Therefore values for a total of 125 slices for each reactor were averaged (5 depth profiles for each reactor × 25 slices per profile).

3.8.3 Thresholding

Thresholding can be viewed as segmenting an image into foreground and background pixels based on the choice of a specific gray scale value. The foreground is the biomass and the background is the interstitial space. If the image is manually thresholded, the operator manipulates the image until it looks good. Although it is impossible to specify precisely how to select the threshold, the parameters calculated from thresholded images depend on the selected gray-scale level. It was suggested that an algorithm for automatic thresholding

could help in the process (Lewandowski et al.2002; Yang et al., 2000; Lewandowski, 2000). The iterative selection method and Otsu's method were integrated as the automatic thresholding methods in ISA3D. The interative selection was incorporated into a new version of ISA3D software as the automatic thresholding algorithm. An interative selection performed better than the other algorithms used (Lewandowski et al., 2002; Yang et al., 2000), and thus was used in this study.

3.8.4 Areal Porosity

Areal porosity is the ratio of combined areas of the voids to the total area of the image. The ISA3D software converts the digital image in the grayscale to the binary image and calculates the areal porosity of the two dimensional image as:

$$\text{Areal porosity} = \frac{\text{Number of void pixels}}{\text{Total number of pixels}} \qquad [3]$$

Areal porosity for a two dimensional image ranges in value from 0 to 1; the higher the value, the more pores and interstitial space within the image. It should be noted that the term "areal porosity" is not a correct use of the term because porosity characterizes three-dimensional space, while the calculated parameter is evaluated from two-dimensional images (Lewandowski, 2000). However with the use of CLSM the areal porosity values calculated from individual slices can be arranged into a depth profile. The depth profiles of areal porosity are then directly related to the three-dimensional porosity. Additionally, porosity appears to be a continuous function of biofilm depth and nutrients can be expected to penetrate biofilm at different rates, depending on the slope of the areal porosity profiles (Lewandowski, 2000).

3.8.5 Fractal Dimension

Fractal dimension measures the degree of raggedness of biofilm cell cluster perimeters. For a two-dimensional image the fractal dimension can range from 1 to 2, where the higher the number, the more ragged the perimeter of the cluster. A straight line has the fractal dimension 1, and a line so ragged that it covers a two-dimensional subplane has a fractal dimension 2. For the purposes of the analysis, the rougher the biofilm boundary, the

higher the fractal dimension. The ISA program uses the Minkowski Sausage algorithm to perform the calculations.

3.8.6 Diffusion Distance

The diffusion distance for a cluster is a measure of the distance from the cells in the cluster to interstitial space. In terms of ISA3D, the diffusion distance for an individual pixel within a cluster is the distance from that pixel to the nearest void pixel. The diffusion distances are only calculated for cluster pixels (Yang et al., 2000). For any cell in a cell cluster, the distance to each pixel that is on the boundary of the cluster can be calculated. Diffusion distances are initially calculated as a number of pixels, and then converted into distances (μm). Diffusional distances measure the distances over which the substrate has to diffuse from the void space to reach bacteria within the cluster.

The average diffusion distance is the average of the minimum distance from each cluster pixel to the nearest void pixel over all cluster pixels in the image. In ISA3D, an eight-point Euclidean distance mapping algorithm, is used to calculate the average diffusion distance (Lewandowski et al., 1999).

3.9 Statistical Analysis

Variability in measurements was calculated using the standard deviation of the average and is shown as mean ± standard deviation. When studying the effect of P-limitation on the physicochemical properties of biomass, a t-test was used to determine the significance between treatment means. All calculations were performed with Microsoft Excel (Windows EXP). The null hypothesis that there is no significant difference in the physicochemical properties at the P-rich and P-limited conditions was tested using a two tailed student's t-test at 95% confidence. If the probability for the calculated t-statistic was ≤ 0.05, then the null hypothesis was rejected and the two conditions, P-rich and P-limited, were concluded to be different and statistically significant.

CHAPTER 4 RESULTS

This study investigated the effect of the nutrients (COD: N: P) on floc properties and the operational parameters of activated sludge processes (i.e. COD removal efficiency and MLSS), in a well controlled laboratory sequencing a batch reactors (SBRs) system. Four parallel SBRs were fed glucose based synthetic feed, and the COD: N: P ratio was varied to stimulate P-rich and P-limited conditions. Reactor 1 (R1) and reactor 2 (R2), were controls with their COD: N: P ratio maintained at 100:5:1. Reactor 3 (R3) and reactor 4 (R4), were fed a P-limited feed with COD: N: P ratio maintained at 100:5:0.1. Before the experimental stage there was an acclimation period (see Table 4.1). Three sludge retention times (SRT) is the period typically recommended to fully acclimate biomass to new conditions. The assumption was generally valid, since stable COD removal efficiencies and MLSS concentrations were obtained before the 4th SRT. The acclimation period lasted 27 days. The SRT of 9 days was used for this experiment since Whittaker (2002) study showed that at low SRT (6 days), the biomass present in the reactors could not sustain itself. A higher SRT (12 days) proved to be much more sustainable in Whittaker's study, but because of a time constraint a compromise of 9 day SRT was made.

Table 4.1: Duration of the experiment at SRT of 9 days and the COD: N: P ratio of each of the SBRs used in this study

COD: N: P Ratio in SBRs		Acclimatization Period (days)	Experimental Period (days)	Total Length of Experiment (days)
R1 and R2 100: 5: 1	R3 and R4 100: 5: 0.1	27	20	47

The overall performance of the SBR system fed with synthetic feed was determined by monitoring the mixed liquor suspended solids (MLSS) and the chemical oxygen demand (COD) removal efficiencies. The measurements were done during the acclimatization period and throughout stable system operating conditions (experimental period). The floc properties that were investigated included: surface charge, hydrophobicity, and EPS composition. Confocal laser scanning microscopy (CLSM) combined with lectin-conjugate analysis were employed to observe EPS distribution. By applying CLSM and an image analysis, the areal

parameters such as porosity, fractal dimension, and average diffusional distance were examined.

Several of the floc properties measured were used to assess the effects of nutrients on floc by comparing the results from the experimental reactors (R3 and R4, COD: N: P = 1000:5:0.1), to that of the controls (R1 and R2, COD: N: P = 100:5:1). The COD: N: P loading scenario was always run in duplicate throughout the duration of acclimation and experimentation. Prior to any pairing of data from duplicate reactors, the collected data was always subjected to a paired two-tailed t-test at 95% confidence, to ensure the data collected from each of the paired reactors (i.e. those reactors run under the same COD:N:P loading) was not significantly different from one another. The paired t-tests were used for comparing the concentrations of EPS components extracted from flocs obtained from each of four reactors. The null hypothesis (H_o) of no statistical difference was rejected at $\alpha = 0.05$ and it was accepted at $\alpha = 0.20$ for the t-test; otherwise the decision was withheld.

In all cases, the data obtained from the reactors run in duplicate was not significantly different and hence was always paired. Each of the paired sample sets was then analyzed via a paired two-tailed t-test to determine if the analyzed parameters (% COD removal, surface charge and hydrophobicity) in the different COD:N:P loading, were significantly different at the 95% confidence level. The comparisons of floc structure were made using correlative microscopy.

4.1 Sequencing Batch Reactor (SBR) System Performance

The performance of the SBR system was evaluated based on the COD removal efficiency and stability of the mixed liquor suspended solids (MLSS) concentration. Table 4.2 summarized the average COD % removal and MLSS during the acclimation and experimental phase for all four reactors. The observed COD % removal efficiency and MLSS concentration values observed during the acclimation and experimental phase were not significantly different for the duplicate reactors within the same treatments, nor were they significantly different between the two sets of P-conditions at the 95% confidence limit.

The COD removal efficiencies over time for the two P-conditions are shown in Figure 4.1. The COD removal efficiencies of the SBR system varied during the acclimatization phase, but after the acclimation period (27 days, >3rd SRT), the COD removal

efficiencies were steadily leveled off as the stable system operating conditions were reached. High COD removal efficiency was achieved in approximately 4 hours. In general, nutrient rich conditions did not enhance the system performance significantly. Limited P conditions in R3 and R4 did not appear to have a significant effect on the overall COD removal efficiency.

The MLSS concentrations over time for the two P-conditions are shown in Figure 4.2. Figure 4.2 shows quite variable MLSS concentrations during the acclimatization phase, but after the acclimation period (27 days, >3rd SRT), the MLSS concentrations were relatively constant as the stable system operating conditions were reached.

Table 4. 1 Effect of COD: N: P ratio on COD removal efficiency and MLSS

	Parameter	R1	R2	R3	R4
Acclimation	COD: N: P	100: 5: 1	100: 5: 1	100: 5: 0.1	100: 5: 0.1
	COD removal %	77.53±23.3	80.03±20.0	81.88±18.9	72.03±18.2
	MLSS (g/L)	0.1833±1.22	0.2233±1.53	0.27±0.690	0.1983±0.632
Experimental Phase	COD: N: P	100: 5: 1	100: 5: 1	100: 5: 0.1	100: 5: 0.1
	COD removal %	89.37±5.04	87.11±6.70	81.20±10.9	87.37±4.21
	MLSS (g/L)	0.368±0.292	0.332±0.493	0.416±0.292	0.524±0.583

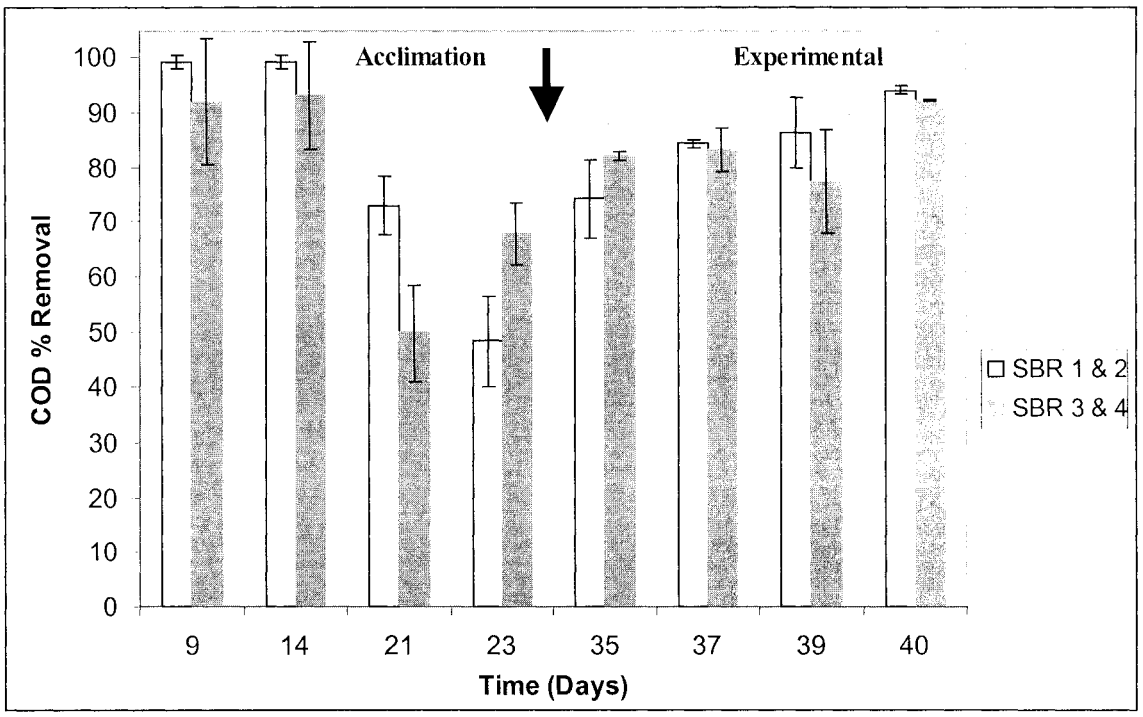

Figure 4.1: COD % Removal in reactors under P-rich conditions (R1 & R2) and in reactors under P-limited conditions (R3 & R4) throughout the acclimation and experimental phase of the study.

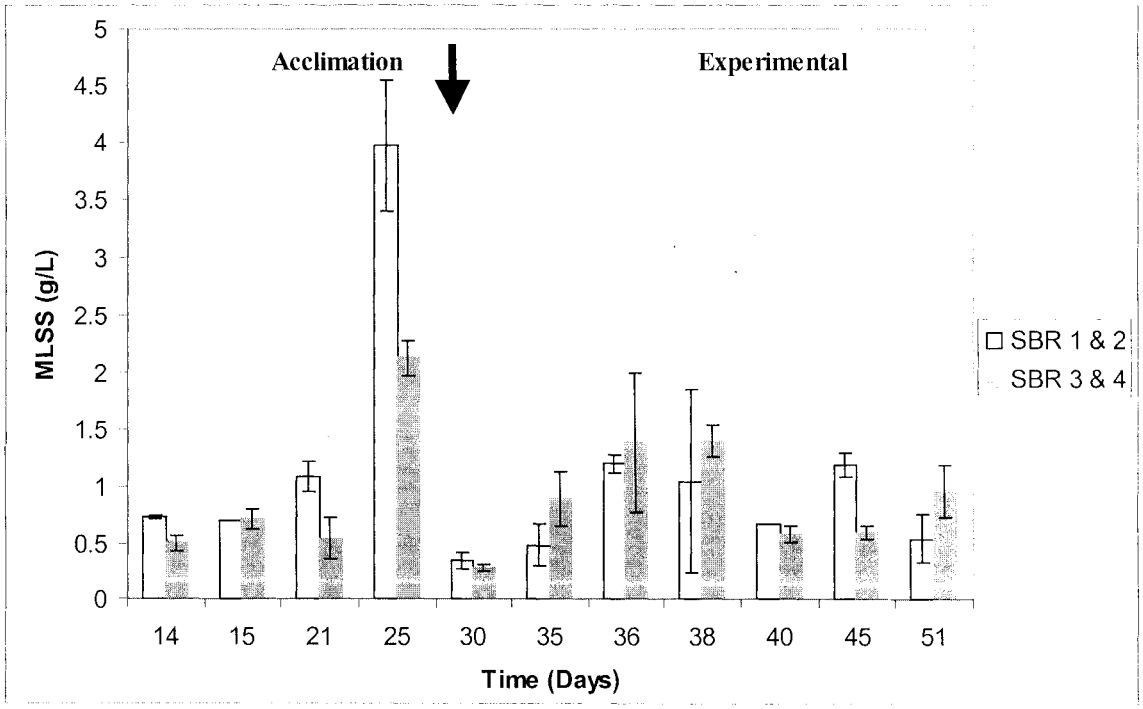

Figure 4.2: Mixed liquor suspended solids concentration in reactors under P-rich conditions (R1 & R2) and in reactors under P-limited conditions (R3 & R4) throughout the acclimation and experimental phase of the study.

4.2 Physicochemical Properties of Floc

Grab samples of the mixed liquor were taken every week and analyzed for surface charge. The hydrophobicity analysis was performed once during the acclimation phase and once during stable system operating conditions. The surface charge analysis was performed twice during acclimation and once during stable system operating conditions. Each analysis was performed in duplicates for each P-condition.

During the acclimation and the experimental phase, the biomass fed a lower than traditional P loading (COD: N; P =100:5:0.1) carried a greater negative surface charge, but the increase was not significant. Also as is shown in Figure 4.3, it is clear that the biomass under both P-conditions underwent a noticeable change with respect to surface charge throughout the duration of the study. An increase in the net negative surface charge was observed as the system was reaching stable system operating conditions. This change may be attributed to the fact that the biomass had not completely been acclimatized to the feed and the bench scale SBR operations. Sludges obtained from full-scale treatment systems typically carry a greater negative surface charge than sludges which have been acclimatized to bench scale SBRs (Liao, 2000).

A similar trend was observed for hydrophobicity, where there was a decrease in relative hydrophobicity as the system was reaching stable operating conditions (Figure 4.4). The surface charge and hydrophobicity values observed during the acclimation and experimental phase were not significantly different for duplicate reactors within the same treatments, nor were they significantly different between the two sets of P-conditions at the 95% confidence limit.

The composition of the extracted EPS during the stable operating conditions is shown in Figure 4.5. Paired two-tailed t-test showed no significant difference between DNA content of the EPS for the two P-loadings. However, there was a significant difference (P=0.028) in the acid polysaccharide content of EPS for the two P-loadings, with acid polysaccharide content being higher for the P-limited conditions. Polysaccharide and protein content was also significantly higher under P-limiting conditions.

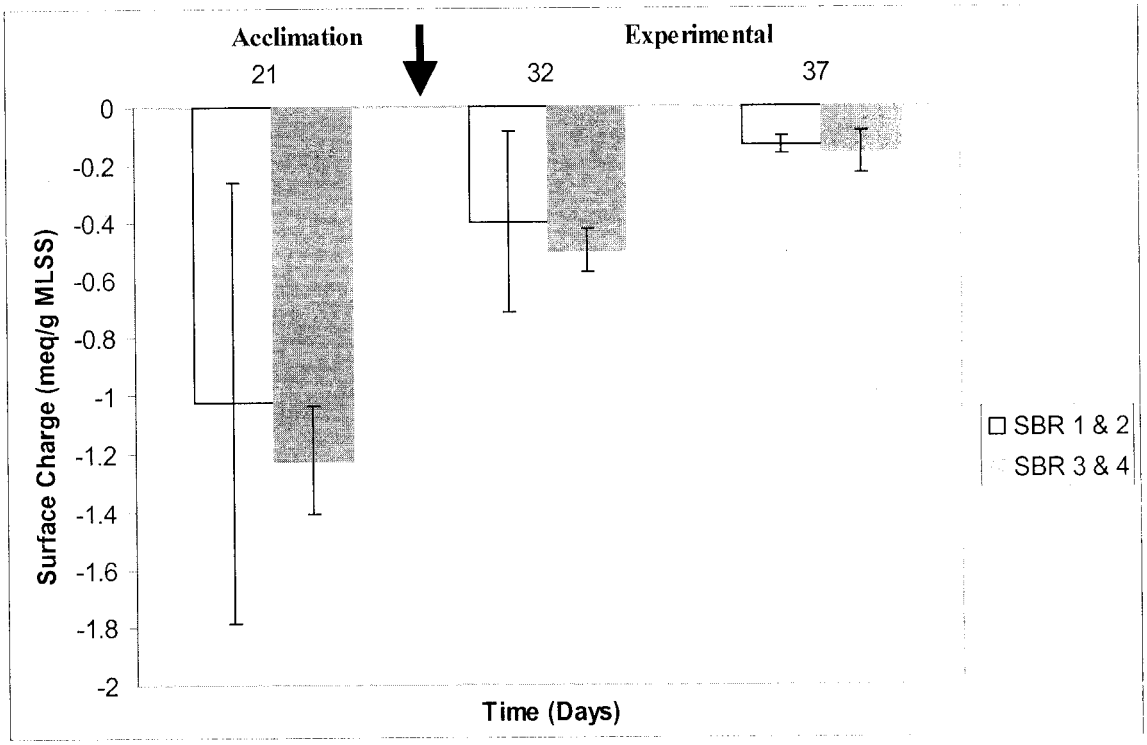

Figure 4.3: Surface charge of the biomass in reactors under P-rich conditions (R1 & R2) and in reactors under P-limited conditions (R3 & R4) throughout the acclimation and experimental phase of the study.

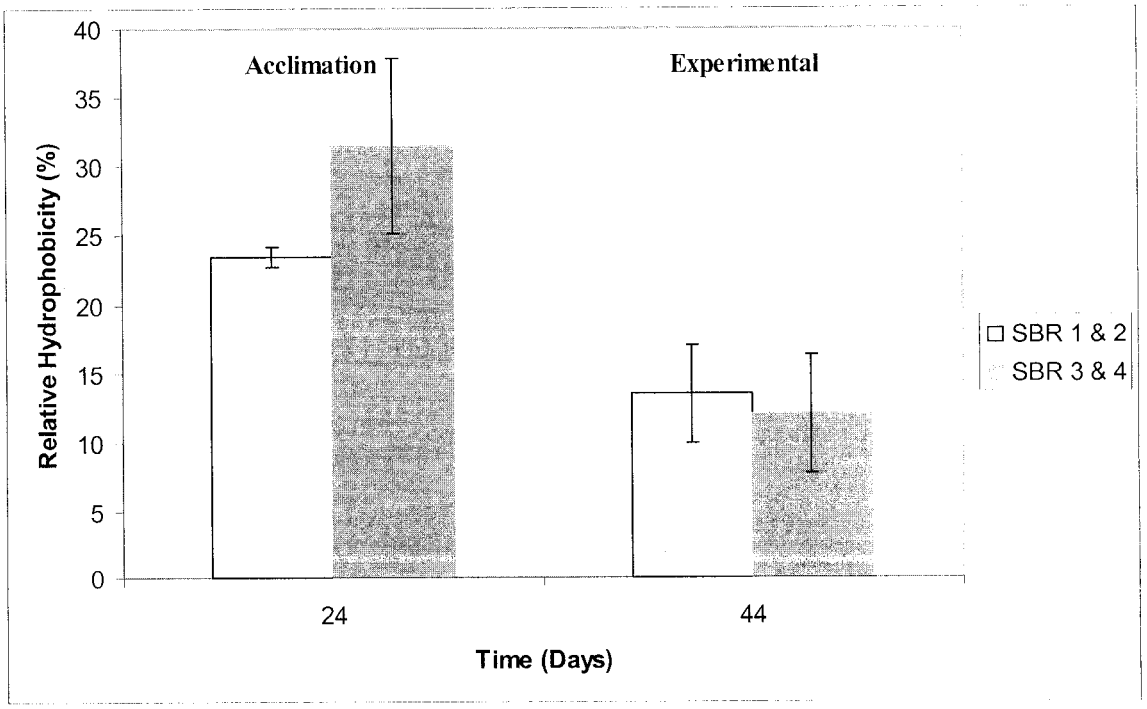

Figure 4.4: Relative hydrophobicity of the biomass in reactors under P-rich conditions (R1 & R2) and in reactors under P-limited conditions (R3 & R4) throughout the acclimation and experimental phase of the study.

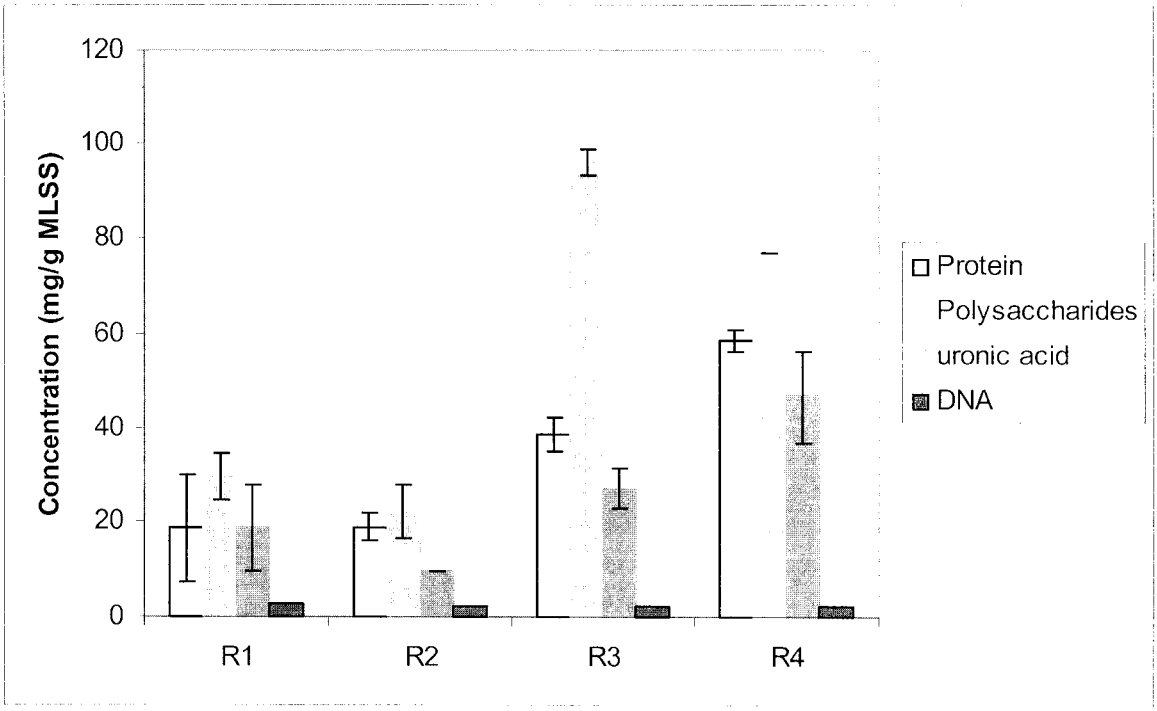

Figure 4.5: EPS composition in all four reactors during stable system operating conditions.

4.3 Microscopic Analysis

4.3.1 Phase Contrast Microscopy

Representative flocs captured in phase contrast for reactors under P-rich and P-limited are shown in Figure 4.6 and Figure 4.7 respectively. A total of 20 images were taken for each condition and they are included in Appendix F. For both P-rich and P-limited conditions, the flocs are irregular in shape and compact (not porous) and contain a diversity of microbes including filamentous bacteria. The flocs under P-rich conditions show internal filament backbone and few filaments growing outwards from the floc. The flocs under P-limited conditions exhibit mostly filament growth outward from the floc.

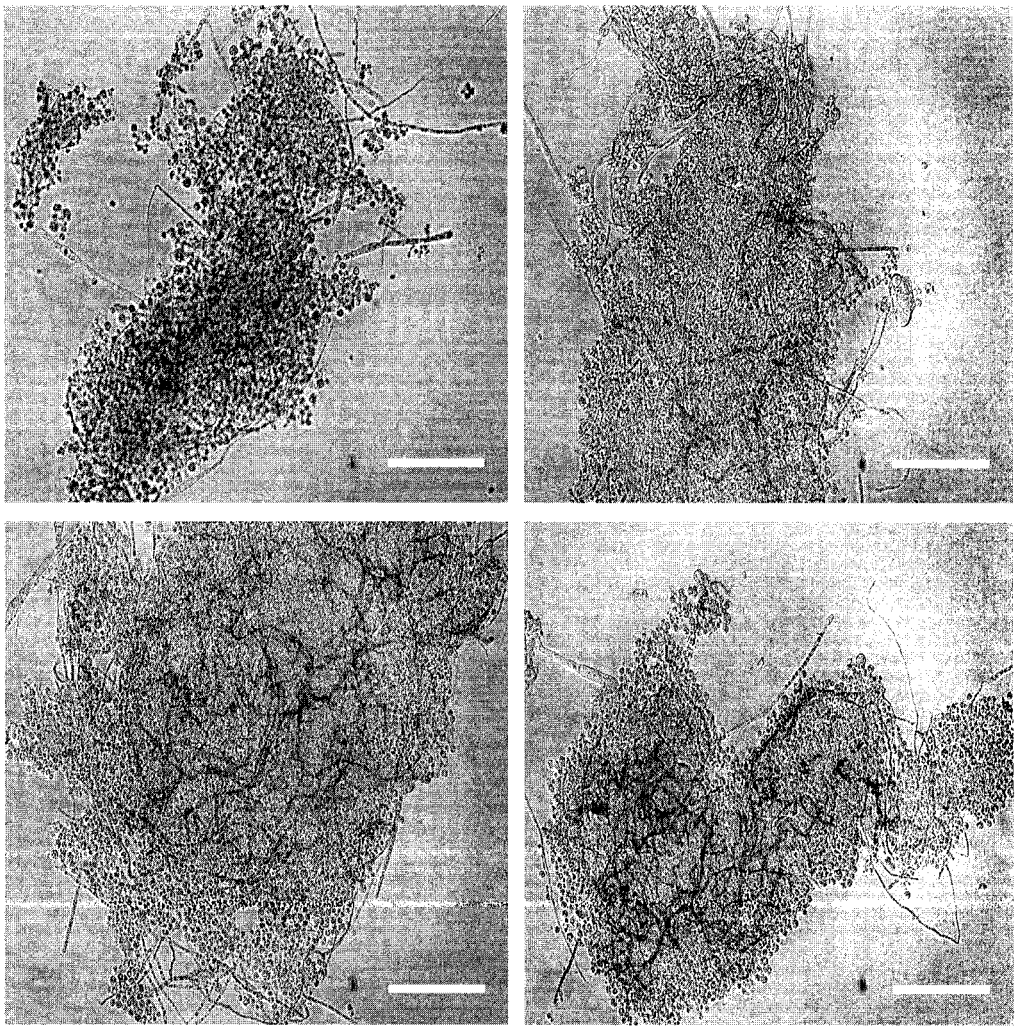

Figure 4.6: Phase contrast micrographs of typical flocs from P-rich condition (reactor 1) during experimental phase (μm scale bar = 100).

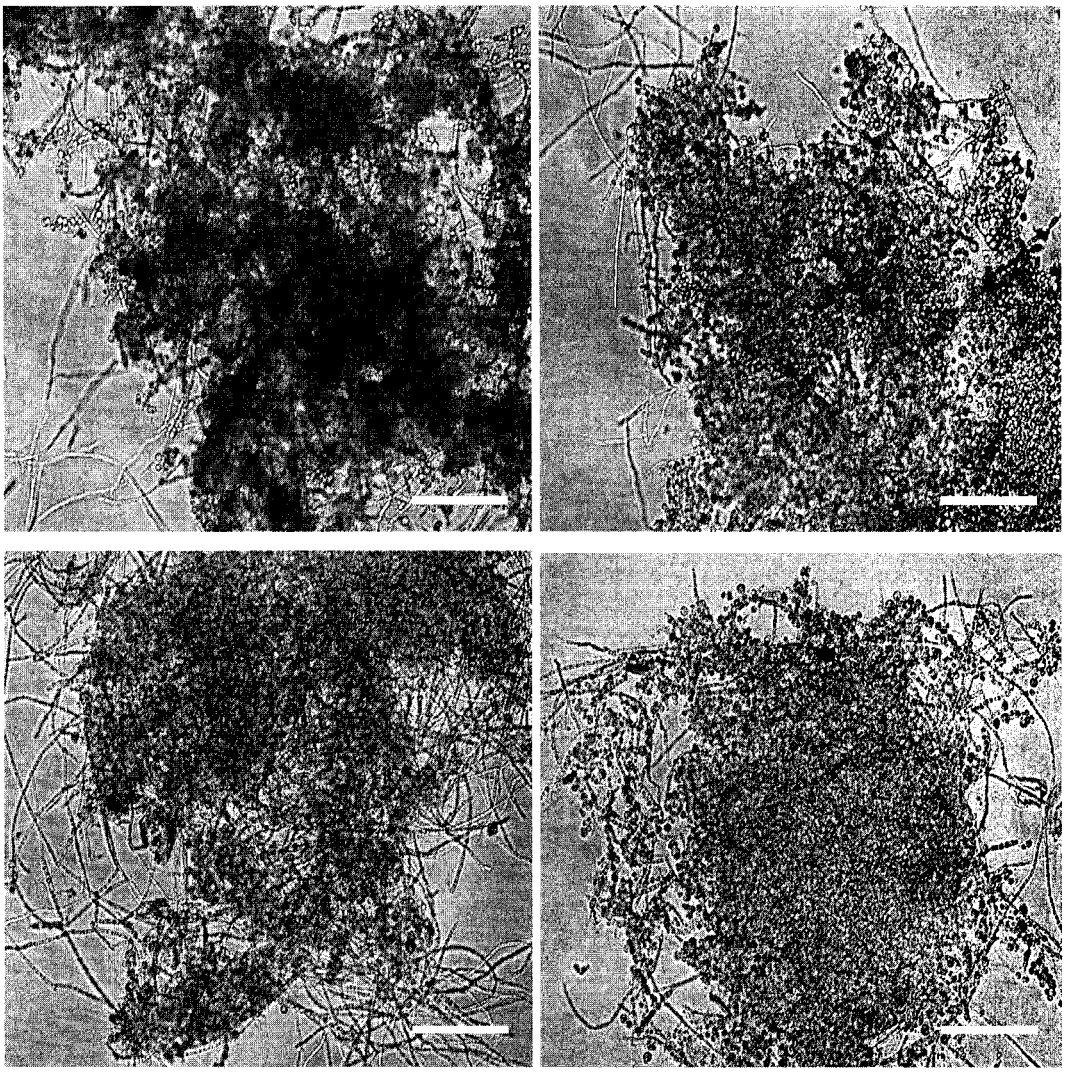

Figure 4.7: Phase contrast micrographs of typical flocs from P-limited condition (reactor 4) during experimental phase (scale bar = 100 μm).

4.3.2 Confocal Laser Scanning Microscopy

In an effort to visualize the biological flocs in the SBRs, images were captured using CLSM in fluorescence and reflectance mode. The microbial flocs were embedded in agarose and stained with lectin-conjugates as outlined in Appendix G. Proceeding staining, the samples were embedded in agarose to maintain the moisture and structural integrity of the flocs. The polysaccharide chains of the agarose in which the floc was stabilized did not fluoresce. The agarose did not generate any erroneous results caused by background florescence or selective redistribution of the stained biological material, and thus was appropriate for this analysis. The lectins employed for CLSM analysis were chosen based on previous studies, as well as for their carbohydrate specificity. The three lectins used were *Canavalia ensiformis* (Concanavalin A, Con A) specific for α-mannopyranosyl and α-glucopyranosyl residues, *Triticum vulgaris* (wheat germ agglutinin, WGA) specific for *N*-acetylglucosaminyl residues, and *Glycine max* (soybean agglutinin, SBA) specific for α and β-*N*-acetylgalactosaminyl and galactopyranosyl residues. All three lectins were detected in all observations, with Con A being always detected in the highest abundance.

The z-stacks were captured using Zeiss 63x/0.9 NA water immersion Apochromat objective, a scan speed of 8.96 μs/pixel, and line averaging of 2. The two-dimensional images were captured the same way as the z-stacks, except that the scan speed of 71.68 μs/pixel was used. The stacked images of flocs were taken at 1μm distance intervals between the optical sections. Distances of <1μm were not analyzed since they are not practicable in fluorescent mode due to bleaching effects caused by the extended excitation time. Photo-bleaching of lectins was not observed in this study. Each image in reflectance mode was obtained in the exact location as the corresponding image in fluorescent mode. The excitation source for the fluorescence mode was an Ar ion laser (488 nm) and two HeNe lasers (543 nm and 633 nm). In the fluorescent images, blue represents Con A-AF633 (Channel 1, Ch1), green represent SBA-AF488 (Channel 2, Ch2) and red represents WGA-tmr (Channel 3, Ch3). The pinhole size for Ch1, Ch2 and Ch3 was 190μm, 147μm and 168μm respectively. The excitation source for the reflectance mode was an Ar ion laser (488 nm) and one HeNe laser (633nm). The pinhole size was 147μm.

Individual bacteria and an EPS matrix can be differentiated and their spatial distribution within the floc can be derived through three-dimensional reconstruction of

multiple optical slices from the collected z-stack. Images described as projections show the total floc volume, as derived from a computerized stacking of optical sections obtained at 1 μm intervals. The total depth of each floc shown is noted for both the fluorescent and reflective mode.

4.3.2.1 Acclimation phase

Figure 4.8 and 4.9 demonstrates that the floc structure during the acclimation phase was different at the two P-conditions. Figure 4.8 illustrates the flocs (day 16) when the COD% removal was especially low for the P-rich condition (42% for R1 and 53% for R2) and less then 75% for the P-limited conditions (71.90% for R3 and 63% for R4). Figure 4.9 shows flocs (day 23) when the COD% removal improved for all four reactors (79% for R1 and 69% for R2; 82% for R3 and 83% for R4). As the COD % removal improved, an increase in density and size of microbial aggregates in P-limited conditions (R3 and R4) and decrease in size of microbial aggregates in P-rich conditions (R1 and R2) was observed.

Flocs grown under P-rich conditions are generally much smaller than flocs grown under P-limited conditions. The flocs are characterized by localized dense growth of biomass within a complex filamentous network. There is a significant amount of void space between the individual biomass clumps. Presence of the filaments is both internal and external. The internal filaments form a backbone for the cell growth. The filaments present at the outer part of the floc extend beyond floc boundaries into the bulk solution. The floc grown under P-limited conditions is larger and very dense. The open channels between the biomass clamps are not as apparent. Presence of the filaments was observed both internally and externally.

In general, bacterial cells enmeshed in the rich EPS matrix were observed in the P-limited and P-rich conditions. All three lectins (Con A, WGA and SBA) were always detected, suggesting that extracellular polymers contain glucose, mannose, *N*-acetylglucosamine, and galactose. The spatial distribution of sugars was very heterogeneous throughout the floc. No localized or discrete regions of conjugates were observed. Con A was generally most predominantly detected, and it stained cells and cell surrounding EPS without discrimination. The SBA and WGA stains were more associated with cells and filamentous organisms.

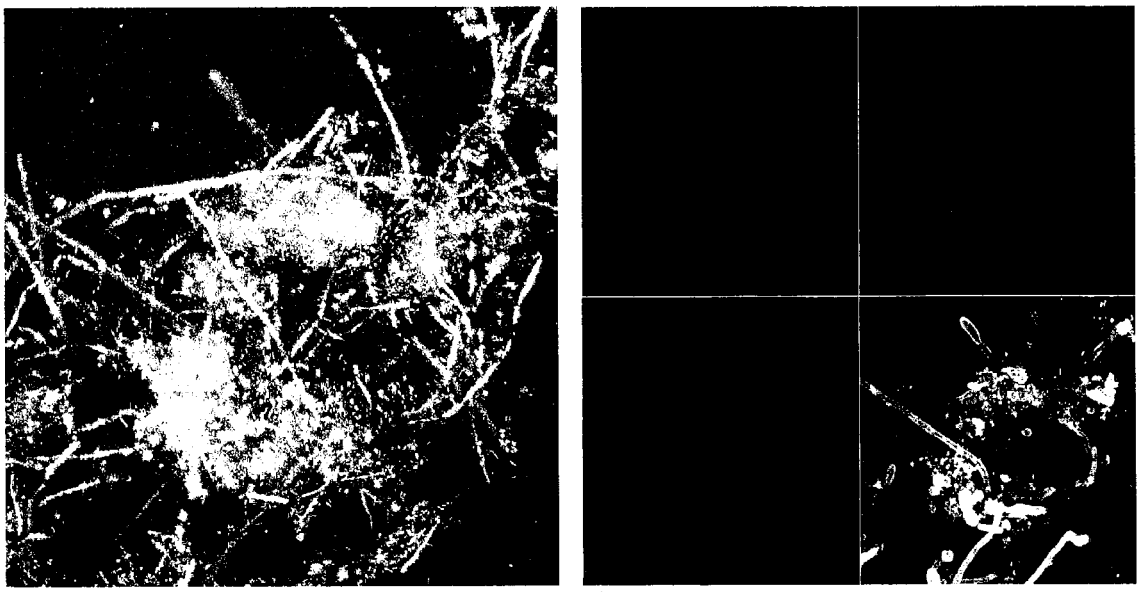

(a) (b)

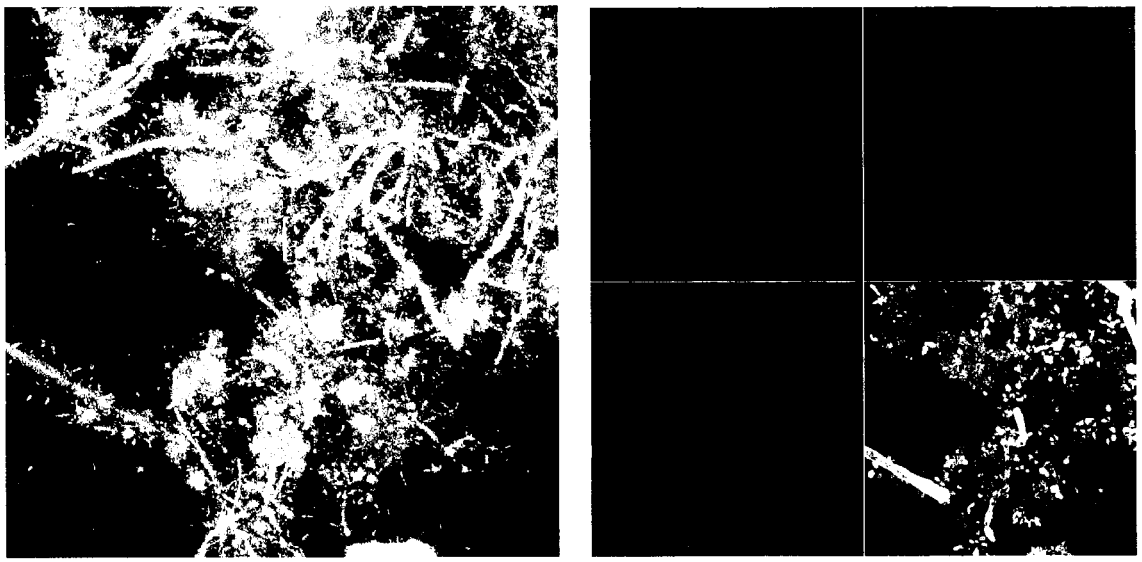

(c) (d)

Figure 4.8: CLSM projections during acclimation (day 16). In the fluorescent images, blue represents ConA-AF633, green represent SBA-AF488, and red represents WGA-tmr (63x/0.9 W objective, scale bar = 20 μm). Micrographs (a) and (b) show floc from reactor 1: (a) in reflectance (projection depth of 143 μm) and (b) fluorescence mode (projection depth 120 μm). Micrographs (c) and (d) show floc from reactor 4: (c) in reflectance (projection depth of 48μm) and (d) fluorescence mode (projection depth 48 μm).

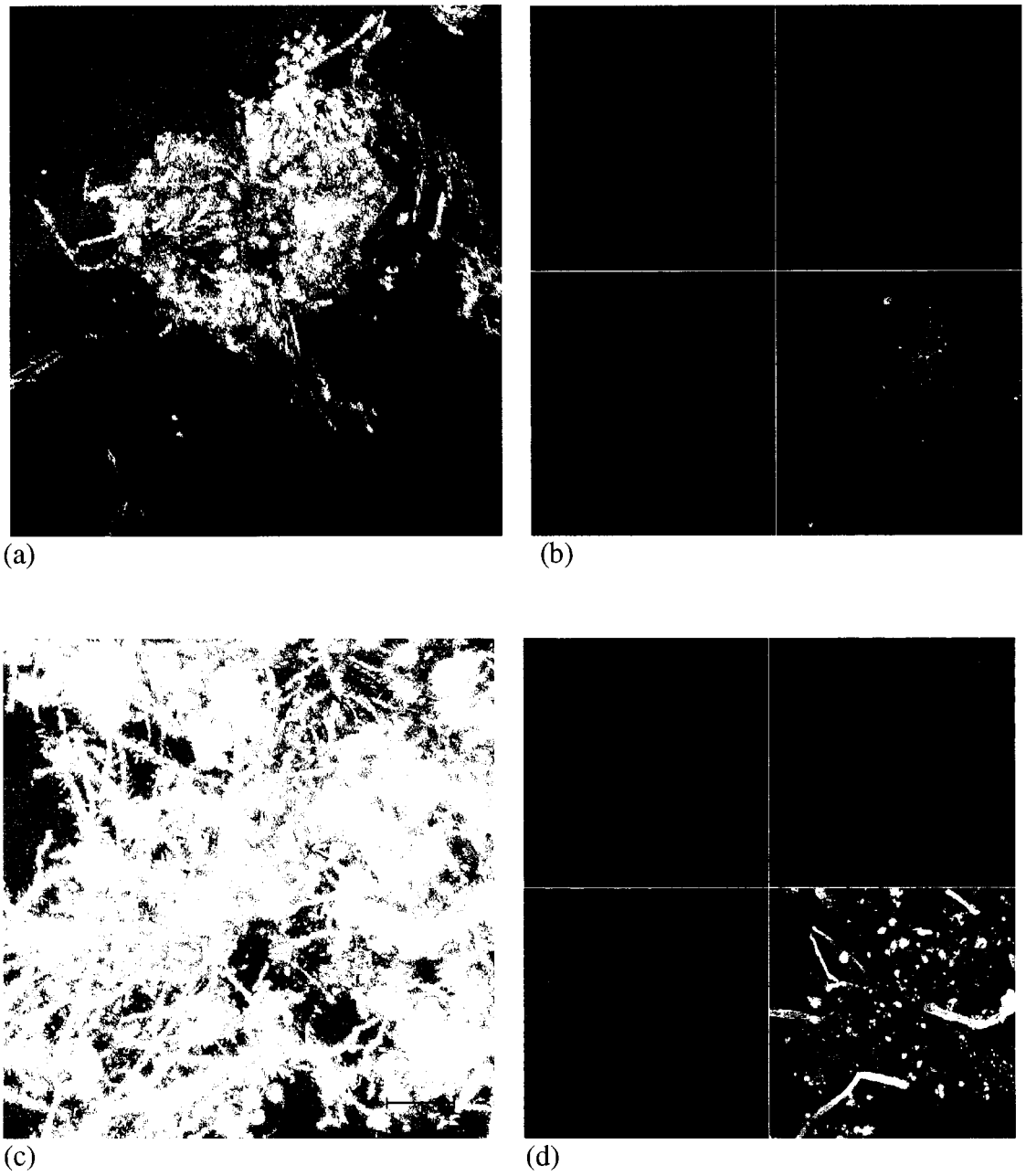

Figure 4.9: CLSM projections during acclimation (day 23). In the fluorescent images, blue represents ConA-AF633, green represent SBA-AF488, and red represents WGA-tmr (63x/0.9 W objective, scale bar = 20 μm). Micrographs (a) and (b) show floc from reactor 2: (a) in reflectance (projection depth of 111 μm) and (b) fluorescence mode (projection depth 83 μm). Micrographs (c) and (d) show floc from reactor 3: (c) in reflectance (projection depth of 114μm) and (d) fluorescence mode (projection depth 111 μm).

4.3.2.2 Stable System Operating Conditions

During stable system operating conditions three zstacks in fluorescence mode and three zstacks in corresponding reflectance mode were acquired for each reactor. Additionally 20 two-dimensional images for each reactor were captured in fluorescent mode to determine the specific carbohydrates distribution. The two-dimensional images were captured the same way as the z-stacks, except that the scan speed of 71.68 μs/pixel was used.

Figure 4.10 and Figure 4.11 illustrate typical two-dimensional images of flocs under P-rich and P-limited conditions during stable system operational conditions. The reproducibility of the observed trend was consistent for each reactor (Appendix G includes the entire gallery of images captured for each reactor). All three conjugates were equally well represented under the P-rich condition. Whereas conjugates stained by WGA and SBA were less abundant than ones stained by Con A for the P-limited conditions.

Figure 4.12 and 4.13 shows the microbial flocs projections under P-rich and P-limited conditions, respectively. In general, bacterial cells enmeshed in the rich EPS matrix were observed under the P-limited and P-rich conditions. The spatial distribution and concentrations of polysaccharides stained by Con A seems to be unaffected by the nutrient limited condition and appear similar to that of the nutrient balanced controls (R1 and R2). However, the spatial concentration of polysaccharides stained specifically by SBA and WGA (specific for α and β-*N*-acetylgalactosaminyl/galactopyranosyl and *N*-acetylglucosaminyl residues respectively) appear to be less abundant in the P-limited conditions (R3 and R4), when compared to that of the nutrient balanced controls (R1 and R2). This may suggest that nutrient limited conditions can cause the changes in EPS distribution within floc structure, which in turn appears to cause compositional changes of the floc.

The depth profile of lectin binding (Figure 4.14) demonstrates a high degree of horizontal and vertical heterogeneity in the distribution of glycoconjugates in the floc. Such heterogeneity was observed in all four reactors. No localized regions of glycoconjugates were found. In contrast, a significant overlap in lectin binding throughout the floc was observed.

The images taken in fluorescence/reflectance mode indicate that the flocs from all four reactors are very dense. The filamentous organisms are present mostly within the floc under P-rich conditions. Flocs from P-limited conditions show excessive filament networks

within the floc and on the outer parts of the floc and dispersed microbial growth. These observations will be further examined by applying image analysis, to the images in reflectance mode, to calculate porosity, fractal dimension and diffusional distances (see Section 4.3).

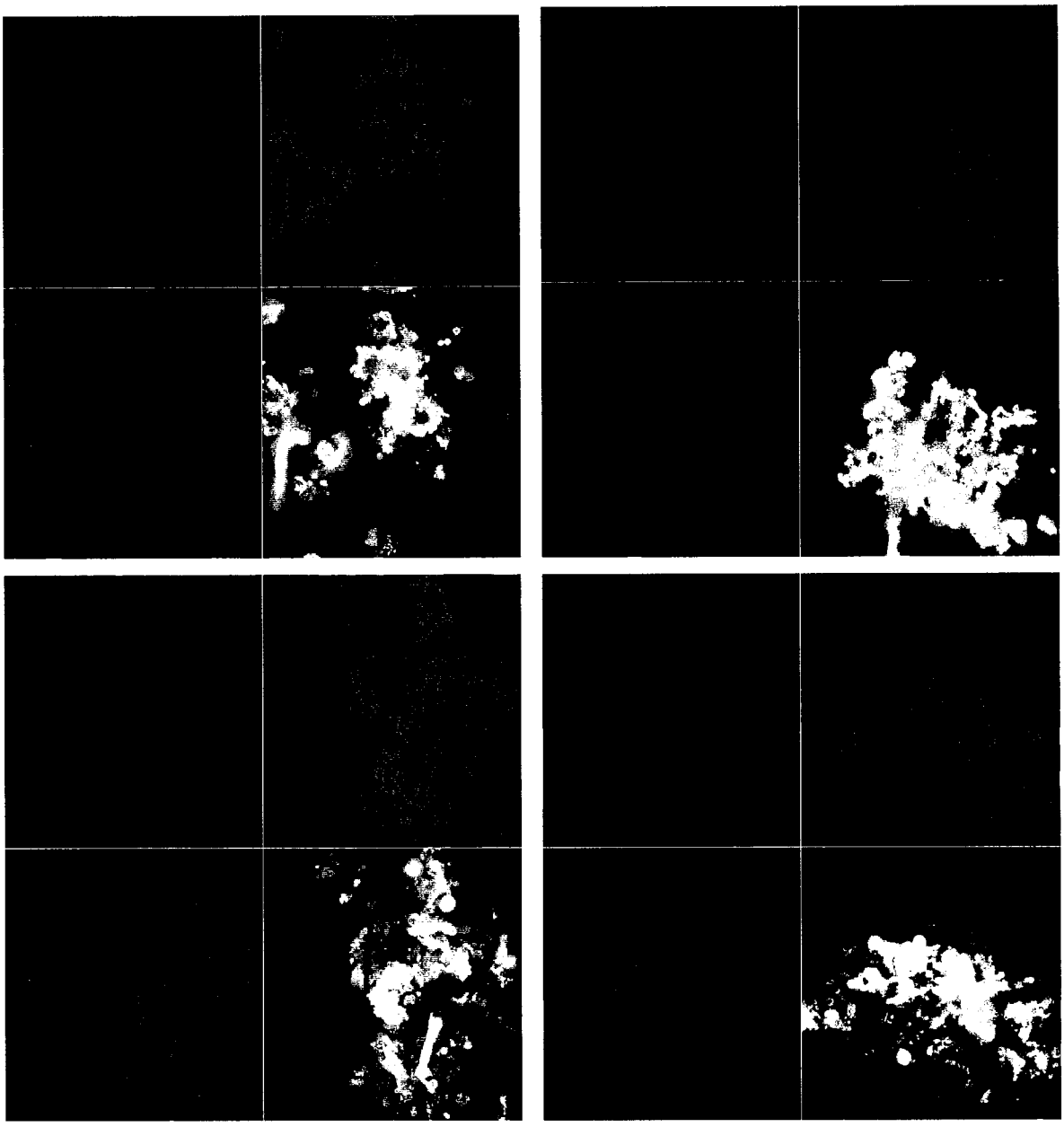

Figure 4.10: CLSM two-dimensional micrographs (146.2μm x146.2μm) showing the composition of microbial flocs under P-rich conditions (Reactor 1) during stable system operating conditions. In the fluorescent images, blue represents ConA-AF633, green represent SBA-AF488, and red represents WGA-tmr (63x/0.9 W objective, scale bar = 20 μm).

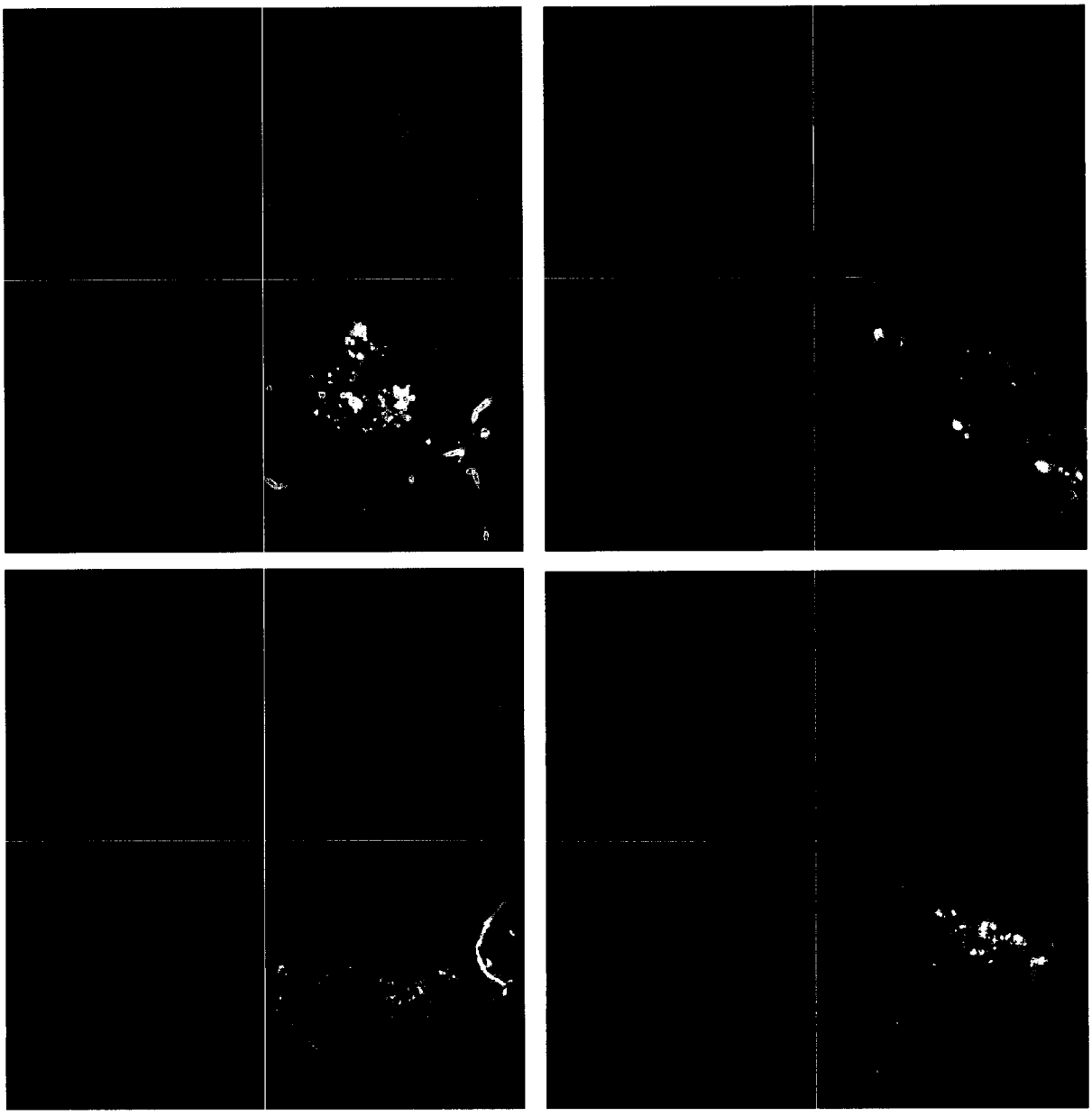

Figure 4.11: CLSM two-dimensional micrographs (146.2μm x146.2μm) showing the composition of microbial flocs under P-limited conditions (Reactor 4) during stable system operating conditions. In the fluorescent images, blue represents ConA-AF633, green represent SBA-AF488, and red represents WGA-tmr (63x/0.9 W objective, scale bar = 20 μm).

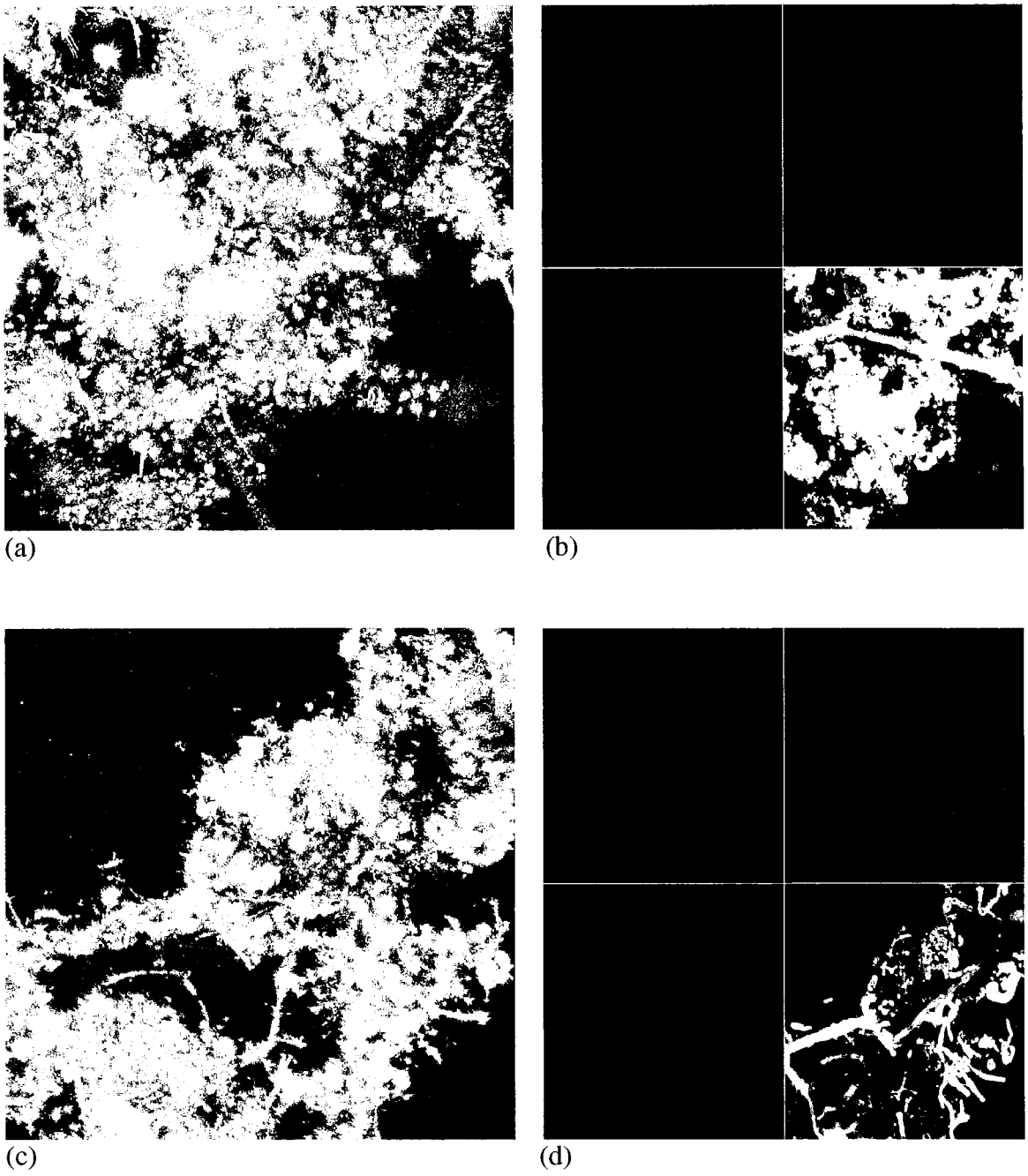

Figure 4.12: CLSM projections during stable system operating conditions (day 40). In the fluorescent images, blue represents ConA-AF633, green represent SBA-AF488, and red represents WGA-tmr (63x/0.9 W objective, scale bar = 20 μm). Micrographs (a) and (b) show floc from reactor 1: (a) in reflectance (projection depth is 66 μm) and (b) fluorescence mode (projection depth is 70μm); Micrographs (c) and (d) show floc from reactor 2: (c) in reflectance (projection depth is 77 μm) and (d) fluorescence mode (projection depth is 81 μm).

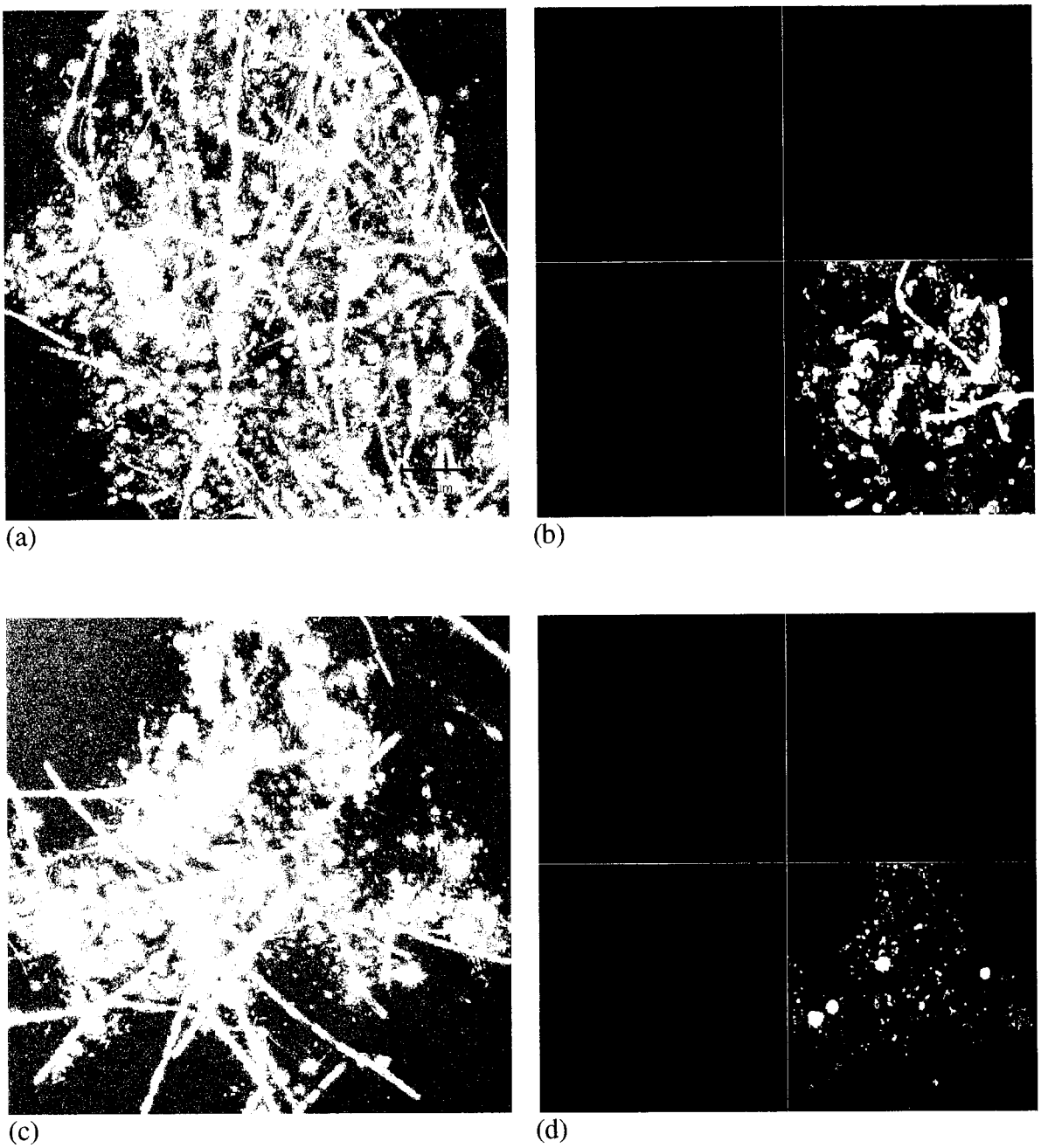

Figure 4.13: CLSM projections under stable system operating conditions (day 40). In the fluorescent images, blue represents ConA-AF633, green represent SBA-AF488, and red represents WGA-tmr (63x/0.9 W objective, scale bar = 20 μm). Micrographs (a) and (b) show floc from reactor 3: (a) in reflectance (projection depth is 98μm) and (b) fluorescence mode (projection depth is 98μm). Micrographs (c) and (d) show floc from reactor 4: (c) in reflectance (projection depth is 93μm) and (c) fluorescence mode (projection depth is 93μm).

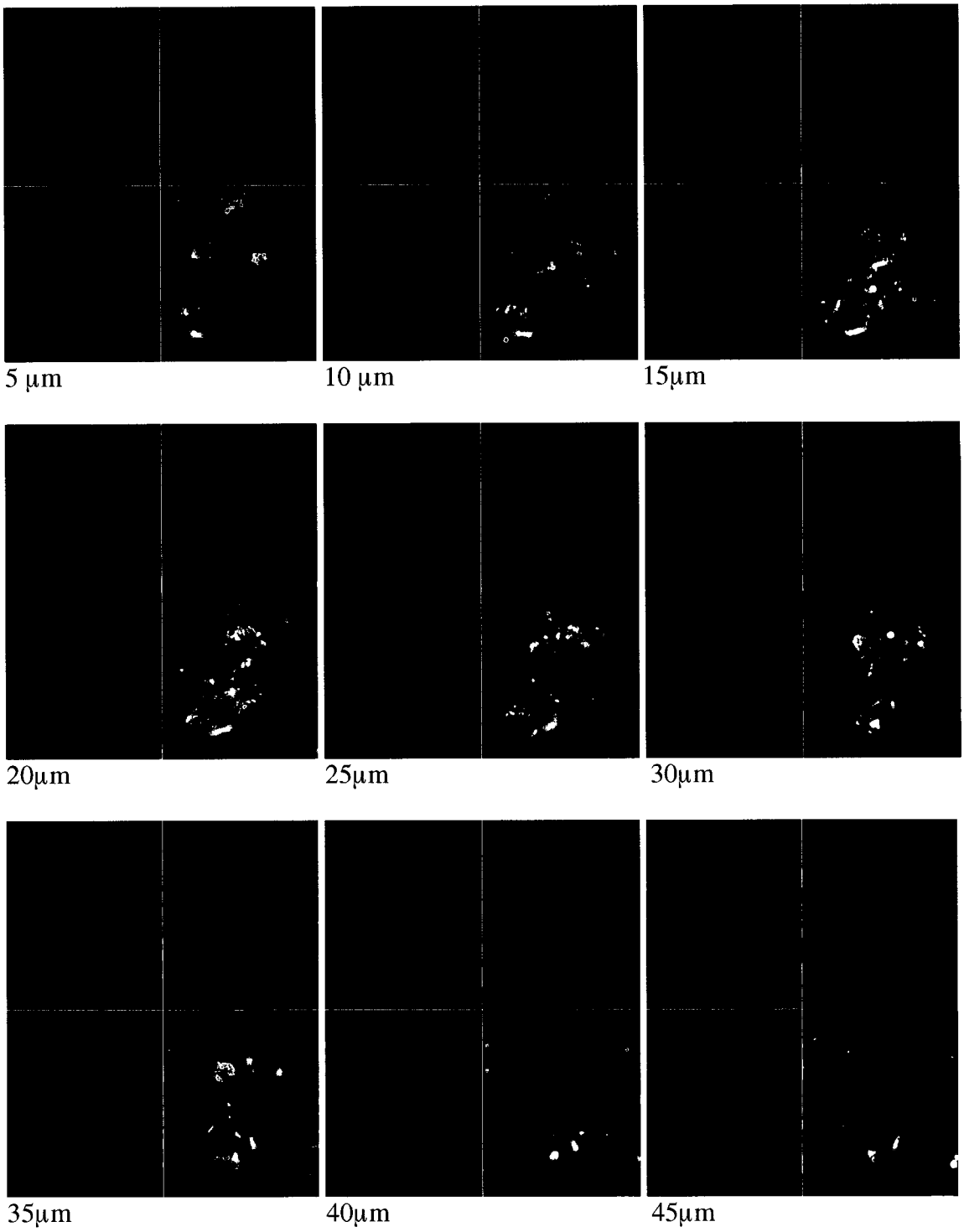

Figure 4.14: Depth profile of lectin binding demonstrating a high degree of horizontal and vertical heterogeneity in the distribution of glycoconjugates in the floc from R3.

4.4 Image Analysis

Analysis of the digital images was conducted using a program called Image Structure Analyzer 3 (ISA3D), a software package developed by the Biofilm Structure-Function research group, Center for Biofilm Engineering, Montana State University. The program calculates many different structure parameters from a two-dimensional image. Each parameter measures a unique characteristic of either the cell cluster or interstitial space within the floc. These parameters are concerned with the size and shape of surface features of the constituent parts and include fractal dimension, porosity, and diffusional distances.

The digital analysis was performed only on the images captured in reflectance mode under 630 x magnification during stable system operating conditions. After CLSM z-stack acquisition, individual sections were removed from each stack image. The two-dimensional image size was 146.2 μm x 146.2μm. Within each image, a square in relative center of the floc was cropped for the image analysis. The size of the cropped square was 20.56μm x 20.56μm (or 422.69μm^2). The ISA3d software thresholded the images using the interative selection algorithm before converting the image into a binary image (Figure 4.15).

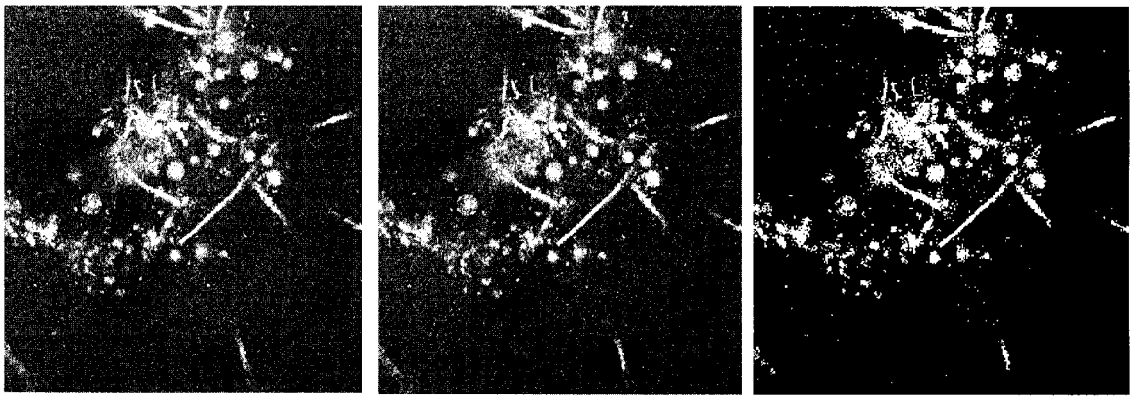

(a) (b) (c)

Figure 4.15: ISA3d image conversion: a) gray scale image b) thresholded image c) binary image

The data for this section was represented in two ways. First the calculated parameters from the 25 slices series across the floc were arranged into depth profiles shown in Figure 4.16. The x-axis represents the distance across the floc, where 1.0 μm represents the top slice of the z-stack. Each graph shows 10 separate lines, where each line represents a cross-

section of the floc in a given location (25 slices, top to bottom). Five non-overlapping locations within the CLSM zstacks were chosen to represent each reactor (10 locations to represent P-rich condition, and additional 10 to represent P-limited condition). Each location was 25 μm deep (25 slices). Additionally to the depth profiles, the structure parameters can be reported as average values and standard deviation. 125 measurements were performed for flocs from each reactor (Appendix H). Average values are listed in Table 4.3.

Table 4. 2 Average values for the image analysis parameters

Parameter	Reactor 1	Reactor 2	Reactor 3	Reactor 4
	COD:N:P =100/5/1		COD:N:P = 100/5/0.1	
Porosity	0.804034 ± 0.0516911	0.802522 ± 0.037043438	0.861784 ± 0.025428744	0.729927 ±0.043156111
Fractal Dimension	1.551325 ± 0.093705	1.59268 ± 0.030856	1.378322 ± 0.076687	1.620537 ± 0.070535
Average diffusion distance	1.097796 ± 0.030877	1.221694 ± 0.109648	1.386401 ± 0.297289	1.331189 ± 0.208305

Porosity and fractal dimension profiles for the P-limited conditions show inherent variability of each measure, indicating more irregular structure/surface across the floc as compared to the P-rich conditions. Porosity and fractal dimension profiles for the floc from the P-rich conditions show low variability of measures across the floc, indicating that cluster porosity remained constant across the floc. Average porosity for flocs from R1 and R2 was 0.80 (no statistical difference within duplicate). The statistical analysis of the porosity values for the duplicate reactors under P-limited conditions indicates that the R3 and R4 are significantly different. Average porosity across the floc for R3 was 0.86 and was significantly different from the P-rich conditions. The average porosity across the floc for R4 was 0.73 and was also significantly lower from the P-rich conditions.

The fractal dimension for R1 and R2 was 1.57 (no significant difference within duplicate). Statistical analysis on the duplicate reactors under P-limited conditions indicates that the R3 and R4 are significantly different. Average fractal dimension for floc from R3

was 1.38 and was significantly different and lower as compared to P-rich conditions. The average fractal dimension for the floc from R4 was 1.62 and was not significantly different from the P-rich conditions.

The statistical analysis on the image analysis results, revealed that the average diffusional distance was significantly different and higher for P-limited conditions (ADD of 1.36 μm) when compared to P-rich conditions (ADD of 1.16 μm).

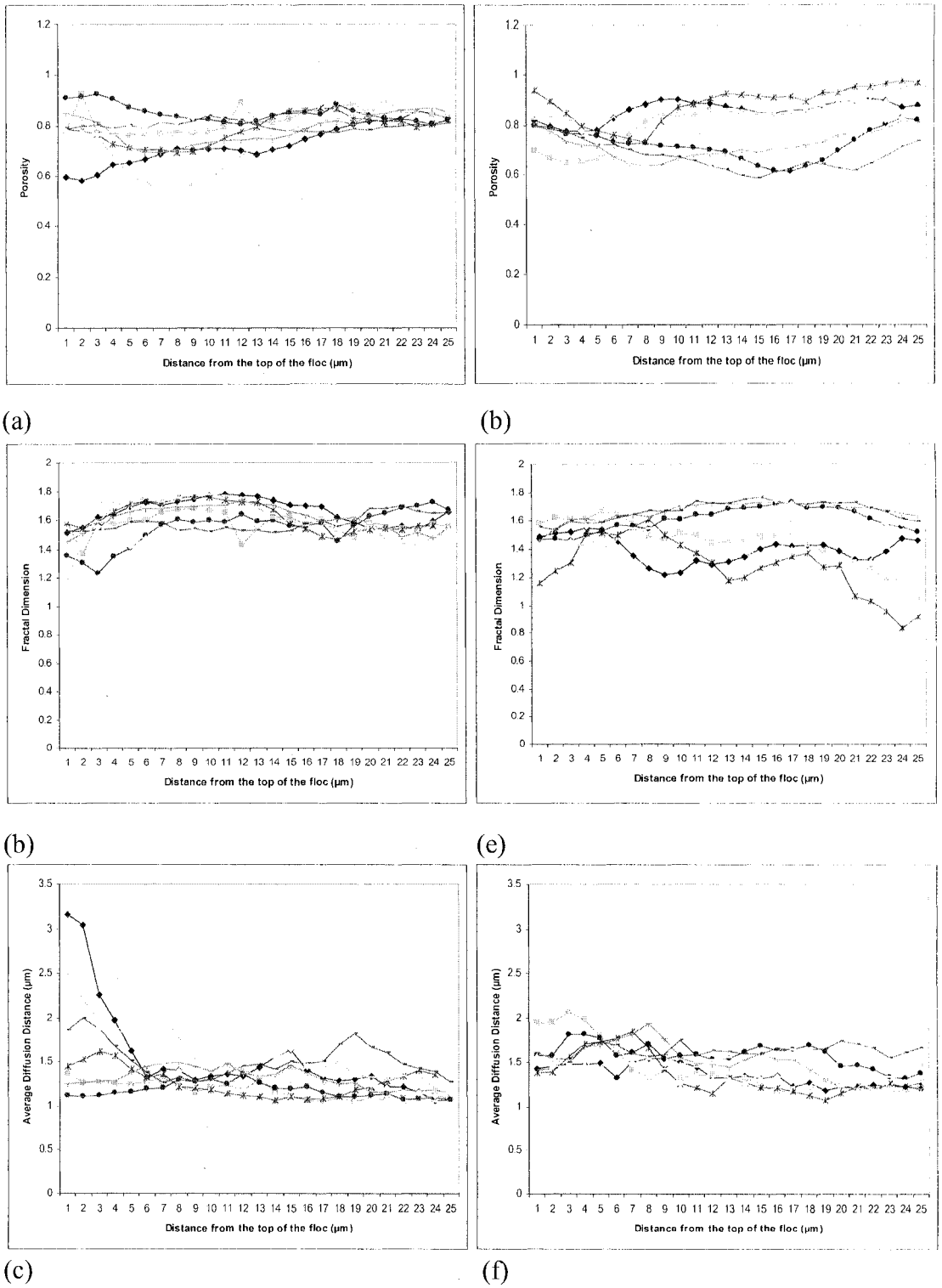

Figure 4.16: Depth profile under P-rich conditions (COD: N: P = 100/5/1): (a) areal porosity, (b) fractal dimension, (c) average diffusion distance.

Depth profile under P-limited conditions (COD: N: P = 100/5/0.1): (d) areal porosity, (e) fractal dimension, (f) average diffusion distance

CHAPTER 5 DISCUSSION

5.1 Sequencing Batch Reactor (SBR) System Performance

A laboratory scale SBR system fed with a synthetic feed was used in this experiment. The SBR system is designed to operate under non-steady state conditions and has been previously shown to be excellent in the removal efficiency of biochemical oxygen demand (BOD), total suspended solids, nitrogen and phosphorus (Norcross, 1992). A SBR system offers several advantages, including a smaller reactor volume requirement than a conventional reactor, its resemblance of a plug flow reactor, minimal feed requirements, and good foaming and bulking control. The use of the synthetic feed as opposed to industrial wastewater allowed easy manipulation of nutrient levels and a well controlled environment in the reactors. The use of industrial wastewater, which fluctuates daily, weekly and seasonally, makes the control of nutrients levels, and concentration of toxin substances entering the reactor nearly impossible. Operational parameters of the SBR system performance were monitored throughout the duration of the experimentation to determine if the COD: N: P ratios applied to the biomass would significantly affect the operational reactor performance. The operational parameters included COD removal efficiency and MLSS. These parameters were chosen because they are typically employed at full-scale treatment facilities, since they are very good indicators of reactor performance. Similar SBR systems fed on glucose based feed have been used in other wastewater research and performed well in chemical oxygen demand removal efficiency (Lee, 1997). The COD removal efficiencies were higher but comparable to the results in this study. The COD removal in Lee's (1997) study averaged 95% for both P-rich (COD:N:P of 100/5/1) and P-limited (COD:N:P of 100/5/0.2) conditions. The COD removal efficiencies in this study averaged 88% for P-rich (COD:N:P of 100/5/1) and 84% for P-limited (COD:N:P of 100/5/0.1) conditions.

Nutrients are important in the activated sludge process. An activated sludge system should be maintained at nutrient adequate conditions in order to produce good COD reduction. The non-limiting conditions were found to have no significant effect (P=0.348) on the SBR system performance, similar to that obtained by Lee (1997). Although excess nutrients were available to the microorganisms in the system, no significant improvement in performance was observed. Similarly, P-limitation did not affect significantly the COD removal efficiency of the system and levels of MLSS concentrations.

It has been previously postulated that P-limitation among other environmental stresses, can cause excessive growth of filamentous organisms. Furthermore the excessive quantities of filaments were correlated with sludge bulking. In this study, filamentous bacterial growth was never excessive even at P-limited conditions. The filaments were commonly observed in all flocs but at low densities. The absence of foaming and bulking might be attributed to the SBR system, since previous researchers have demonstrated that studies using the SBR system are excellent for controlling bulking (Lee, 1997; Norcross, 1992)

The high COD removal efficiencies measured during stable system operating conditions and reproducibility of the measurements, as well as absence of foaming and bulking conditions, suggest that the SBR system was an appropriate tool for studying the biomass produced by simulated wastewater. The SBR system was easy to operate and produced relatively stable operational parameters. Furthermore, this approach permitted the determination of changes in floc physicochemical characteristics and floc structure that might be due to changes in COD: N: P ratio, which was the focus of this study.

5.2 Physicochemical Properties of Floc

A number of mechanisms, such as charge neutralization, hydrophobic interactions, hydrogen bonds, ionic interactions, and EPS enmeshment, have been suggested to be important in controlling the formation of sludge floc and its stability (Liao et al., 2002; Zita and Hermansson, 1994; Zita and Hermansson, 1997a/b; Jorand et al., 1998). The concentration and/or nature of EPS present at sludge surfaces may influence the relative hydrophobicity and surface charge of sludge samples (Jorand et al., 1998; Morgan et al., 1990; Liao et al., 2002; Bura et al., 1998). Jorand et al. (1998) found that the hydrophobic fraction of EPS was made up of proteins. Liao et al. (2000) found that large amount of hydrophilic and mainly neutral carbohydrates may have contributed to the more hydrophilic (less hydrophobic) nature of the sludge.

The relative hydrophobicities were much higher during acclimation for both P-conditions than during stable system operating conditions, indicating the system was not acclimated to the synthetic feed and SBR operation. During stable system operating conditions, the relative hydrophobicity was not significantly different between the two

P-conditions (P=0.657), but lower for the P-limited than for the P-rich condition. Hydrophobicity of sludge flocs appear to be affected by variations in the protein, total carbohydrate, and DNA content in the EPS, and the protein to carbohydrate ratio (Jorand et al., 1998; Liao et al., 2001). Thus, the slightly lower hydrophobicity of biomass from a P-limited condition can be related to variations in the protein and carbohydrate content in the EPS and a reduced protein: carbohydrate ratio.

The net surface charge was more negative for all reactors during the acclimation phase than during the stable system operating conditions. This may be attributed to the fact that the biomass had not completely acclimated to the glucose-based synthetic feed and the SBR operation. Sludges obtained from full-scale treatment systems typically carry a greater negative surface charge than sludges that have been acclimatized to bench scale SBRs (Liao, 2000). During stable system operating conditions, the net surface charge was not significantly different between the two P-conditions (P=0.731), but it showed to be more negative for the P-limited than for the P-rich condition. The increase in surface charge for biomass from P-limited condition can be attributed to significantly higher acid polysaccharide content in the EPS.

The chemical composition of the EPS matrix is reported to be very heterogeneous. Carbohydrate and protein are usually found as the major EPS components having a protein to carbohydrate ratio between 0.2-5 (w/w) (Frølund et al., 1995). In this study the predominant component of EPS were carbohydrates and protein, with a protein to carbohydrate ratio of 0.63 and 0.86 for R1 and R2 respectively, and ratio of 0.40 and 0.76 for R3 and R4 respectively. The protein to carbohydrate ratio measures in this study, lies in the range of 0.2-5 (w/w) found by Frølund et al. (1995), who used a cation exchange resin for EPS extraction. However the carbohydrates were more predominant than protein and recent studies of mixed cultures in wastewater treatment systems found that protein was a predominant constituent in EPS (Lee, 1997; Frølund et al., 1995; Nielsen et al., 1996; Dignac et al., 1998; Liu and Fang, 2002). On the other hand, carbohydrates were considered the main constituent of EPS in pure cultures fed a synthetic substrate (Morgan et al., 1990). Thus, the predominance of proteins in activated sludge EPS could be due to the complexity of the substrate present in wastewater (presence of large quantities of exoenzymes and structural proteins), while the synthetic glucose based feed added to the SBR is much

simpler. Additionally, the variation in EPS composition in this study can be attributed to many other factors. First, it was also shown that the composition and production of EPS varied with species, environmental and operation conditions and type of organics in wastewater (Sponza, 2003; Lee, 1997; Bura et al., 1998). Second, different extraction procedures are used in different studies, which strongly affect the yield of EPS and EPS composition analysis. And finally, different analytical tools are used for analyzing the chemical composition of the extracted EPS, which can cause further variability in results (Frølund et al., 1995).

The compositions of EPS were affected by the nutritional condition in the synthetic feed. The protein content in R3 and R4 was significantly different (P=0.02) within the experimental duplicate. The protein content in both R3 and R4 (compared separately) was significantly higher (P=0.00987 and P=0.0004) than in R1 and R2. Also the total polysaccharide (P=0.0002) and acid polysaccharide (P=0.0285) content was significantly higher for P-limited than for P-rich conditions. There was no significant difference in the DNA content for P-limited and P-rich conditions. Lee (1997) found similar results under the P-limited condition, with significant increases in carbohydrates, uronic acid, DNA and protein concentration. An enhanced EPS production under conditions of depletion of external substrate is expected, since the bacteria have the ability to acclimatize and produce enzymes which can hydrolyze and assimilate the EPS surrounding and bonding their surface (Andreadakis, 1993). Thus the increase in the total carbohydrates and proteins under P-limited conditions could be reflecting the accumulation of extracellular polymeric material.

Although the chemical composition of EPS and the relative abundance of components can be accurately assessed using EPS extraction and EPS composition analysis, the characterization of the spatial arrangements of the EPS components within the microbial floc is not shown. The CLSM and lectin-conjugate mapping analysis was performed to determine glycoconjugate distribution within the floc.

5.3 Microscopic Analysis

CLSM was employed using triple lectin-conjugates which have shown to work effectively in all cases. Subsequent to staining, the floc samples were embedded in agarose to retain their moisture and 3-dimensional arrangements. Previous studies have shown

successful results when imaging microbial cells and EPS stabilized in low melting point agarose (Droppo et al., 1996), thus this method was employed in this study and shown to be successful at maintaining the flocs moisture content as well as its structural integrity. Using this stabilization technique also allowed for long periods of microscopic observation.

Previous studies have successfully utilized various lectin-conjugates to study extracellular polymers produced by bacterial cells (Del Gallo, 1989; Michael and Smith, 1995; Lawrence et al., 1998; Wolfaardt et al., 1998; Decho and Kawaguchi, 1998; Johnsen et al., 2000). The floc under P-rich and P-limited conditions was analyzed using three lectins: *Conavalia ensiformis* (concanavalin A, ConA), *Triticum vulgaris* (wheat germ agglutinin, WGA), *Glycine max* (soybean agglutinin, SBA). The lectins were selected on the basis of other studies and their specificity to common polysaccharides. Glucose, mannose and galactose are present everywhere simultaneously in the environment and are always found as major constituents of bacterial extracellular polymers in sludge biomass (Dignac et al., 1998). The polysaccharides produced by bacteria associate with bacterial cells as intracellular polysaccharides, as capsular or bound polysaccharide (CPS) and as extracellular or soluble polysaccharides (EPS) (Figueroa and Silverstein, 1989; Del Gallo et al., 1989). If the assumption is made that lectins will have a higher binding affinity to the polysaccharides in the CPS and EPS, then there will be a low probability that the lectins will penetrate the bacterial cell wall. Johnsen et al. (2000) demonstrated that fluorescence from WGA and Con A is closely associated with the cells. Although some SBA and WGA binding was intimately associated with the cells under P-limited conditions, most of the lectins bound to EPS are in the environment surrounding the cells.

Lectin binding revealed bacterial cells enmeshed in the rich EPS matrix under both P-limited and P-rich conditions. The EPS was observed in interstitial spaces and between the substrate. The lectin analysis demonstrated a high degree of horizontal and vertical heterogeneity in the distribution of glycoconjugates in the flocs grown under both conditions, which is consistent with previous studies (Neu and Lawrence, 1997; Decho and Kawaguchi, 1999; Wolfaardt et al., 1998). The heterogeneous fluorescence throughout the EPS matrix could suggest that EPS may consist of varying compositions.

Del Gallo et al. (1998) found that each lectin (WGA, SBA and Con A) had localized discrete domains of binding on the marine biofilm surface. Wolfaardt et al. (1998) found that

Con A and SBA had both discrete regions and considerable overlap in lectin binding within the degradative biofilm. No apparent localized or discrete domain of binding for either lectin was found in this study, although WGA and SBA seemed to be associated with cells and the EPS matrix. Generally a considerable overlap in lectin binding within the floc was observed. Strong fluorescence conferred by bound Con A was always observed under both P-conditions, which is in agreement with previous studies. The spatial distribution and relative abundance of polysaccharides stained by Con A seem to be unaffected by the nutrient limited condition and appeared similar to that of the nutrient balanced controls (R1 and R2). However, the relative abundance of polysaccharides stained specifically by SBA and WGA (specific for α and β-*N*-acetylgalactosaminyl/ galactopyranosyl and *N*-acetylglucosaminyl residues respectively) appeared to be less abundant in the P-limited conditions (R3 and R4), when compared to that of the nutrient balanced controls (R1 and R2). This may suggest that nutrient limited conditions can cause the changes in microbial populations within the floc structure, which in turn appears to cause compositional changes of EPS.

5.4 Image Analysis

The image analysis on the images in reflective mode was performed to assess the average diffusional distances, fractal dimension, and porosity. When using image analysis to estimate floc structure parameters from confocal images there are two things to consider. The first is the difficulty in the thresholding of the original image. The images taken by a camera are gray scale images, while the images processed to extract the structural parameters are binary images (Figure 4.15). The thresholding process relies on an arbitrary selection of a gray scale value, in order to segment a gray scale image into a binary image. Thresholding is a subjective operation. The choice of gray-scale intensity selected to segment the images depends on the operator's understanding of the image content and the desired relationships between the two segments in the final image. There are no rules for setting the threshold value manually and yet the numerical value prescribed to areal porosity, fractal dimension and diffusion distances depend on this step. The variability between operators in choosing the threshold adversely affects the measurements obtained from the binary image. Additionally, to extract statistically meaningful morphological parameters from a series of images, the thresholding has to be reproducible. Yang et al. (2000) screened available

algorithms, searching for those that generated reproducible results tending toward the average generated by a panel of experts. Iterative selection performed better than the other algorithms used (Lewandowski et al., 2002) and was, thus, used in this study.

Variance in image magnification (field of view) is the second difficulty. For example, if the field of view is very small, then at the usual power of resolution of an optical microscope, the image will show little structural heterogeneity. If the field of view is expanded, then the image will show greater heterogeneity including cell clusters and interstitial voids. The structural parameter calculations are therefore, affected by the area of the field of view. Therefore, the magnification used in other studies has to be noted before the parameters' values are compared. The magnification used in this study (630 ×) was sufficiently large to show multiple cell clusters, but small enough to show heterogeneities at the one μm scale.

The ISA3D software was used to calculate the areal average diffusion distance, the areal porosity, and the fractal dimension. These structure parameters quantify the morphology of the microbial floc. The diffusion distance for a cell cluster is a measure of the distance from any cell in the cluster to the interstitial space. The average diffusion distance is of interest because it reflects the average distance a nutrient must travel from the cell cluster edge to the microorganisms, at different positions in the cell cluster within the floc. The average diffusion distance takes into consideration the size of the cluster and its general shape (Jackson et al., 2001; Yang et al., 2000). The larger the diffusional distance, the greater the distance a substance must diffuse in order to reach the inner parts of a cluster. It can be considered as the average diameter of the cell clusters (Jackson et al., 2001). Hence, the greater the average diffusion distance, the bigger the cell cluster (Jackson et al., 2001; Yang et al., 2000; Lewandowski et al., 1999). The image analysis revealed that average diffusional distance was significantly different and higher for P-limited conditions. A larger diffusion distance indicates a longer distance that the substrate has to diffuse in the cell cluster. This further suggests that cell clusters were larger under P-limited conditions than under non-limiting conditions. Since the diffusion distance increased for P-limited conditions, chances are that the substrate was exhausted before it reached the middle section of the floc. It could be further suggested that the middle of the floc is occupied by different microorganisms than the outer boundary of the floc. It is then possible that the changes in

EPS distribution within floc structure (decreased abundance of α and β-*N*-acetylgalactosaminyl, galactopyranosyl and *N*-acetylglucosaminyl residues) could be due to cell starvation or change in the microbial population in the middle of the floc. On the other hand, the average diffusional distance being lower under P-rich conditions indicates that the cell clusters were smaller than under P-limited conditions. This could further suggest that the substrate was able to reach the middle of the floc (equal abundance of all tested polysaccharide residues).

Areal porosity is the ratio of interstitial void area to the total area of the image. It gives information about the relative coverage of microorganisms. Lower porosity indicates more coverage. Porosity for the flocs from P-rich conditions remained almost the same, indicating that cluster porosity remained constant across the floc (Figure 4.16 (a)). Average porosity for flocs from R1 and R2 was 0.80 (no statistical difference). Porosity profile for the P-limited conditions shows inherent variability of each measure, indicating more irregular structure across the floc as compared to the P-rich conditions (Figure 4.16 (b)). The statistical analysis of the porosity mean values for the duplicate reactors under P-limited conditions indicates that the R3 and R4 are significantly different. Average porosity across the floc for R3 was 0.86 and was significantly different from the P-rich conditions. The average porosity across the floc for R4 was 0.73 and was also significantly different from the P-rich conditions. This indicates that P-limitation resulted in highly irregular floc structure. The results found for the porosity in this study were lower than those found by other researchers. Andreadakis (1993) found activated sludge flocs to have porosities in the range of 85-97%. Li and Logan (2001) found that for fractal aggregates, porosity increases with size. The increase in the aggregate porosity with size becomes larger as the fractal dimension decreases in magnitude. They found porosity to be 92.1% and 99.99% for smaller aggregates (with fractal dimension of 2.5) and larger aggregates (with fractal dimension of 1.7) respectively. There are other factors that will affect the overall porosity of an aggregate that were not considered in the Li and Logan (2001) study, such as EPS filling in the pores between bacteria and coagulated materials. In the calculation of the porosity of activated sludge flocs, the flocs are frequently considered to be composed of only microorganisms and water. However, EPS may have different densities and a different physical state from those

of microbial cells in the flocs (Li and Ganczarczyk, 1989). Therefore the previously reported estimations of porosity of the flocs would certainly be affected.

Fractal dimension reflects the extent of the "raggedness" of the floc's perimeter. Thus, higher fractal dimension indicates an increase in the surface area exposed to the nutrients, and possibly an increase in the local mass transfer coefficient of the cell clusters (Jackson et al., 2001). Furthermore, higher fractal dimension suggests compact structure and smaller values indicate more open structure (Hermanowicz et al., 1995), and thus the inverted proportionality between fractal dimension and porosity is apparent. Although fractal dimension can be used as a tool for the morphological analysis of biological aggregates, it is not a unique characteristic. Thus two objects that vary vastly may have the same fractal dimension (Hermanowicz et al., 1995). The magnitude of the fractal dimension of flocs in this study was within the range of 1.4-2.0, indicated for microbial aggregates (Namer and Ganczarczyk, 1994). Li and Ganczarczyk (1989) found the fractal dimension to be 1.55-2.0 in settled activated sludge. Zahid and Ganczarczyk (1990) found that sludge from a biological filter had the fractal dimension of 1.79. Namer and Ganczarczyk (1994) observed the fractal dimension to be between 1.63-1.66 for settled digested sludge. Logan and Wilkinson (1991) found the fractal dimension to be in the range of 1.8-3.0 for *Zooglea ramigera* grown in the laboratories. The fractal dimension results found in this study indicate that the flocs from laboratory scale SBR are a highly porous structure in comparison to digested sledge (Namer and Ganczarczyk, 1994), or microbial aggregates grown in laboratories (Logan and Wilkinson ,1991), but also as compact as activated sludge (Li and Ganczarczyk, 1989).

The fractal dimension profile remained almost the same for the P-rich conditions indicating that cluster surfaces remained constant and were not as irregular across the floc as for P-limited conditions (Figure 4.16 (c) and (d)). The fractal dimension for R1 and R2 was 1.57 (no significant difference within duplicate). The fractal dimension profile for P-limited conditions shows inherent variability of each measure, indicating highly irregular surfaces across the floc. Statistical analysis on the duplicate reactors under P-limited conditions indicates that the R3 and R4 are significantly different. The average fractal dimension for the floc from R3 was 1.38, and was significantly different and lower as compared to P-rich conditions. The average fractal dimension for the floc from R4 was 1.62 and was not

significantly different from the P-rich conditions. Lower fractal dimension and higher porosity for the flocs from R3 indicate less irregular boundary and more open structure of the floc. The lower irregularity of the cluster boundary decreases the surface area of the cluster, thus allowing less interaction with surrounding bulk fluid.

CHAPTER 6: CONCLUSIONS AND RECOMENDATIONS

The purpose of this study was to achieve a better understanding of floc structure and properties under two different P-levels. On the basis of the results obtained, a more complete knowledge of microbial floc structure has been gained. Specific conclusions that can be drawn from the results presented are listed below:

1. Decreasing the amount of P in the simulated wastewater was found to have no significant impact on the treatment efficiency (COD). However the EPS composition and floc structure were affected by the P-limitation.
2. The composition of EPS was affected by the P-limitation with significant increase of carbohydrate, uronic acid, and protein concentrations.
3. The CLSM analysis revealed that bacterial cells under both P-conditions are enmeshed in a complex EPS matrix that is known to contain glucose, mannose, *N*-acetylglucosamine, and galactose. The heterogeneous fluorescence throughout the EPS matrix could suggest that EPS may consist of varying compositions.
4. The CLSM analysis showed that EPS under both P-conditions was composed predominantly of α –mannopyranosyl and α-glucopyranosyl residues (stained by Con A).
5. P-limitation affected relative abundance of *N*-acetylglucosaminyl residues (stained by WGA) and α and β-*N*-acetylgalactosaminyl and galactopyranosyl residues (stained by SBA), suggesting changes in microbial populations within a floc structure, which in turn appear to cause compositional changes of EPS.
6. P-limitation affected calculated porosity, fractal dimension, and the average diffusion distance. The cell clumps within the floc were larger under P-limited conditions.

This study investigated the importance of nutrients on the physicochemical properties and structure of flocs in the laboratory SBR system. It was demonstrated by EPS extract composition analysis and CLSM combined with glycoconjugate mapping, that the P-limitation influenced EPS composition. EPS composition and distribution is of great interest because it affects bioflocculation, substrate transfer and utilization, bioflocculation, sludge settling and sludge thickening and dewatering. Thus this ability to manipulate natural biopolymers in activated sludge flocs, without affecting a system performance, would aid in the research of their effects on sludge properties. Perhaps, variation of P in the influent wastewater could be used as a control parameter and applied to engineer desired floc properties.

The experimental approach used in this study could be used to investigate the optimum COD:N:P ratio for specific type of plant and wastewater to be treated. Phosphorus can be successfully removed from wastewater either by chemical precipitation or by enhanced biological phosphorus removal (EBPR). EBPR systems have an economical advantage because of their lower sludge production and lower usage of chemicals (Kawaharasaki et al., 2001). For the industrial wastewater treatment plants that practice P-addition, lower P concentrations might save chemical cost to the plants. Lastly, phosphorus is one of the nutrients which cause the eutrophication of rivers and lakes, thus reducing access of P to the aquatic environment would be environmentally beneficial.

The potential of employing CLSM in conjunction with fluorescently labeled probes to study microbial flocs is tremendous. CLSM combined with image analysis can be used not only for detection, but quantitative estimation of exopolymers (Wolfaardt et al., 1998). A variety of probes, including fluorescent antibodies, and nucleic acid stains can be used along lectins to produce multiple labeling of floc materials. A number of nucleic acid stains are available and well suited for use in CLSM to observe the distribution of bacterial biomass. SYTO series, and specifically SYTO 9 (excitation 488, emission 522/532), was shown to be a very effective stain with minimal non-specific binding during the staining of complex microbial communities (Lawrence et al., 1998). Alga and other fluorescent biomolecules or organic matter incorporated into the microbial floc may be visualized through the auto-fluorescence when the correct excitation/emission filters

are used (Lawrence et al., 1998). Lastly, the development of species-selective fluorescently labeled oligonucleotide probes has enabled microscopists to distinguish between morphologically similar cells within the microbial aggregates.

In addition to CLSM, other microscopic techniques can be employed to investigate floc structure. Transmission and scanning electron microscopy (TEM and SEM) could allow high magnification not achieved by COM or CLSM. In addition, there is the option of elemental microanalysis with both electron microscopic techniques. Roman confocal microspectroscopy (RCM) is a non-destructive method that combines chemical information obtained through vibrational spectroscopy with the spatial distribution of chemical constituents within the bulk. Another technique for which partially dehydrated samples can be used, is atomic force microscopy (AFM). The tip of the probe will give information on the surface contours of the sample. AFM reveals a high-resolution image of the topography of single cells and aggregates. Using correlative microscopy techniques such as TEM and SEM, RCM and AFM is advantageous because each one adds to, and overlaps, the understanding of biological structures and interfaces.

CHAPTER 7: REFERENCES

Alphenaar, P.A, Sleyster, R. and P. De Reuver. 1993. Phosphorus requirement in high–rate anaerobic wastewater treatment. *Water Research* 27/5:749-756

Andreadakis, A.D. 1993. Physical and chemical properties of activated sludge floc. *Water Research* 27/12:1707-1714

APHA. 1980. Standard methods for the examination of water and wastewater, 15the edition. American Public Health association, American Water Works Association and Water Pollution Control Federation, Washington, DC.

Barbusinski, K. and H. Koscielniak. 1994. Influence of substrate loading intensity on floc size in activated sludge process. *Water Research* 29/7:1703-1710

Brown, D.A., Beveridge, T.J., Keevil, C.W and B.L. Sherriff. 1998. Evaluation of microscopic techniques to observe iron precipitation in a natural microbial biofilm. *FEM Microbiology Ecology* 26: 297-310

Bura R., Cheung M., Liao B.Q., Finlayson J., Lee B.C., Droppo I.G., Leppard G.G. and S.N. Liss. 1998. Composition of extracellular polymeric substances in the activated sludge floc matrix. *Water Science and Technology* 37/4-5:325-333

Contreras, E.M., Giannuzzi, L., and N.E. Zaritzky. 2000. Growth kinetics of the filamentous microorganism *Sphaerotilus natans* in a model system of a food industry wastewater. *Water Research* 34/18:4455-4463

Cornelissen, A., Burnett, M.G., McCall, R.D. and D.T. Goddard. 1997. The structure of hydrous flocs prepared by batch and continuous flow water treatment systems and obtained by optical, electron and atomic force microscopy. *Water Science and Technology* 36/4: 41-48

Costerton, J.W., Lewandowski, Z., DeBeer, D., Caldwell, D. Korber, D. And G. James. 1994. Biofilms, the customized microniche. *J. Bacteriol.* 176:2137-2142

Costerton, J.W. 1999. Introduction to biofilms. *International Journal of Antimicrobial Agents* 11: 217-221

Decho A.W. and T. Kawaguchi. 1999. Confocal imaging of in situ natural microbial communities and their extracellular polymeric secretion using Nanoplast ® resin. *BioTechniques* 27, 1246-1252

Del Gallo. M., Negi, M. and C.A. Neyra. 1989. Calcofluor- and lectin-binding exocellular polysaccharides of *Azospirillum brasilense* and *Azospirillum lipoferum. Journal of Bacteriology:* 3504-3510

DeLeo P.C., Baveye P., and W.C. Ghiorse. 1997. Use of confocal laser scanning microscopy on soil thin-sections for improved characterization of microbial growth in unconsolidated soils and aquifer material. *Journal of Microbiological Methods* 30, 193-203.

Dignac, M.F., Urbain, V., Rybacki, D., Bruchet, A., Snidaro, D. and P. Scribe. 1998. Chemical description of extracellular polymers: implication on activated sludge floc structure. *Water Science and Technology* 38/8-9:45-53

Droppo I.G., Flannigan D.T., Leppard G.G., and S.N. Liss. 1996. Microbial Floc Stabilization and Preparation for Structural Analysis by Correlative Microscopy. *Water Science and Technology* 34/ (5-6), 155-162.

Droppo, I.G., Leppard, G.G., Flannigan D.T., and S.N. Liss. 1997. The freshwater floc: a functional relationship of water and organic and inorganic floc constituents affecting suspended sediment properties. *Water, Air and soil Pollution* 99:43-54

Ericsson, B. and L. Eriksson. 1988. Activated sludge characteristics in a phosphorus depleted environment. *Water research* 22/2:151-162

Eriksson, L., Steen, I. and M. Tendaj. 1992. Evaluation of sludge properties at an activated sludge plant. *Water Science and Technology* 25/6: 251-265

Figueroa, L. and J.A. Silverstein. 1989. Ruthenium red adsorption method for measurement of extracellular polysaccharides in sludge flocs. *Biotechnology and Bioengineering* 33: 941-947

Filisetti-Cozzi, T.M. and N.C. Carpita. 1991. Measurement of uronic acids without interference from neutral sugars. *Analytical Biochemistry* 197: 159-162

Finlayson J.E., Liao B., Droppo I.G., Leppard G.G. 1998. The relationship between the structure of activated sludge flocs and the sorption of hydrophobic pollutants. *Water science and technology* 37/4-5:353-7

Frølund B., Palmgren R., Keiding K., and Nielsen P.H. 1995. Extraction of extracellular polymers from activated sludge using a cation exchange resin. *Water Research* 30/8, 1749-1758

Ganczarczyk, J.J., Zahid, W.M., and D-H Li. 1992. Physical Stabilization and embedding of microbial aggregates for light microscopy studies. *Water Research* 26/12: 1695-1699

Gaudy, A.F. 1962. Colorimetric determination of protein and carbohydrate. *Industrial Water and Wastes* Jan-Feb: 17-22

Goodwin, J. and C. Foster. 1985. A further examination into the composition of -activated sludge surfaces in relation to their settling characteristics. *Water Research* 19/4: 527-533

Hermanowicz, S.W., Schindler, U., and P. Wilderer. 1995. Anisotropic morphology and fractal dimensions of biofilms. *Water Research* 30/3: 753-755

Horan, N.J. and C.R. Eccles. 1986. Purification and characterization of extracellular polysaccharide from activated sludges. *Water Research* 20/11:1427-1432

Jackson, G., Beyenal, H., Wayne, M.R., and Z. Lewandowski. 2001. Growing reproducible biofilms with respect to structure and viable cell counts. *Journal of Microbiological Methods* 47: 1-10

Jenkins D., Richard, M.G. and G.T. Daigger. 1993. Manual on the Causes and Control of Activated Sludge Bulking and Foaming, 2nd ed. USA: Lewis publishers.

Johnsen, A.R., Hausner, M., Schnell, A., and S. Wuertz. 2000. Evaluation of fluorescently labeled lectins for noninvasive localization of extracellular polymeric substances in *Sphingomonas* biofilms. *Applied and Environmental Microbiology*: 3487-3491

Jorand F., Bouge-Bigne F., Block J.C. and Urbain v. 1998. Hydrophobic/hydrophilic properties of activated sludge exopolymeric substances. *Water Science and Technology* 37 / (4-5), 307-316

Jorand F., Guicherd P., Urbain V., Manem J., and Block J.C. 1994. Hydrophobicity of Activated Sludge Flocs and Laboratory-Grown Bacteria. *Water Science and technology* 30/11: 211-218

Kawaharasaki, M., Manome A., Kanagawa T., and K. Nakamura. 2001. Flow cytometric sorting and RFLP analysis of phosphate accumulating bacteria in and enhanced biological phosphorus removal system. *Proceedings of 3rd IWA International Specialised Conference on Microorganisms in Activated Sludge and Biofilm Processes:* 92-97

Kreamer, H.E. 2002. Characterization of microbial aggregates in relation to membrane biofouling in submerged membrane bioreactors. MASc. Thesis, Graduate Department of Environmental Applied Science and Management, Ryerson University

Lau A.O., Strom P.F., and Jenkins D. 1984. The competitive growth of floc forming and filamentous bacteria: a model for activated sludge bulking. *Journal of Water Pollution Control* 56/1, 52-61

Lawrence, J.R., Korber, D.R., Hoyle B.D., Costerton, J.W. and D.E. Caldwell. 1991. Optical sectioning of microbial biofilms. *J. Bacteriol.* 173: 6558-6567

Lawrence J.R., Neu, T.R and G.D.W Swerhone.1998. Application of multiple parameter imaging for the quantification of algal, bacterial and exopolymer components of microbial biofilms. *Journal of Microbiological Methods* 32:253-261

Lee, Boon Chong. 1997. The influence of nutrients on floc physicochemical properties and structure in activated sludge processes. MASc. Thesis, Graduate Department of Chemical Engineering and Applied Chemistry, University of Toronto

Lewandowski, Z., Webb, D., and M. Hamilton. 1999. Quantifying biofilm structure. *Water Science and Technology* 39-7: 71-76

Lewandowski, Z. 2000. Notes on biofilm porosity. *Water Research*34/9: 2620-2624

Lewandowski, Z., Harkin, G., and H. Beyenal. 2002. Author's response. *Water Research* 36: 807

Li, D.H. and J.J. Ganczarczyk. 1990. Structure of activated sludge flocs. *Biotechnology and Bioengineering* 35, 57-65

Li, D.H. and J.J. Ganczarczyk. 1987. Stroboscopic determination of settling velocity, size and porosity of activated sludge flocs. *Water Research* 21/3: 257-262

Li, D.L and J. Ganczarczyk. 1989. Fractal geometry of particle aggregates generated in water and wastewater treatment processes. 1989. *Environmental Science and Technology* 23: 1385-1389

Li, D.L and J. Ganczarczyk. 1989. Structure of activated sludge flocs. *Biotechnology and Bioengineering* 35: 57-65

Li, X.Y. and B.E. Logan. 2001. Permeability of fractal aggregates. *Water Research* 35/14: 3373-3380

Liao B.Q. 2000. Physicochemical Studies of Microbial Flocs. Ph.D. Thesis, Department of Chemical Engineering and Applied Chemistry, University of Toronto.

Liao B.Q., Allen D.G., Droppo L.G., G.G. Leppard and S.N. Liss. 2000. Bound water content of activated sludge and its relationship to solid retention time, floc structure, and surface properties. *Water Environment Research* 72/6: 722-730

Liao B.Q., Allen D.G., Droppo L.G., G.G. Leppard and S.N. Liss. 2001. Surface properties of sludge and their role in bioflocculation and settleability. *Water Resources* 35/2, 339-350

Liao B.Q., Allen D.G., Droppo L.G., G.G. Leppard and S.N. Liss. 2002. Interparticle interactions affecting the stability of sludge flocs. *Journal of Colloid and Interface science* 249, 372-380

Liss, S.N., Droppo, I.G., Flannigan, D.T., and G.G. Leppard. 1996. Floc architecture in wastewater and natural riverine systems. *Environmental Science and Technology* 30/2:680-686

Liu, H. and H.H.P. Fang. 2002. Extraction of extracellular polymeric substances of sludges. *Journal of Biotechnology* 95: 249-256

Logan, E.B. and D.B. Wilkinson. 1991. Fractal dimensions and porosities of *Zoogloea ramigera* and *Saccharomyces cerevisae* aggregates. *Biotechnology and Bioengineering* 38: 389-396

Lowry, O.H., Rosenbrough, N.J., Farr, A.L. and R.J. Randall. 1951. Protein measurement with the Folin phenol reagent. *Journal of Biological Chemistry* 193: 265-275

Manz, W., Schumann-Kindel G., Szewzyk U., and Reitner, J. 2000. Wide Field Deconvolution epifluorescence microscopy combined with fluorescence in situ hybridization reveals the spatial arrangement of bacteria in sponge tissue. *Journal of Microbiological Methods* 40, 125-134

Michael, T. and C.M. Smith. 1995. Lectins probe molecular films in biofouling: characterization of early films on non-living and living surfaces. *Marine Ecology Progress Series* 119/1-3:229-236

Morgan JW, Forster CF, Evison L. 1990. A comparative study of the nature of biopolymers extracted from anaerobic and activated sludges. Water Resources 24:743-750

Namer, J. and J. Ganczarczyk. 1994. Fractal dimensions and shape factors of digested sludge particle aggregates. *Water Poll. Res. J. Canada* 29/4:441-455

Norcross, K.L. 1992. Sequencing batch reactors – an overview. *Water Science Technology* 26/9-11: 2523-2526

Neu T.R., Eitner A., Staudt C., and J.R. Lawrence. 2002. Off-line, multi-parameter monitoring of major biofilms features. *International Specialized Conference on Biofilm Monitoring,* 314-316

Neu, T.R. and J.R. Lawrence. 1997. Development and structure of microbial biofilms in river water studied by confocal laser scanning microscopy. *FEMS Microbiology Ecology* 24: 11-25

Nielsen P.H., Frølund B., and Keiding K. 1996. Changes in the composition of Extracellular polymeric substances in activated sludge during anaerobic storage. *Applied Microbiol. Biotechnology* 44, 823-830

Ozkanca, R. and K.P. Flint. 1996. Alkaline phosphatase activity of *Escherichia Coli* starved in sterile lake water microcosms. *J. App. Bact.* 80:252-258

Palmer R.J. and C. Stenberg. 1999. Modern microscopy in biofilm research; confocal microscopy and other approaches. *Current Opinions in Biotechnology* 10: 263-268

Palmgren R., Jorand F., Nielsen P.H. and J.C. Block. 1998. Influence of oxygen limitation of the cell surface properties of bacteria from activated sludge. *Wat. Sci. Tech.* 37/ (4-5), 349-352.

Parker, D.S., Kaufman, W.J., and D. Jenkins. 1971. Physical conditioning of the activated sludge floc. *J. Wat. Pollut. Control Fed.* 43, 1817-1833

Rosenberg, M., Gutnick, D. and E. Rosenberg. 1980. Adherence of bacteria to hydrocarbons: a simple method for measuring cell-surface hydrophobicity. *FEM Microbiology Letters* 9: 29-33

Saunamaki, R. 1994. Experimental study on the control of nutrients in activated sludge treatment. *Water science and technology* 29/5-6:329-342

Scherer P., Lippert H. and G. Wolff. 1983. Composition of the major elements and trace elements of 10 methanogenic bacteria determined by inductively coupled plasma emission spectrometry. *Biol. Trace Elem. Res.* 5: 149-163

Schramm A., Larsen, L., Revsbech, N., Ramsing, N., Amann, R., and K.H. Schleifer. 1996. Structure and function of a nitrifying biofilm as determined by *in situ* hybridization and the use of microelectrodes. *Applied Environmental Microbiology* 62: 4641-4647

Silyn-Roberts G. and G.Lewis. 1997. A technique in confocal laser microscopy for establishing biofilms coverage and thickness. *Wat. Sci. Tech.* 36/10, 117-124

Sponza D.T. 2002. Extracellular polymer substances and physicochemical properties of flocs in steady- and unsteady-state activated sludge systems. *Process Biochemistry* 37, 983-998

Sponza D.T. 2003. Investigation of Extracellular polymer substances and physicochemical properties of different activated sludge flocs under steady-state conditions. *Enzyme and Microbial Technology* 32, 375-385

Stanier R.Y., Adelberg E.A. and J.L. Ingraham. 1977. *General Microbiology,* 4th edition. Macmillan Press, London

Stewart P.S., Murga, R, Srinivasan, R. and D. de Beer. 1994. Biofilm structural heterogeneity visualized by three microscopic methods. *Water Research* 29/8:2006-2009

Surman S.B., Walker J.T., Goddard D.T., Morton L.H.G., Keevil C.W., Weaver W., Skinner A., Hanson K., Caldwell D., and J. Kurtz. 1996. Comparison of microscope techniques for the examination of biofilms. *Journal of Microbiological Methods* 25, 57-70

Thill, A., Veerapaneni, S., Simon, B., Wiesner, M., Bottero, J.Y. and D. Snidaro. 1998. Determination of structure of aggregates by confocal scanning laser microscopy. *Journal of Colloid and Interface Science* 204: 357-362

Urbain, V., Block, J.C., and J. Manem. 1993. Bioflocculation in Activated Sludge: An Analytical Approach. *Water Research* 27/5, 829-838

Wolfaardt, G.M., Lawrence, J.R., Robarts, R.D. and D.E. Caldwell. 1998. In situ characterization of biofilm exopolymers involved in the accumulation of chlorinated organics. *Microb. Ecol.*35:213-223

Wilen B.M., Keiding I.K., Nielsen P.H. 2000. Anaerobic deflocculation and aerobic reflocculation of activated sludge. *Water Research* 34, 3933-3942

Wilen, B.M., Jin, B. and P. Lant. 2003. The influence of key chemical constituents in activated sludge on surface and flocculation properties. *Water Research* 37: 2127-2139

Whittaker, Dean. 2002. The effect of phosphorus on phosphorus metabolism, metal accumulation and floc properties in activated sludge processes. MASc. Thesis, Graduate Department of Chemical Engineering and Applied Chemistry, University of Toronto

Wu, Y.C, and J.D. Casey. 1978. Effective removal of copper and cadmium by phosphate-restricted activated sludge. *Wire Technology* 1/ 2:60-64

Yang, X., Beyenal, H., Harkin, G., and Z. Lewandowski. 2000. Quantifying biofilm structure using image analysis. *Journal of Microbiological Methods* 39: 109-119

Yang, X., Beyenal, H., Harkin, G., and Z. Lewandowski. 2000. Evaluation of biofilm image thresholding methods. *Water Research* 35/5: 1149-1158

Zahid, W.M., and J.J. Ganczarczyk. 1990. Suspended solids in biological filter effluents. *Water Research* 24/2: 215-220

Zita A. and M. Hermansson. 1994. Effects of ionic strength on bacterial adhesion and stability of flocs in a wastewater activated sludge system. *Applied Environmental Microbiology* 60: 3041-3048

Zita A. and Hermansson M. 1997a. Effects of bacterial cell surface structure and hydrophobicity on attachment to activated sludge flocs. *Applied Environmental Microbiology* 63, 1168-1170

Zita A. and Hermansson M. 1997b. Determination of bacterial cell surface hydrophobicity of single cells in cultures and in wastewater in situ. *FEMS Microbiology Letters* 152, 299-306

APPENDIX A: COD Removal Data and Statistical Analysis

Acclimation Phase % COD Removal

Date	Time (Days)	R1 % Removal	R2 % Removal	R3 % Removal	R4 % Removal
15-Jan-03	9	98.31	100.00	100.00	83.79
20-Jan-03	14	98.31	100.00	100.00	86.21
27-Jan-03	21	69.13	76.88	55.92	43.7
29-Jan-03	23	42.46	53.99	71.9	63.75
10-Feb-03	35	79.42	69.26	81.57	82.68

Average	77.526	80.03	81.88	72.026
Std. Dev.	23.27903413	20.00998951	18.90956689	18.19299123

R1 and R2

t-Test: Two–Samples Assuming Unequal Variance

	Variable 1	*Variable 2*
Mean	77.526	80.026
Variance	541.9134	400.3997
Observations	5	5
Hypothesized Mean Difference	0	
Df	8	
t Stat	-0.18211	
P(T<=t) one-tail	0.430014	
t Critical one-tail	1.859548	
P(T<=t) two-tail	0.860028	
t Critical two-tail	2.306006	

R3 and R4

t-Test: Two-Samples Assuming Unequal Variance

	Variable 1	*Variable 2*
Mean	81.878	72.026
Variance	357.5717	330.9849
Observations	5	5
Hypothesized Mean Difference	0	
Df	8	
t Stat	0.839536	
P(T<=t) one-tail	0.212772	
t Critical one-tail	1.859548	
P(T<=t) two-tail	0.425544	
t Critical two-tail	2.306006	

COD:N:P	**Grouped COD % Removal**									
100/5/1	98.31	98.31	69.13	42.46	79.42	100	100	76.88	53.99	69.26
100/5/0.1	100	100	55.92	71.9	81.57	83.79	86.21	43.7	63.75	82.68

COD: N: P 100/5/1 and 100/5/0.1

t-Test: Two – Samples Assuming Unequal Variance

		Variable 1	*Variable 2*
Mean		78.776	76.952
Variance		420.5419378	332.9868178
Observations		10	10
Hypothesized	Mean		
Difference		0	
Df		18	
t Stat		0.210123642	
P(T<=t) one-tail		0.417965646	
t Critical one-tail		1.734063062	
P(T<=t) two-tail		0.835931292	
t Critical two-tail		2.100923666	

Experimental Phase % COD Removal

Date	Time (Days)	R1 %Removal	R2 % Removal	R3 % Removal	R4 % Removal
12-Feb-03	37	83.78	84.95	80.46	85.98
14-Feb-03	39	90.77	81.75	70.67	84.03
15-Feb-03	40	93.56	94.62	92.46	92.09

Average	89.37	87.10666667	81.19666667	87.36666667
Std.Dev.	5.038065105	6.700569628	10.91366269	4.205119895

R1 and R2

t-Test: Two–Samples Assuming Unequal Variance

	Variable 1	*Variable 2*
Mean	89.37	87.10667
Variance	25.3821	44.89763
Observations	3	3
Hypothesized Mean Difference	0	
Df	4	
t Stat	0.467621	
P(T<=t) one-tail	0.332198	
t Critical one-tail	2.131846	
P(T<=t) two-tail	0.664395	
t Critical two-tail	2.776451	

R3 and R4

t-Test: Two-Samples Assuming Unequal Variance

	Variable 1	*Variable 2*
Mean	81.19667	87.36667
Variance	119.108	17.68303
Observations	3	3
Hypothesized Mean Difference	0	
Df	3	
t Stat	-0.91373	
P(T<=t) one-tail	0.214117	
t Critical one-tail	2.353363	
P(T<=t) two-tail	0.428235	
t Critical two-tail	3.182449	

Grouped COD % Removal

COD:N:P	% Removal					
100/5/1	83.78	90.77	93.56	84.95	81.75	94.62
100/5/0.1	80.46	70.67	92.46	85.98	84.03	92.09

COD: N: P 100/5/1 and 100/5/0.1

t-Test: Two – Samples Assuming Unequal Variance

		Variable 1	*Variable 2*
Mean		88.23833333	84.28166667
Variance		29.64869667	66.13709667
Observations		6	6
Hypothesized Difference	Mean	0	
Df		9	
t Stat		0.99027209	
P(T<=t) one-tail		0.17395801	
t Critical one-tail		1.833113856	
P(T<=t) two-tail		0.347916019	
t Critical two-tail		2.262158887	

APPENDIX B: MLSS Data and Statistical Analysis

Acclimation Phase

Date	Time (days)	R1 MLSS (g/L)	R2 MLSS (g/L)	R3 MLSS (g/L)	R4 MLSS (g/L)
20-Jan-03	14	0.74	0.72	0.56	0.46
21-Jan-03	15	0.7	0.7	0.78	0.66
27-Jan-03	21	1.00	1.18	0.68	0.42
30-Jan-03	25	3.56	4.38	2.24	2.02
5-Feb-03	30	0.4	0.3	0.28	0.32
10-Feb-03	35	0.36	0.62	1.06	0.73

Average	0.183333	0.223333	0.27	0.198333
Std. dev.	1.21528	1.526953	0.689541	0.632026

R1 and R2

t-Test: Two–Samples Assuming Unequal Variance

	Variable 1	*Variable 2*
Mean	0.989091	1.192727
Variance	0.797629	1.283302
Observations	11	11
Hypothesized Mean Difference	0	
Df	19	
t Stat	-0.46819	
P(T<=t) one-tail	0.322487	
t Critical one-tail	1.729131	
P(T<=t) two-tail	0.644974	
t Critical two-tail	2.093025	

R3 and R4

t-Test: Two-Samples Assuming Unequal Variance

	Variable 1	*Variable 2*
Mean	0.932727	0.893636
Variance	0.271942	0.356245
Observations	11	11
Hypothesized Mean Difference	0	
Df	20	
t Stat	0.163579	
P(T<=t) one-tail	0.435852	
t Critical one-tail	1.724718	
P(T<=t) two-tail	0.871704	
t Critical two-tail	2.085962	

COD:N:P	Grouped MLSS (g/L)											
100/5/1	0.74	0.7	1	3.56	0.4	0.36	0.72	0.7	1.18	4.38	0.3	0.62
100/5/0.1	0.56	0.78	0.68	2.24	0.28	1.06	0.46	0.66	0.42	2.02	0.32	0.73

COD: N: P 100/5/1 and 100/5/0.1

t-Test: Two – Samples Assuming Unequal Variance

		Variable 1	*Variable 2*
Mean		1.2216667	0.85083333
Variance		1.7409788	0.40511742
Observations		12	12
Hypothesized	Mean		
Difference		0	
Df		16	
t Stat		0.8768893	
P(T<=t) one-tail		0.1967614	
t Critical one-tail		1.7458842	
P(T<=t) two-tail		0.3935228	
t Critical two-tail		2.1199048	

Experimental Phase

Date	Time (days)	R1 MLSS (g/L)	R2 MLSS (g/L)	R3 MLSS (g/L)	R4 MLSS (g/L)
11-Feb-03	36	1.14	1.26	0.96	1.82
13-Feb-03	38	0.48	1.62	1.3	1.5
15-Feb-03	40	0.68	0.68	0.64	0.54
20-Feb-03	45	1.12	1.26	0.64	0.56
26-Feb-03	51	0.7	0.4	1.12	0.8

Average	0.368	0.332	0.416	0.524
Std. dev.	0.29237	0.493031	0.292438	0.582649

R1 and R2

t-Test: Two–Samples Assuming Unequal Variance

	Variable 1	*Variable 2*
Mean	0.824	1.044
Variance	0.08548	0.24308
Observations	5	5
Hypothesized Mean Difference	0	
Df	7	
t Stat	-0.858223373	
P(T<=t) one-tail	0.209591088	
t Critical one-tail	1.894577508	
P(T<=t) two-tail	0.419182176	
t Critical two-tail	2.36462256	

R3 and R4

t-Test: Two-Samples Assuming Unequal Variance

	Variable 1	*Variable 2*
Mean	0.932	1.044
Variance	0.08552	0.33948
Observations	5	5
Hypothesized Mean Difference	0	
Df	6	
t Stat	-0.38416	
P(T<=t) one-tail	0.357054	
t Critical one-tail	1.943181	
P(T<=t) two-tail	0.714108	
t Critical two-tail	2.446914	

COD:N:P	Grouped MLSS (g/L)									
100/5/1	1.14	0.48	0.68	1.12	0.7	1.26	1.62	0.68	1.26	0.4
100/5/0.1	0.96	1.3	0.64	0.64	1.12	1.82	1.5	0.54	0.56	0.8

COD: N: P 100/5/1 and 100/5/0.1

t-Test: Two – Samples Assuming Unequal Variance

		Variable 1	*Variable 2*
Mean		0.934	0.988
Variance		0.159471111	0.192373333
Observations		10	10
Hypothesized	Mean		
Difference		0	
Df		18	
		-	
t Stat		0.287884585	
P(T<=t) one-tail		0.388361765	
t Critical one-tail		1.734063062	
P(T<=t) two-tail		0.776723529	
t Critical two-tail		2.100923666	

APPENDIX C: Surface Charge and Statistical Analysis

Surface Charge (meq/g MLSS)					
Date	Day	R1	R2	R3	R4
27-Jan-03	21	-0.483	-1.562	-1.089	-1.354
7-Feb-03	32	-0.625	-0.179	-0.446	-0.556
12-Feb-03	37	-0.114	-0.156	-0.211	-0.105

R1 and R2

t-Test: Two–Samples Assuming Unequal Variance

	Variable 1	*Variable 2*
Mean	-0.40733	-0.63233
Variance	0.069574	0.648342
Observations	3	3
Hypothesized Mean Difference	0	
Df	2	
t Stat	0.459945	
P(T<=t) one-tail	0.345358	
t Critical one-tail	2.919987	
P(T<=t) two-tail	0.690716	
t Critical two-tail	4.302656	

R3 and R4

t-Test: Two-Samples Assuming Unequal Variance

	Variable 1	*Variable 2*
Mean	-0.582	-0.67167
Variance	0.206593	0.400034
Observations	3	3
Hypothesized Mean Difference	0	
Df	4	
t Stat	0.199403	
P(T<=t) one-tail	0.425837	
t Critical one-tail	2.131846	
P(T<=t) two-tail	0.851674	
t Critical two-tail	2.776451	

COD:N:P	Grouped Data- Surface Charge (meq/g MLSS)					
100/5/1	-0.483	-0.625	-0.114	-1.562	-0.179	-0.156
100/5/0.1	-1.089	-0.446	-0.211	-1.354	-0.556	-0.105

COD: N: P 100/5/1 and 100/5/0.1

t-Test: Two – Samples Assuming Unequal Variance

		Variable 1	*Variable 2*
Mean		-0.51983	-0.62683
Variance		0.302354	0.245063
Observations		6	6
Hypothesized	Mean		
Difference		0	
Df		10	
t Stat		0.354242	
P(T<=t) one-tail		0.365257	
t Critical one-tail		1.812462	
P(T<=t) two-tail		0.730513	
t Critical two-tail		2.228139	

APPENDIX D: Hydrophobicity and Statistical Analysis

Hydrophobicity (%)					
Date	Time (Days)	R1	R2	R3	R4
30-Jan-2003	24	24	23	27	36
19-Feb-2003	44	11	16	15	9

R1 and R2

t-Test: Two–Samples Assuming Unequal Variance

	Variable 1	*Variable 2*
Mean	17.5	19.5
Variance	84.5	24.5
Observations	2	2
Hypothesized Mean Difference	0	
Df	2	
t Stat	-0.2709142	
P(T<=t) one-tail	0.40592791	
t Critical one-tail	2.91998731	
P(T<=t) two-tail	0.81185583	
t Critical two-tail	4.30265573	

R3 and R4

t-Test: Two-Samples Assuming Unequal Variance

	Variable 1	*Variable 2*
Mean	21	22.5
Variance	72	364.5
Observations	2	2
Hypothesized Mean Difference	0	
Df	1	
t Stat	-0.10153	
P(T<=t) one-tail	0.467791	
t Critical one-tail	6.313749	
P(T<=t) two-tail	0.935582	
t Critical two-tail	12.70615	

COD:N:P	Grouped Data- Hydrophobicity (%)			
100/5/1	24	11	23	16
100/5/0.1	27	15	36	9

COD: N: P 100/5/1 and 100/5/0.1

t-Test: Two – Samples Assuming Unequal Variance

		Variable 1	*Variable 2*
Mean		18.5	21.75
Variance		37.6666667	146.25
Observations		4	4
Hypothesized Difference	Mean	0	
Df		4	
t Stat		-0.4792949	
P(T<=t) one-tail		0.32837774	
t Critical one-tail		2.13184649	
P(T<=t) two-tail		0.65675548	
t Critical two-tail		2.77645086	

APPENDIX E: EPS Composition and Statistical Analysis

EPS Extraction--Polysaccharides			
	COD: N: P	Polysaccharide (mg Glucose/g MLSS)	
R1	100/5/1	32.9	26
R2	100/5/1	17.8	25.8
R3	100/5/0.1	98	93.9
R4	100/5/0.1	77	77

R1 and R2

t-Test: Two–Samples Assuming Unequal Variance

	Variable 1	*Variable 2*
Mean	29.45	21.8
Variance	23.805	32
Observations	2	2
Hypothesized Mean Difference	0	
df	2	
t Stat	1.448237794	
P(T<=t) one-tail	0.142269404	
t Critical one-tail	2.91998731	
P(T<=t) two-tail	0.284538808	
t Critical two-tail	4.302655725	

R3 and R4

t-Test: Two-Samples Assuming Unequal Variance

	Variable 1	*Variable 2*
Mean	95.95	77
Variance	8.405	0
Observations	2	2
Hypothesized Mean Difference	0	
df	1	
t Stat	9.2439024	
P(T<=t) one-tail	0.0343012	
t Critical one-tail	6.3137486	
P(T<=t) two-tail	0.0686024	
t Critical two-tail	12.70615	

COD:N:P	Grouped Data- Polysaccharides			
100/5/1	32.9	26	17.8	25.8
100/5/0.1	98	93.9	77	77

COD: N: P 100/5/1 and 100/5/0.1

t-Test: Two – Samples Assuming Unequal Variance

	Variable 1	*Variable 2*
Mean	25.625	86.475
Variance	38.10917	122.5025
Observations	4	4
Hypothesized Mean Difference	0	
df	5	
t Stat	-9.60289	
P(T<=t) one-tail	0.000104	
t Critical one-tail	2.015049	
P(T<=t) two-tail	0.000208	
t Critical two-tail	2.570578	

EPS Extraction--Acid Polysaccharides			
	COD: N: P	Acid Polysaccharides (mg Glucuronic Acid/g MLSS)	
R1	100/5/1	12.32	24.9
R2	100/5/1	9.68	9.68
R3	100/5/0.1	29.93	23.82
R4	100/5/0.1	53.29	39.55

R1 and R2

t-Test: Two–Samples Assuming Unequal Variance

	Variable 1	*Variable 2*
Mean	18.61	9.68
Variance	79.1282	0
Observations	2	2
Hypothesized Mean Difference	0	
df	1	
t Stat	1.419713831	
P(T<=t) one-tail	0.195331189	
t Critical one-tail	6.313748599	
P(T<=t) two-tail	0.390662378	
t Critical two-tail	12.7061503	

R3 and R4

t-Test: Two-Samples Assuming Unequal Variance

	Variable 1	*Variable 2*
Mean	26.875	46.42
Variance	18.66605	94.3938
Observations	2	2
Hypothesized Mean Difference	0	
df	1	
t Stat	-2.59954	
P(T<=t) one-tail	0.1168939	
t Critical one-tail	6.3137486	
P(T<=t) two-tail	0.2337879	
t Critical two-tail	12.70615	

COD:N:P	Grouped Data- Acid Polysaccharides			
100/5/1	12.32	24.9	9.68	9.68
100/5/0.1	29.93	23.82	53.29	39.55

COD: N: P 100/5/1 and 100/5/0.1

t-Test: Two – Samples Assuming Unequal Variance

	Variable 1	*Variable 2*
Mean	14.145	36.6475
Variance	52.9577	165.0223
Observations	4	4
Hypothesized Mean Difference	0	
df	5	
t Stat	-3.048263109	
P(T<=t) one-tail	0.014240359	
t Critical one-tail	2.015049176	
P(T<=t) two-tail	0.028480718	
t Critical two-tail	2.570577635	

EPS Extraction--Proteins			
	COD: N: P	Proteins (mg Bovine/g MLSS)	
R1	100/5/1	10.43	26.48
R2	100/5/1	16.56	20.81
R3	100/5/0.1	41.18	35.84
R4	100/5/0.1	56.99	60

R1 and R2

t-Test: Two–Samples Assuming Unequal Variance

	Variable 1	*Variable 2*
Mean	18.455	18.685
Variance	128.80125	9.03125
Observations	2	2
Hypothesized Mean Difference	0	
df	1	
t Stat	-0.027705565	
P(T<=t) one-tail	0.4911833	
t Critical one-tail	6.313748599	
P(T<=t) two-tail	0.9823666	
t Critical two-tail	12.7061503	

R3 and R4

t-Test: Two-Samples Assuming Unequal Variance

	Variable 1	*Variable 2*
Mean	38.51	58.495
Variance	14.2578	4.53005
Observations	2	2
Hypothesized Mean Difference	0	
df	2	
t Stat	-6.520496	
P(T<=t) one-tail	0.0113608	
t Critical one-tail	2.9199873	
P(T<=t) two-tail	0.0227215	
t Critical two-tail	4.3026557	

COD:N:P	Grouped Data- Proteins			
100/5/1	10.43	26.48	16.56	20.81
100/5/0.1-R3	41.18	35.84		
100/5/0.1-R4	56.99	60		

COD: N: P 100/5/1 and 100/5/0.1(R3)

t-Test: Two–Samples Assuming Unequal Variance

	Variable 1	*Variable 2*
Mean	18.57	38.51
Variance	45.9618	14.2578
Observations	4	2
Hypothesized Mean Difference	0	
df	4	
t Stat	-4.62107	
P(T<=t) one-tail	0.004937	
t Critical one-tail	2.131846	
P(T<=t) two-tail	0.009873	
t Critical two-tail	2.776451	

COD: N: P 100/5/1 and 100/5/0.1(R4)

t-Test: Two–Samples Assuming Unequal Variance

	Variable 1	*Variable 2*
Mean	18.57	58.495
Variance	45.9618	4.53005
Observations	4	2
Hypothesized Mean Difference	0	
df	4	
t Stat	-10.7648	
P(T<=t) one-tail	0.000211	
t Critical one-tail	2.131846	
P(T<=t) two-tail	0.000422	
t Critical two-tail	2.776451	

APPENDIX F: Phase Contrast Microscopy

Phase contrast micrographs (20x/DICII objective) of typical flocs from P-rich condition (reactor 1) during stable system operating conditions.

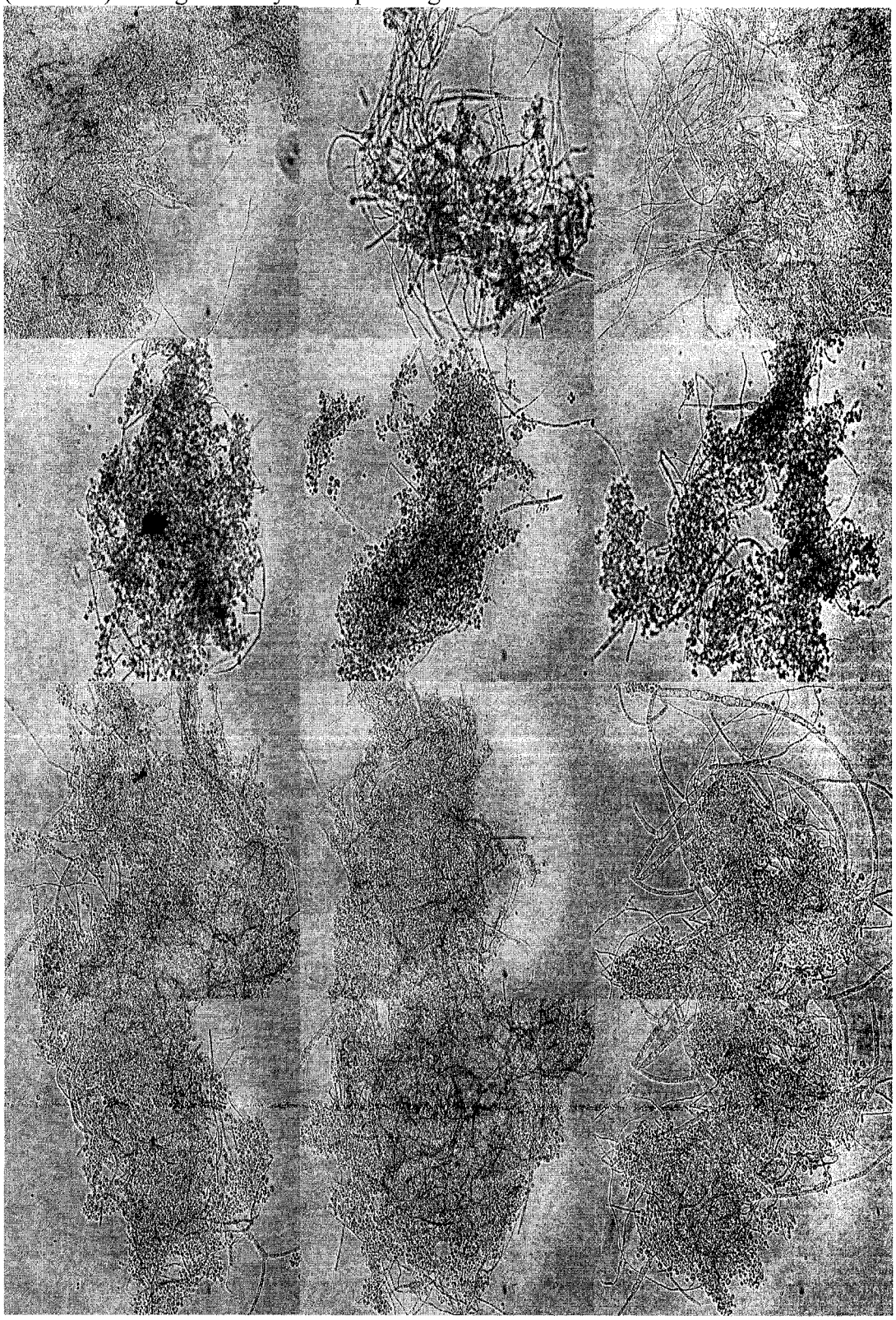

(continuation)

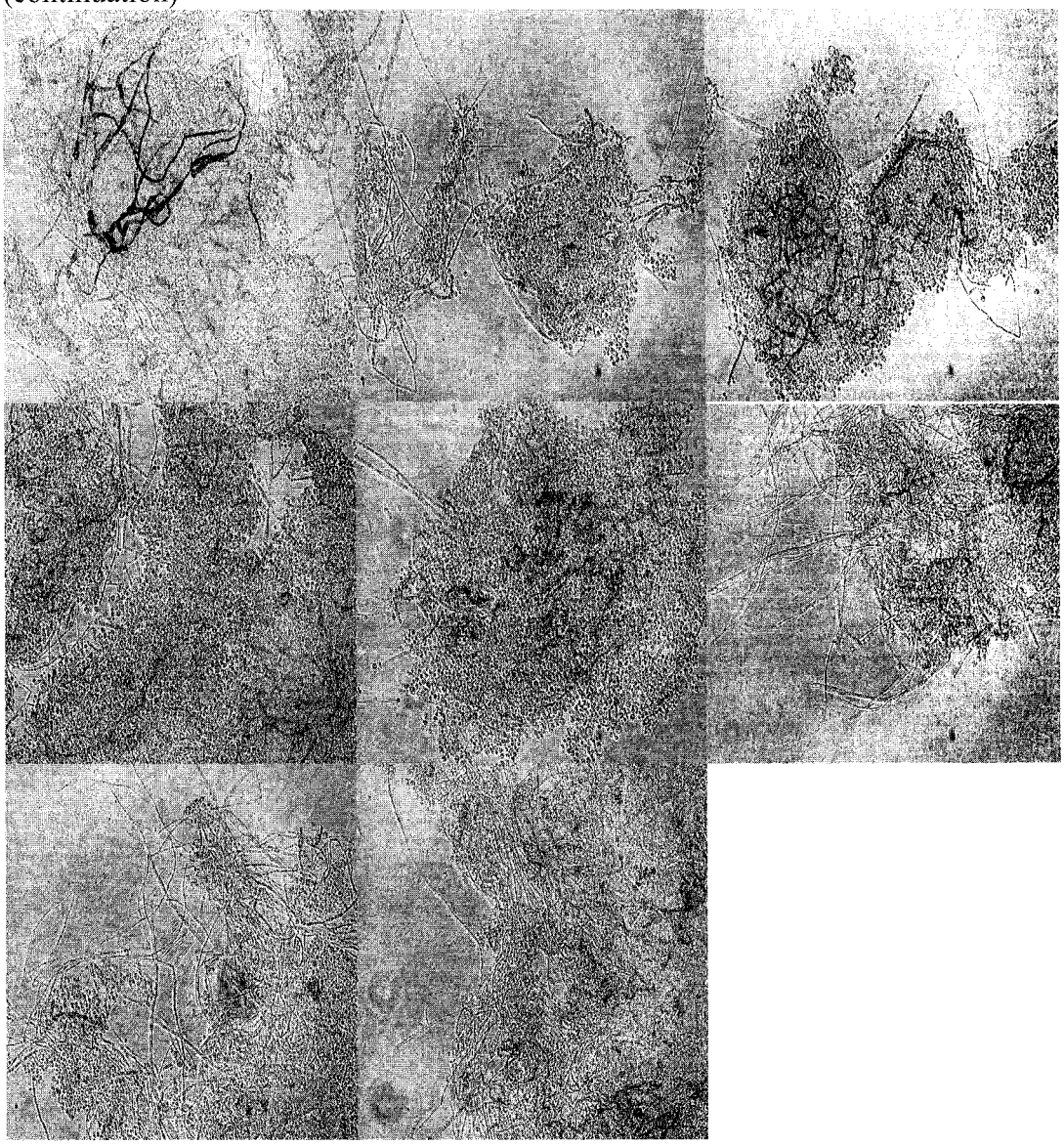

Phase contrast micrographs (20x/DICII objective) of typical flocs from P-limited condition (reactor 4) during stable system operating conditions.

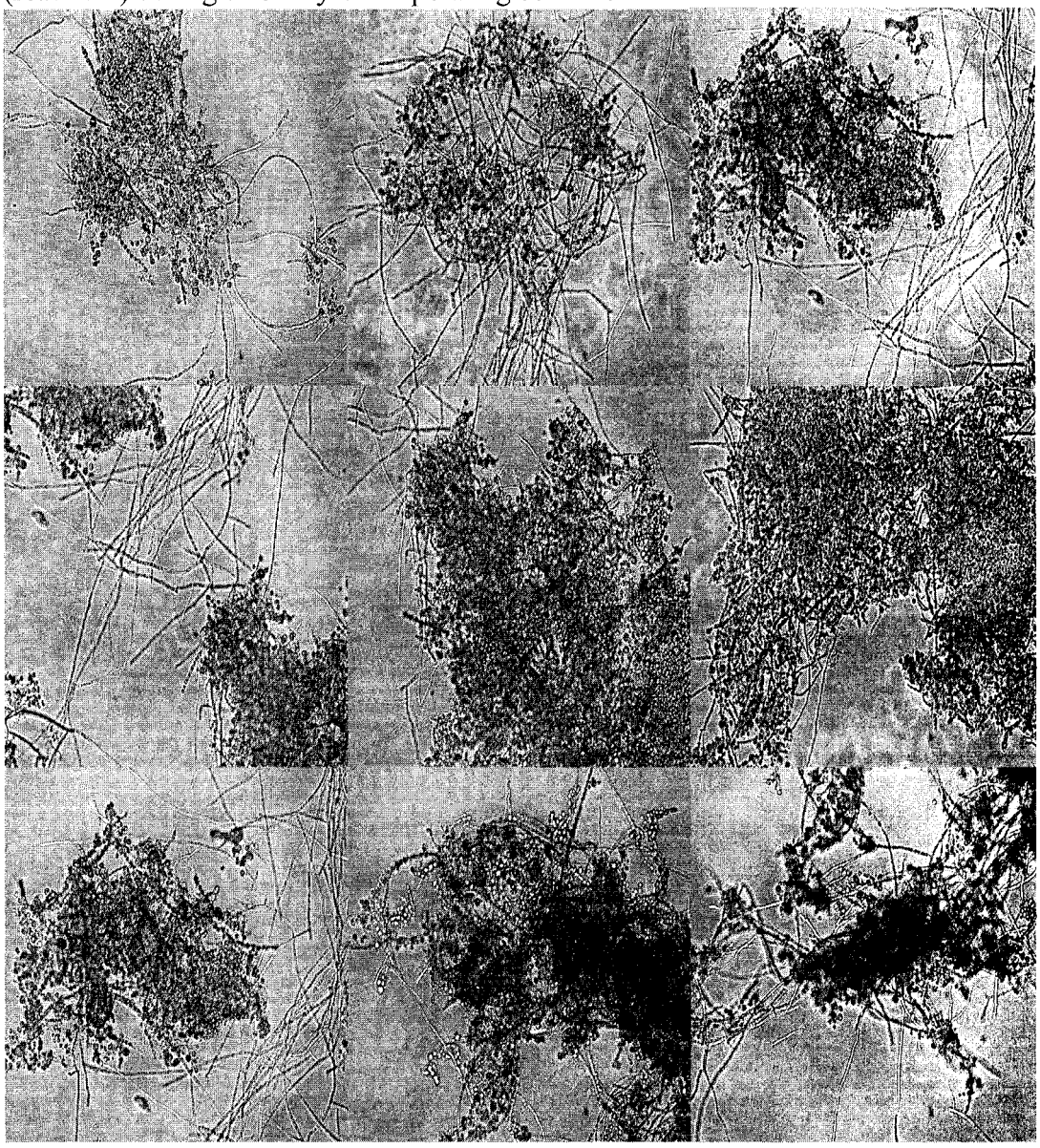

(continuation)

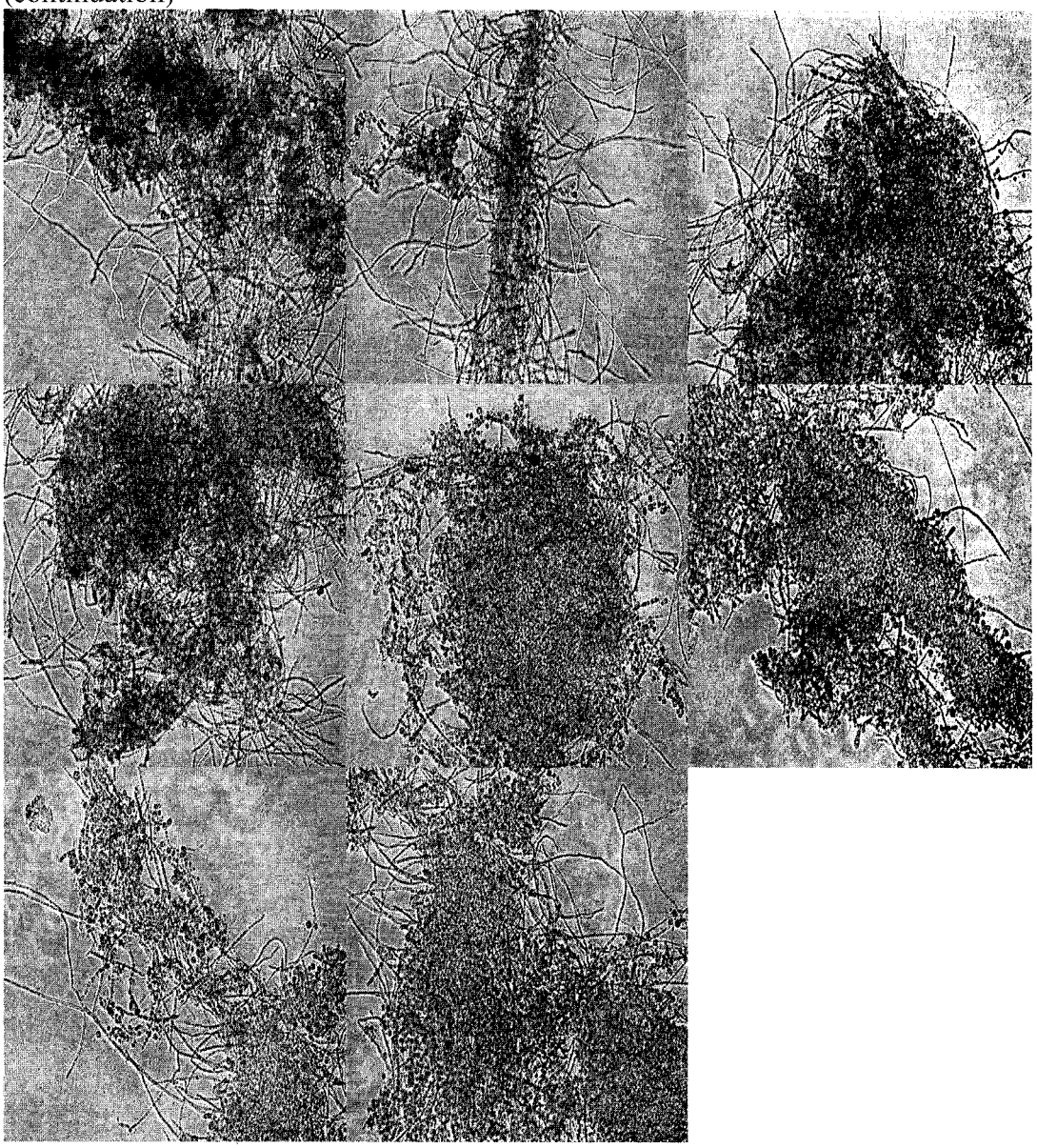

APPENDIX G: CLSM Analysis of Flocs

1 Prepare each lectin-conjugate stain according to the stock concentration listed below.

Lectin-conjugate	Stock Concentration	Working Concentration
Wheat germ agglutinin-tetramethylrhodamine	1-2 mg/mL in 0.1 M $NaHCO_3$ containing 1 mM Mn^{2+} and 1 mM Ca^{2+} at pH 8.3	10 µg/mL in 0.1 M NaHCO3 containing 1 mM Mn^{2+} and 1 mM Ca^{2+} at pH 8.3
Concanavalin A-Alexa Fluor 647	2 mg/mL in 0.1 M $NaHCO_3$ containing 1 mM Mn^{2+} and 1 mM Ca^{2+} at pH 8.3	100 µg/mL in 0.1 M NaHCO3 containing 1 mM Mn^{2+} and 1 mM Ca^{2+} at pH 8.3
Soybean agglutinin- Alexa Fluor 488	2 mg/mL in distilled deionized water	10 µg/mL in 0.1 M NaHCO3 containing 1 mM Mn^{2+} and 1 mM Ca^{2+} at pH 8.3

2 Centrifuge each lectin-conjugate for 2 minutes at 14 000 g.

3 Using a wide mouth pipet (opening around 5 mm in diameter to prevent destruction of floc structure) obtain 500 µL MLSS sample from each reactor during mixing phase.

4 Mix the 500 µL sample with 1.00 mL low melting point agarose solution in a 1.5 mL microcentrifuge tube by inverting several time and pour the mixture into plankton chambers. Allow the agarose to solidify for around 15 minutes.

5 Using 1.5 mL microcentrifuge tubes wrapped in aluminum foil, add the appropriate volume of lectin-conjugate to 0.1 m $NaHCO_3$ containing 1 mM Mn^{2+} and 1 mM Ca^{2+} at pH 8.3 to make 1 mL working solution. Mix thoroughly by pipetting up and down several times.

6 Pour the 1 mL of lectin-conjugate working solution over the floc embedded in agarose.

7 Incubate at room temperature in the dark for 10 min.

8 Draw off lectin-conjugate working solution with pipet or dropper, or by inverting the plankton chamber over a waste container.

9 Wash the agarose embedded sample three times with 1 mL 0.1 M $NaHCO_3$ containing 1 mM Mn^{2+} and 1 mM Ca^{2+} at pH 8.3 and incubate for 10 minutes each time at room temperature in the dark.

10 Observe samples by CLSM using the FITC, Rhodamine, and Cy 5 configurations installed with the Zeiss LSM 510 Release 2.3 software.

CLSM Projections of flocs during acclimation stage

CLSM projections in reflectance and fluorescence mode from day 16 during acclimation phase. In the fluorescent images, blue represents ConA-AF633, green represent SBA-AF488, and red represents WGA-tmr. 63x/0.9 W objective, scale bar = 20 µm

Reactor 1 (P-rich conditions)

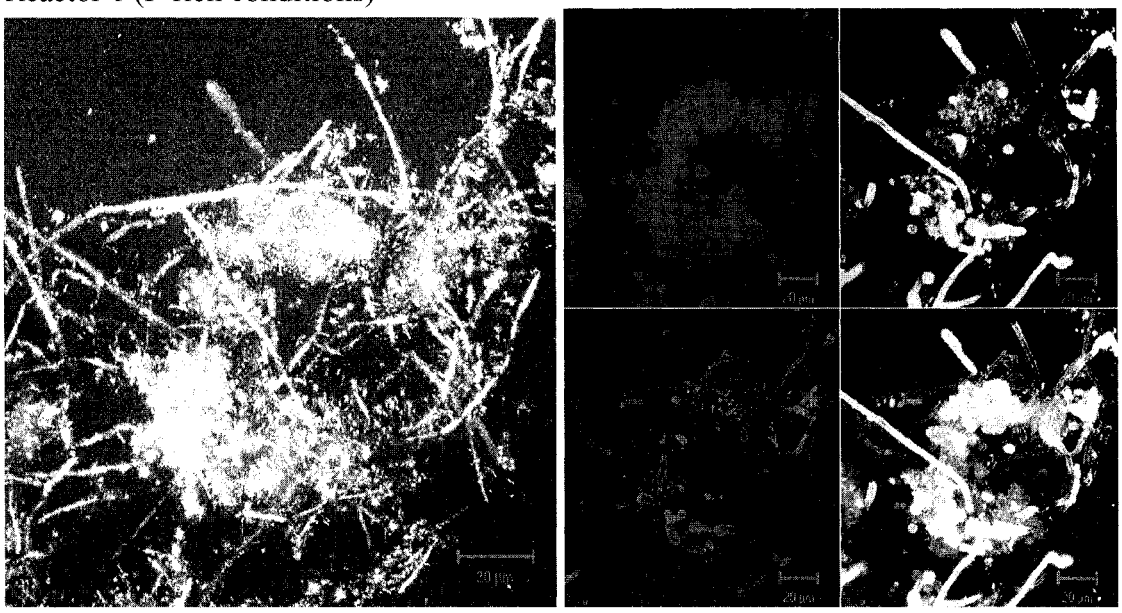

(a) reflectance (b) fluorescence

Reactor 2 (P-rich conditions)

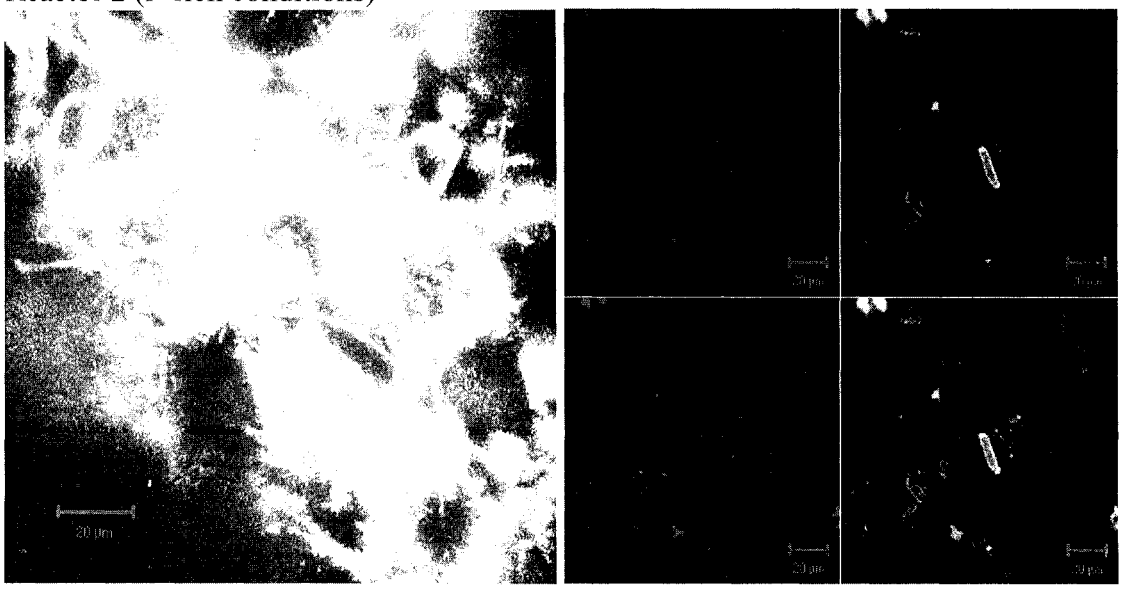

(a) reflectance (b) fluorescence

Reactor 3 (P-limited conditions)

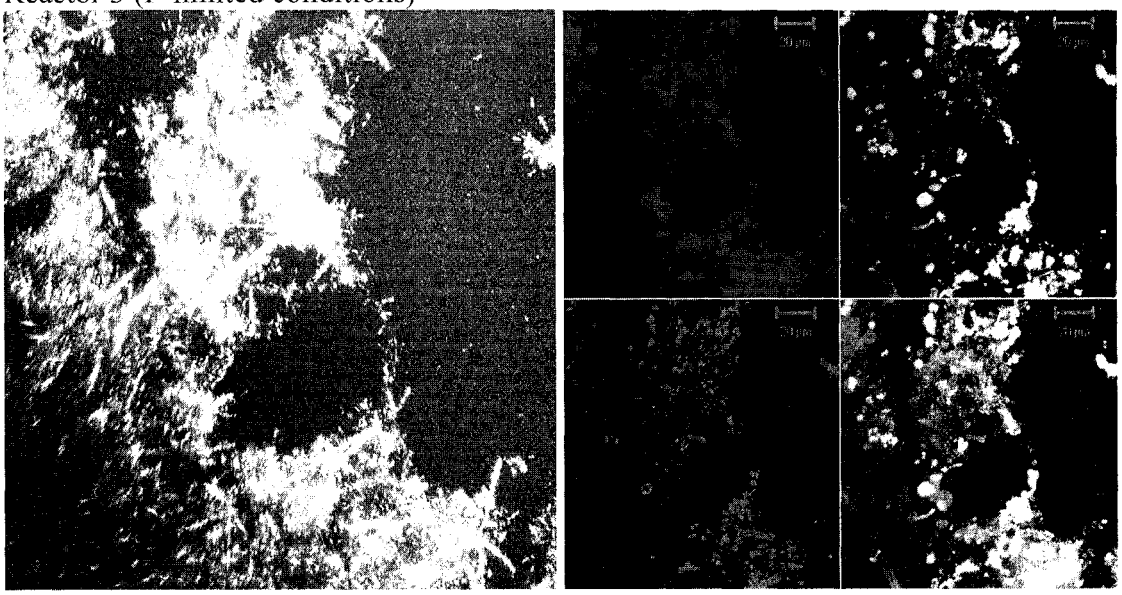

(a) reflectance (b) fluorescence

Reactor 4 (P-limited conditions)

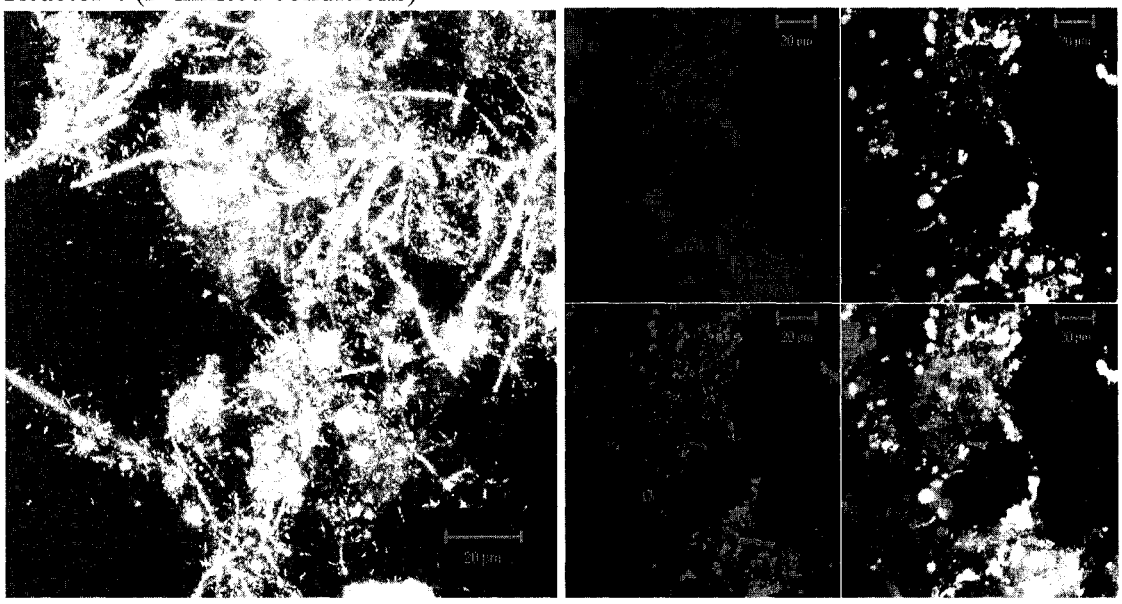

(a) reflectance (b) fluorescence

CLSM projections in reflectance and fluorescence mode from day 23 during acclimation phase. In the fluorescent images, blue represents ConA-AF633, green represent SBA-AF488, and red represents WGA-tmr. 63x/0.9 W objective, scale bar = 20 μm

Reactor 1 (P-rich conditions)

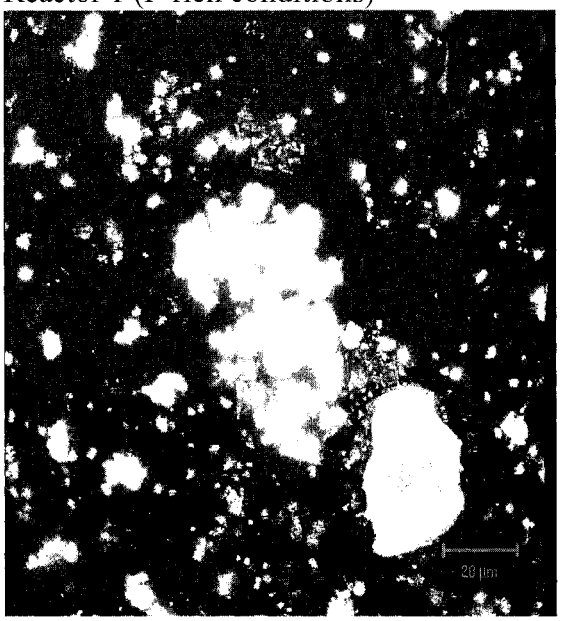

(a) reflectance

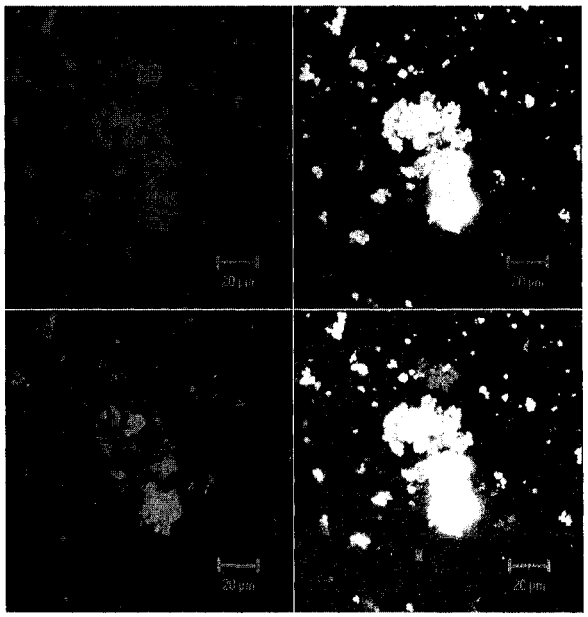

(b) fluorescence

Reactor 2 (P-rich conditions)

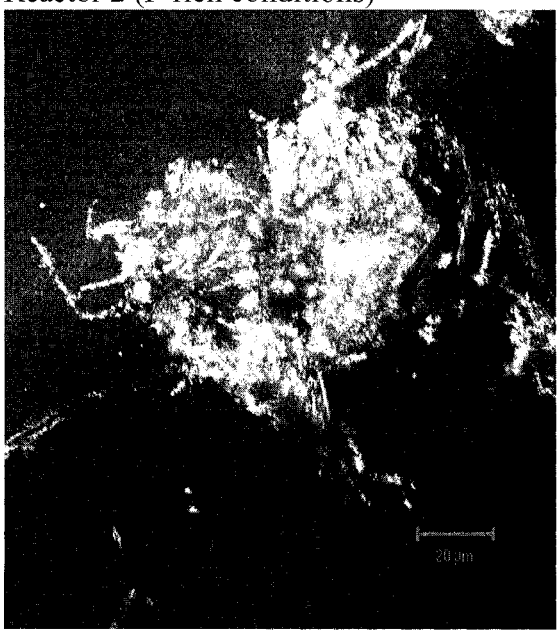

(a) reflectance

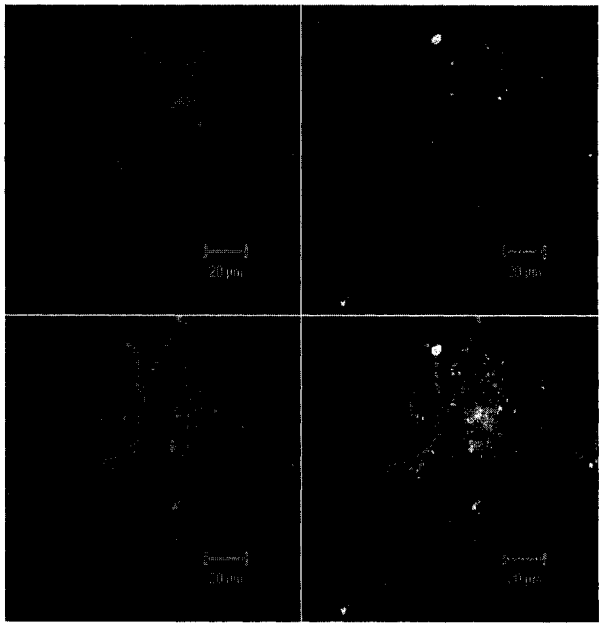

(b) fluorescence

Reactor 3 (P-limited conditions)

(a) reflectance

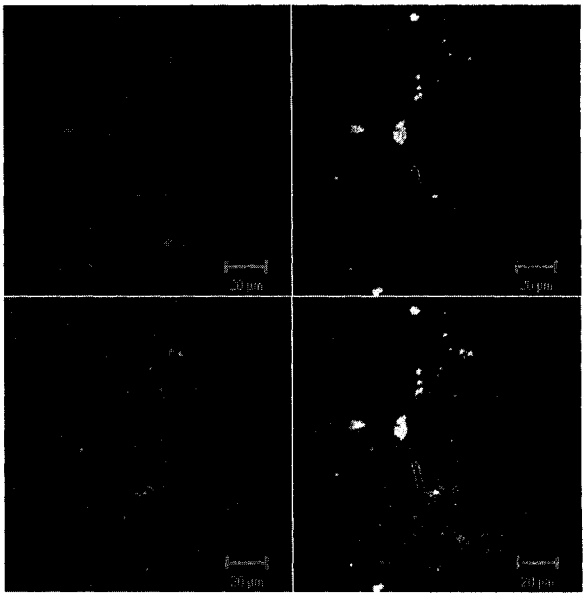

(b) fluorescence

Reactor 4 (P- limited conditions)

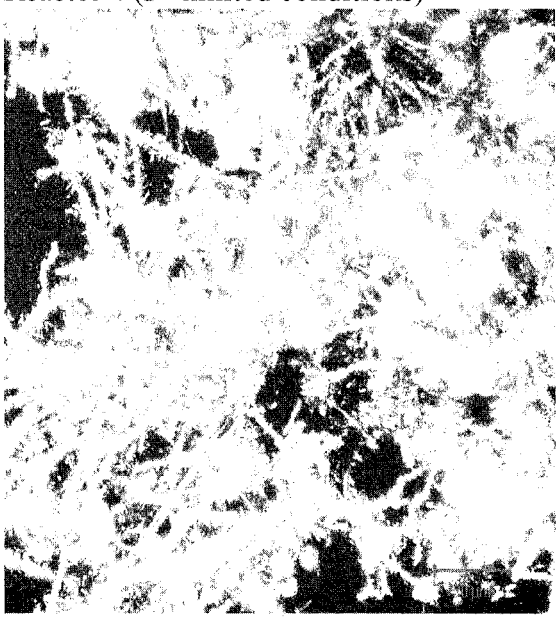

(a) reflectance

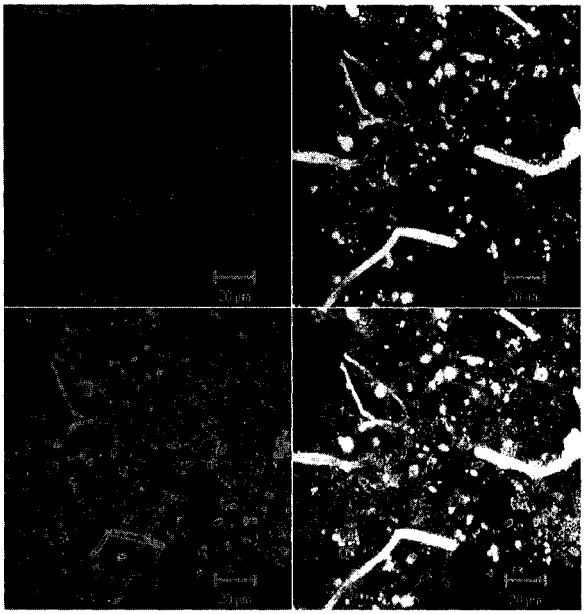

(b) fluorescence

Two–dimensional CLSM Analysis of flocs during stable system operating conditions

Gallery of CLSM two-dimensional plane micrographs (8 bit, 146.2μm x146.2μm) showing the composition of microbial flocs from Reactor 1(P-rich conditions). The images are captured with 63x objective in fluorescence mode, where blue represents ConA-AF633, green represent SBA-AF488, and red represents WGA-tmr.
Scale bar = 20 μm

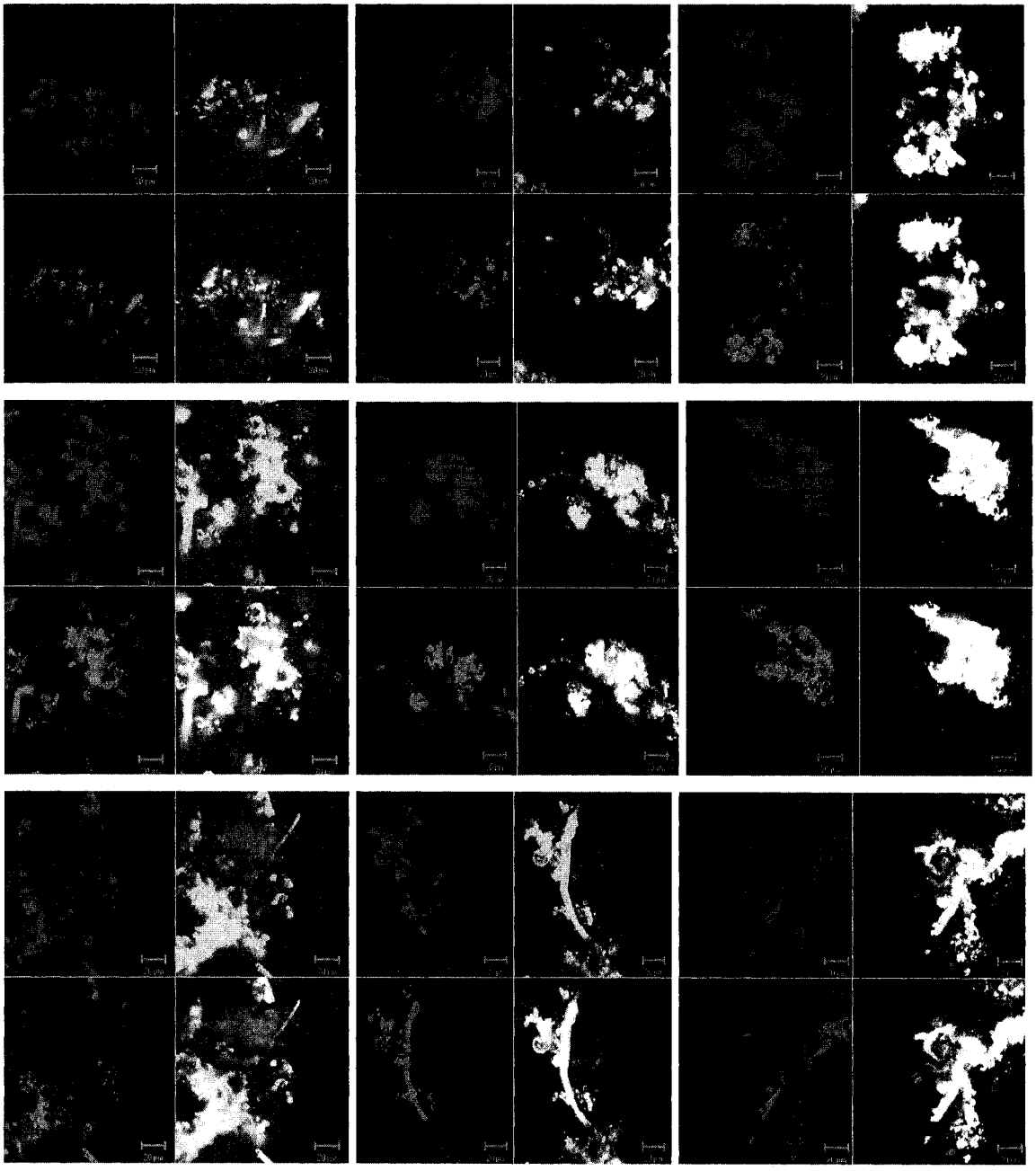

(continuation)

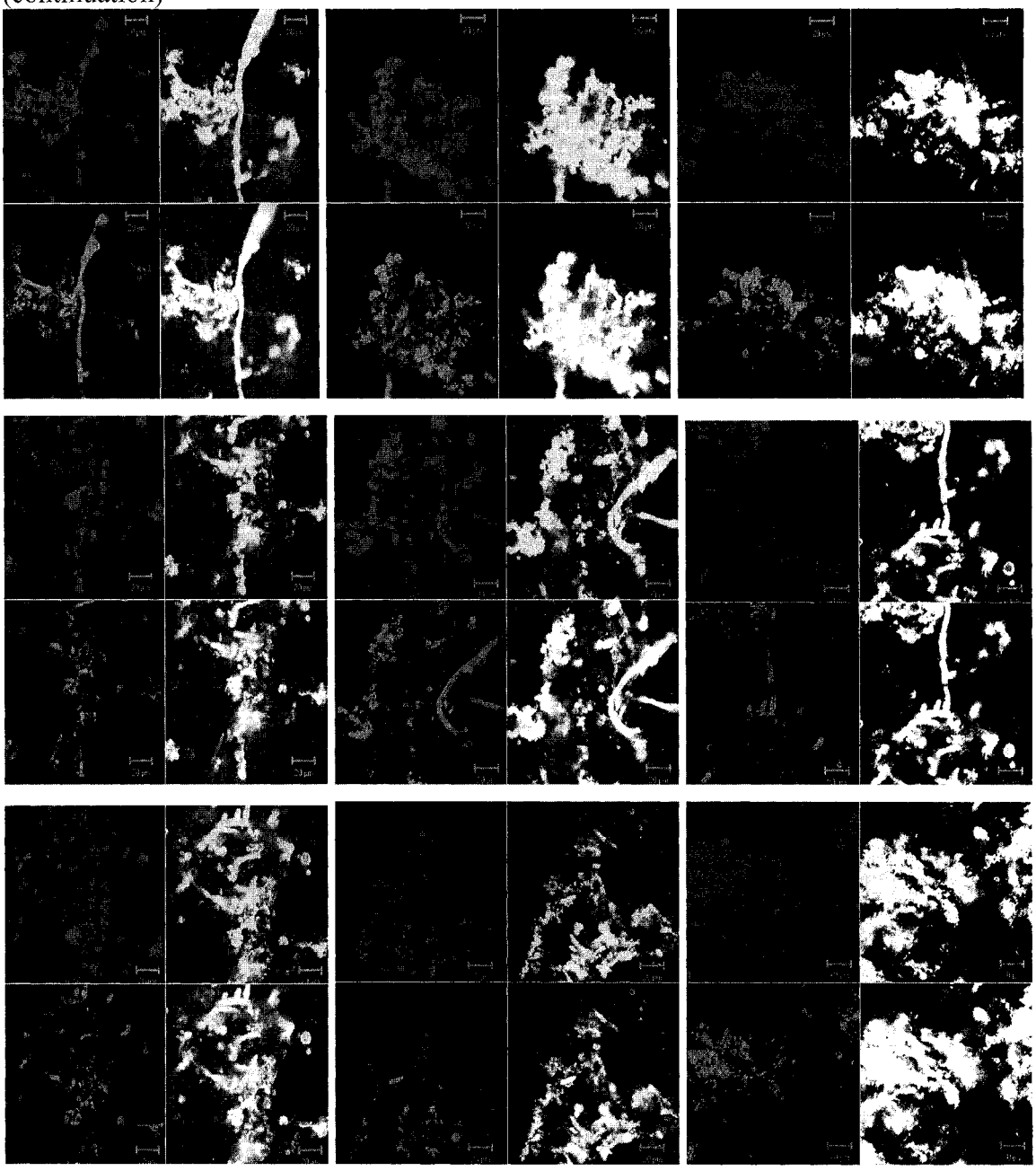

(continuation)

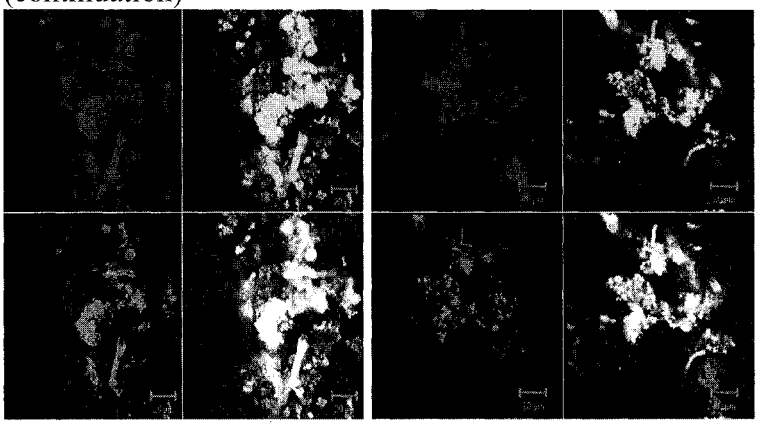

Gallery of CLSM two-dimensional plane micrographs (8 bit, 146.2μm x146.2μm) showing the composition of microbial flocs from Reactor 2(P-rich conditions). The images are captured with 63x objective in fluorescence mode, where blue represents ConA-AF633, green represent SBA-AF488, and red represents WGA-tmr.
Scale bar = 20 μm

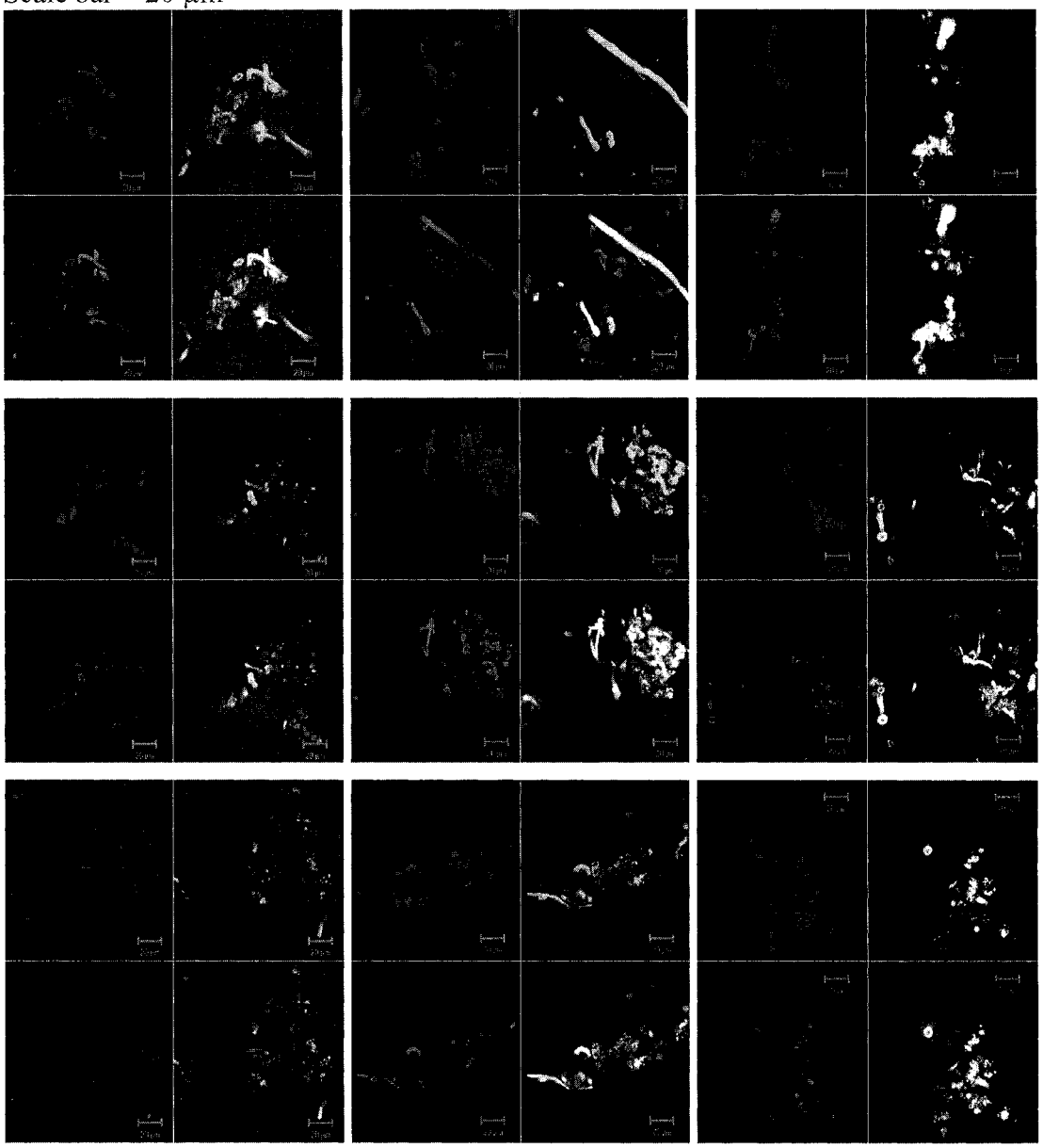

(continuation)

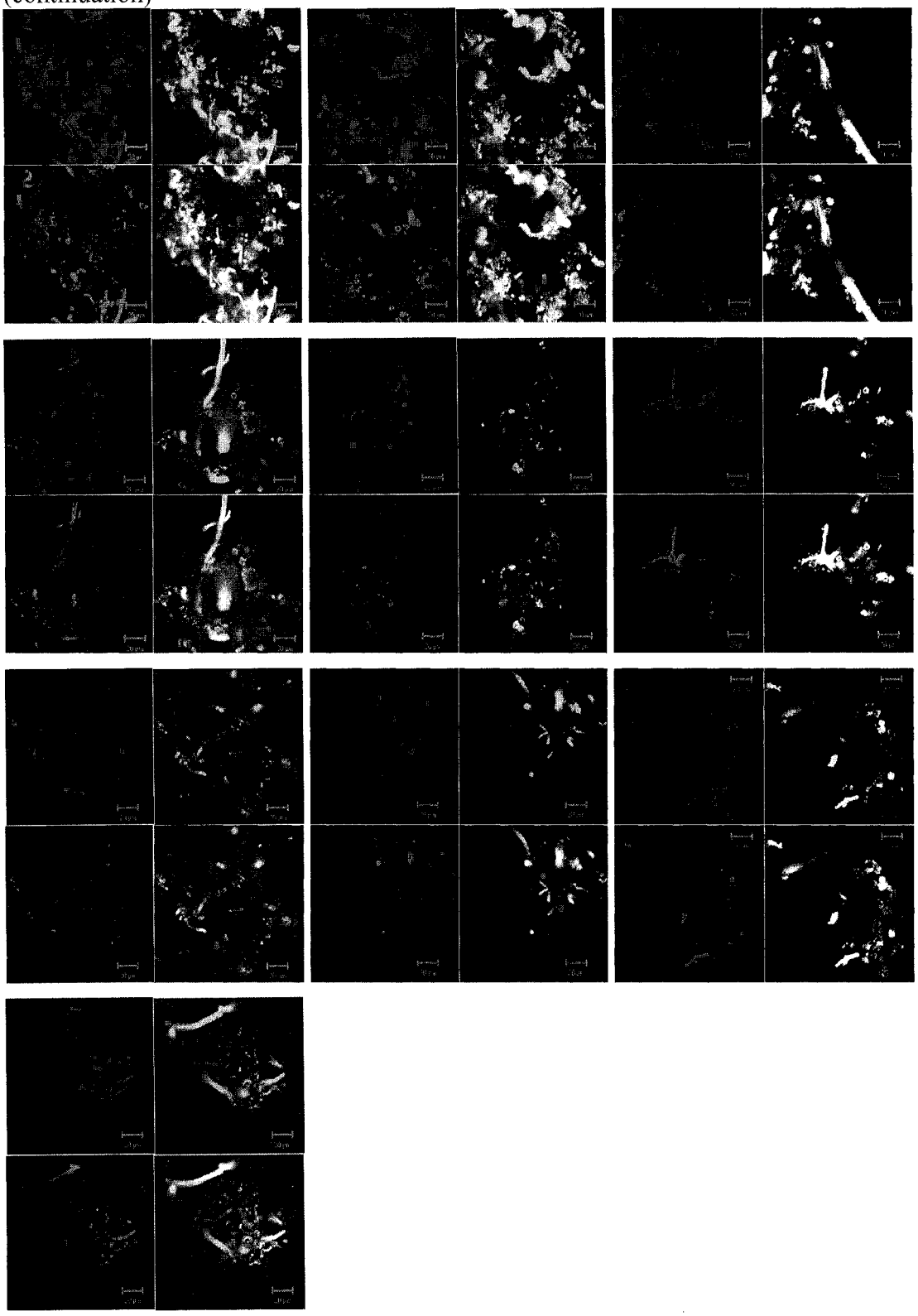

Gallery of CLSM two-dimensional plane micrographs (8 bit, 146.2μm x146.2μm) showing the composition of microbial flocs from Reactor 3(P-limited conditions). The images are captured with 63x objective in fluorescence, where blue represents ConA-AF633, green represent SBA-AF488, and red represents WGA-tmr. Scale bar = 20 μm

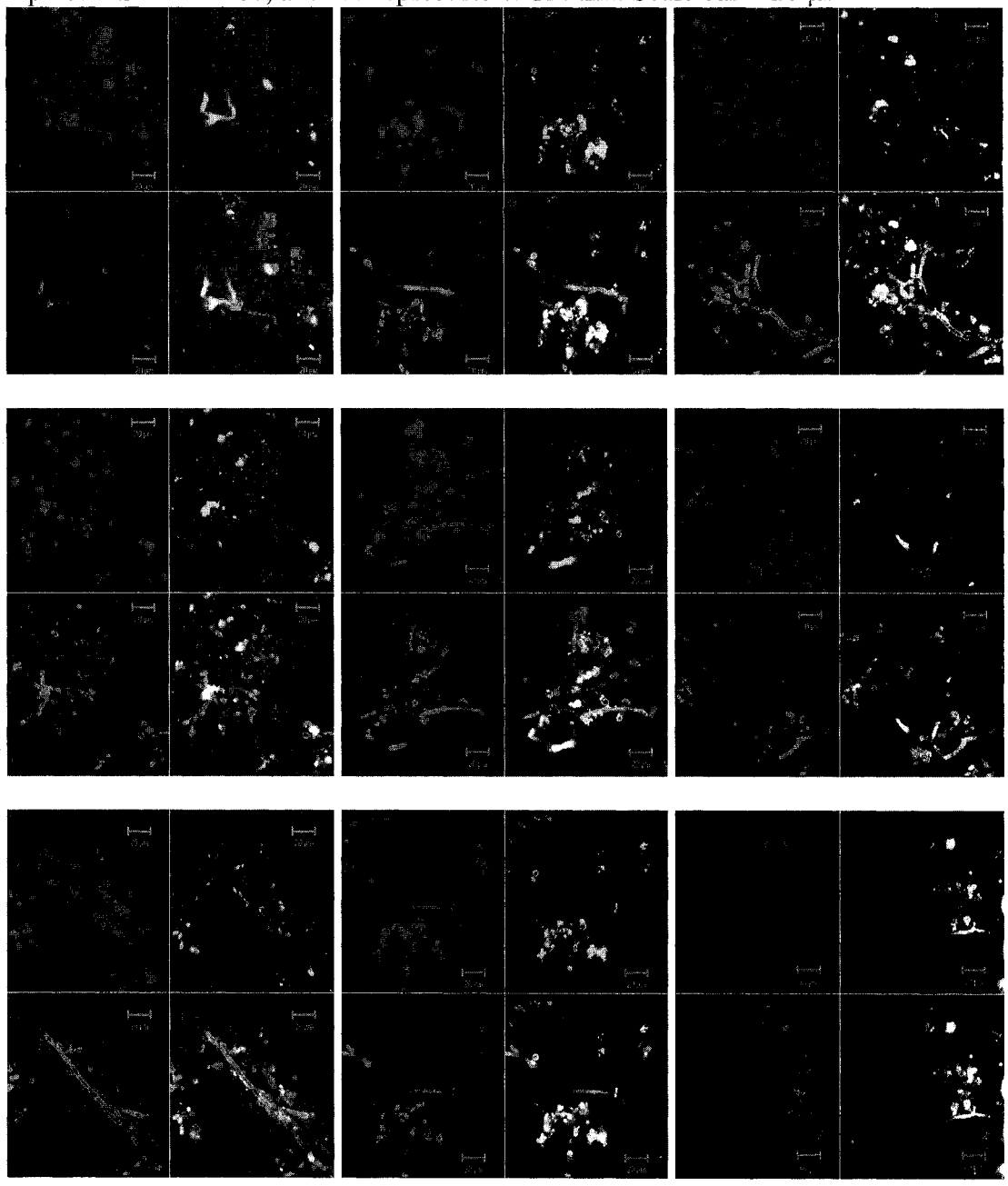

(continuation)

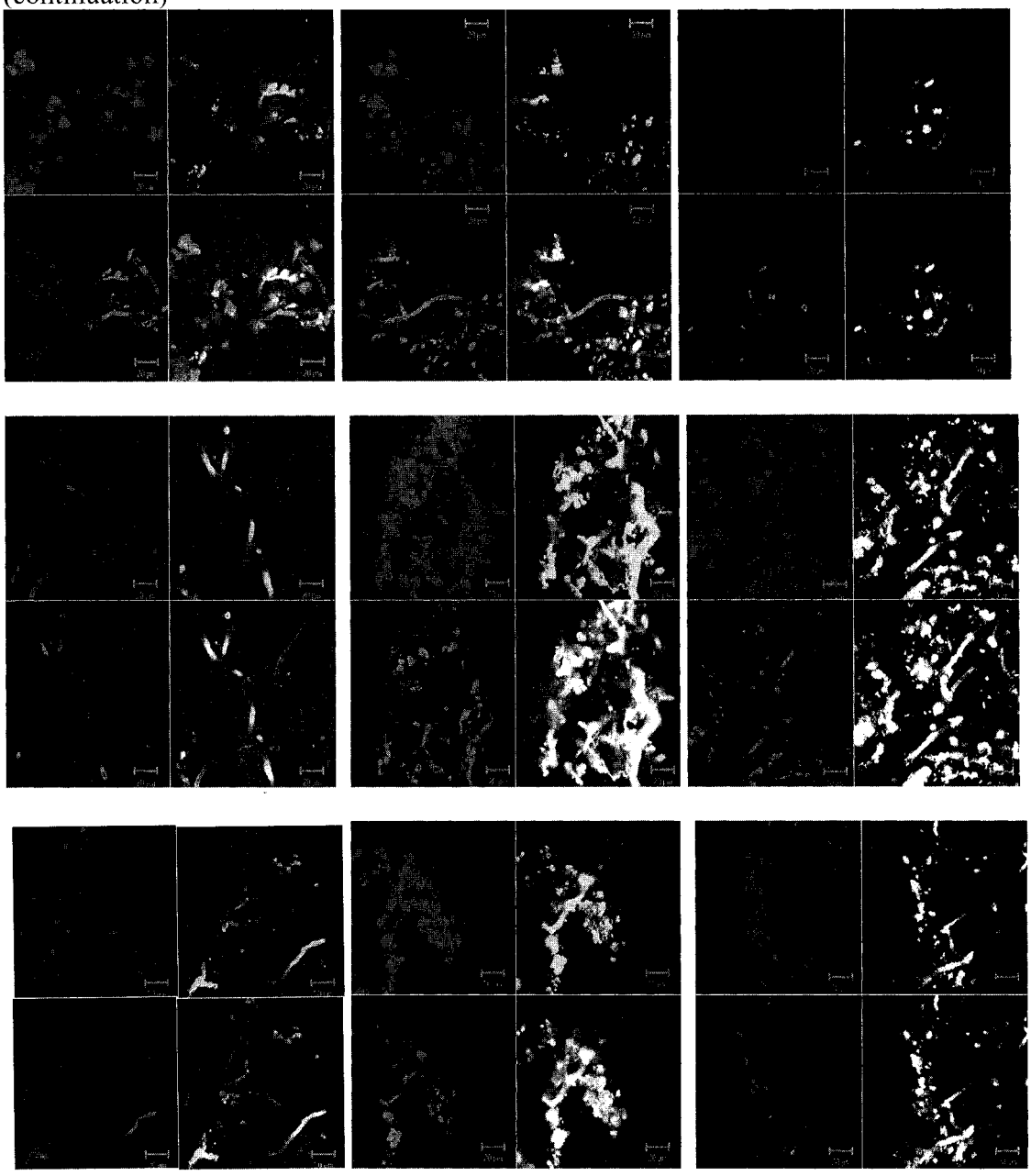

(continuation)

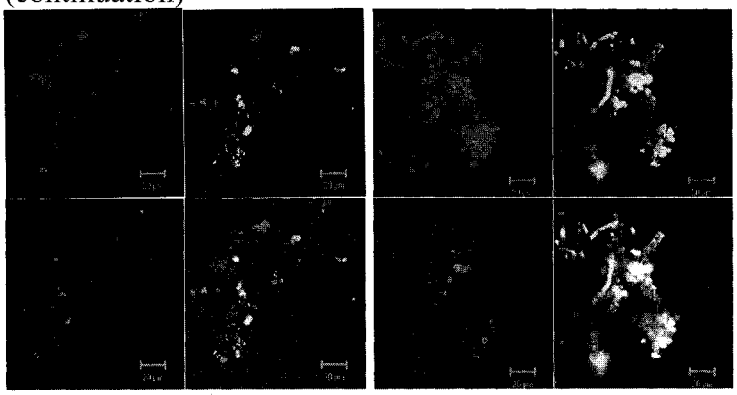

Gallery of CLSM two-dimensional plane micrographs (8 bit, 146.2μm x146.2μm) showing the composition of microbial flocs from Reactor 4 (P-limited conditions). The images are captured with 63x objective in fluorescence mode, where blue represents ConA-AF633, green represent SBA-AF488, and red represents WGA-tmr.
Scale bar = 20 μm

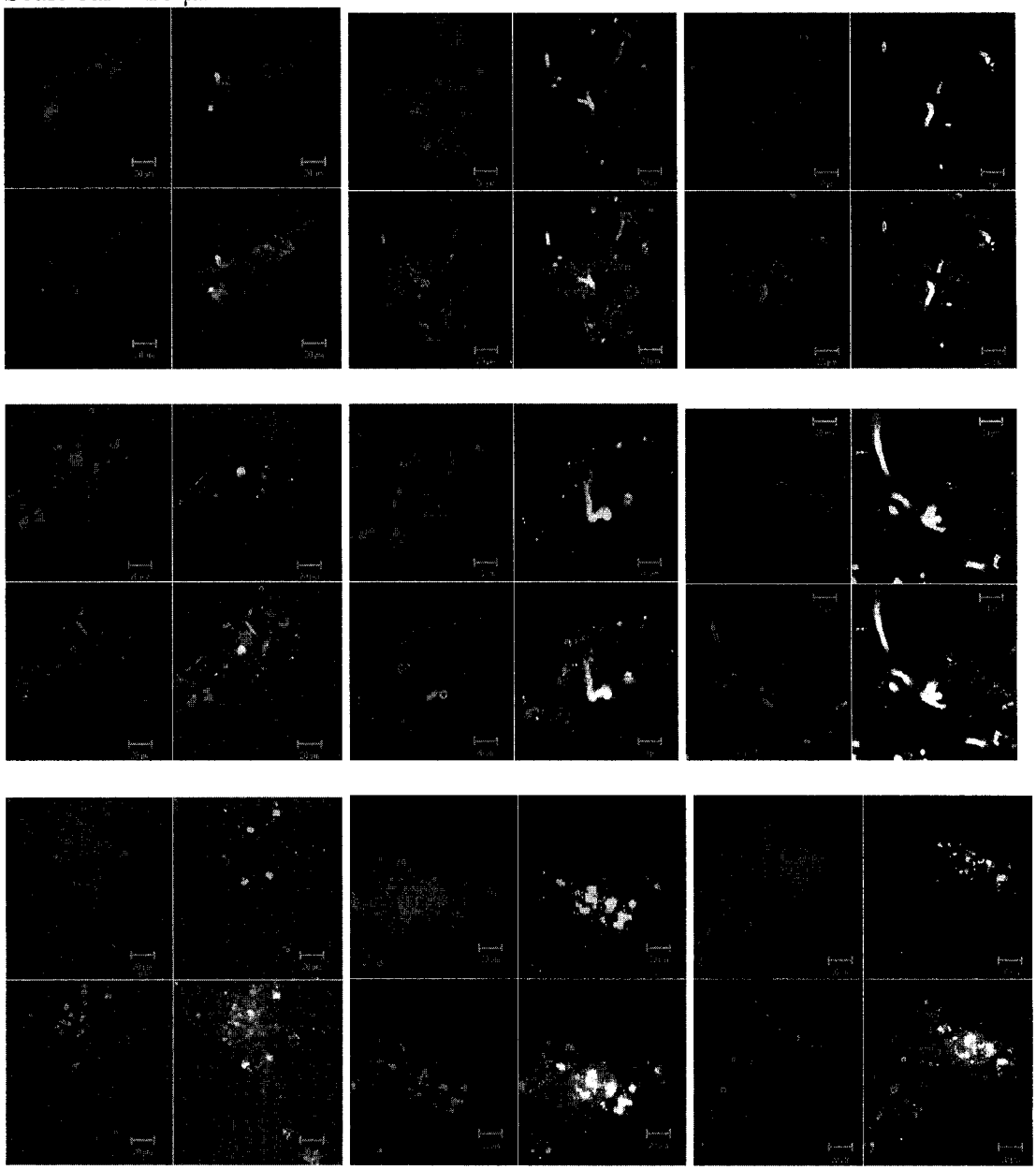

(continuation)

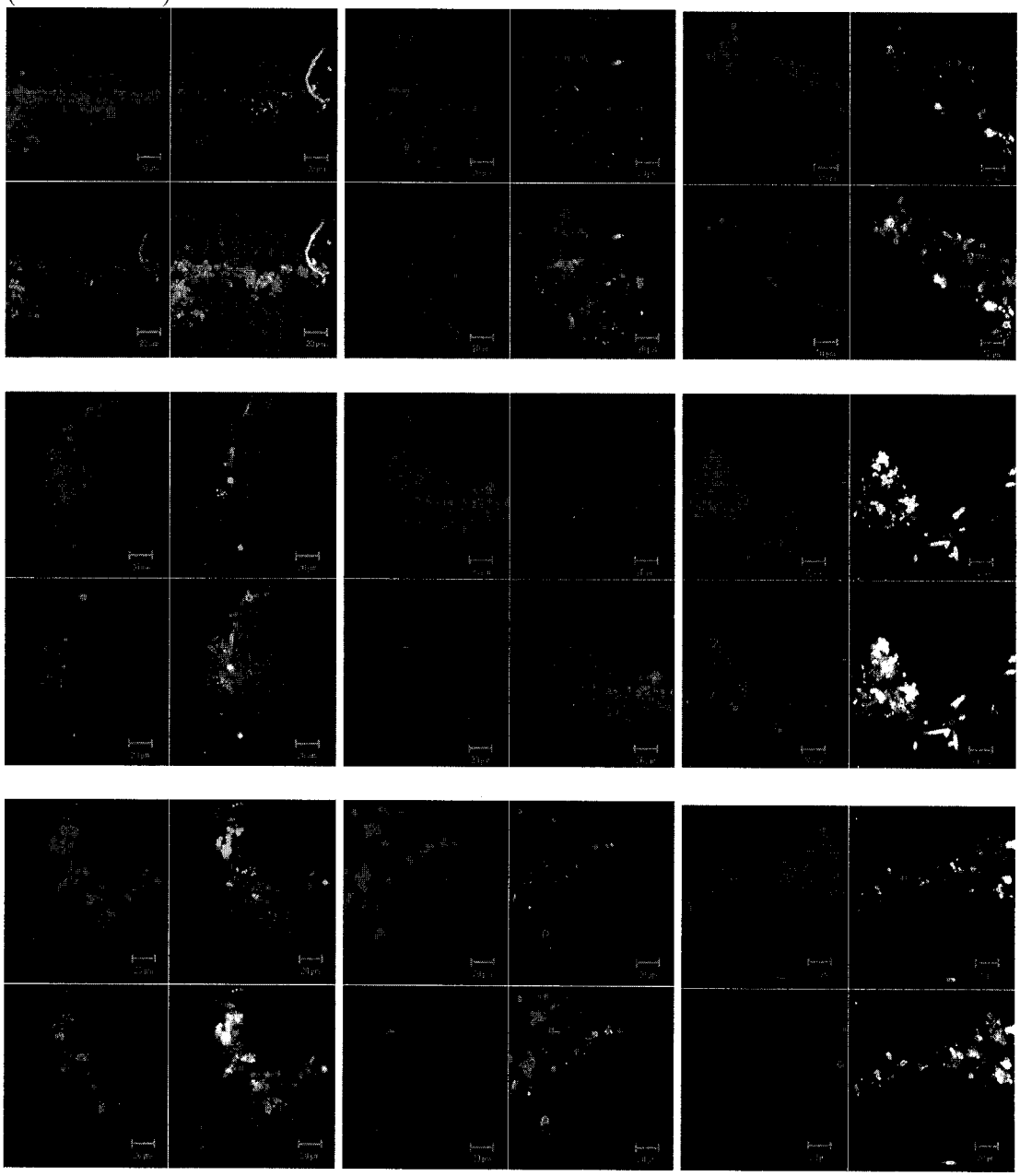

(continuation)

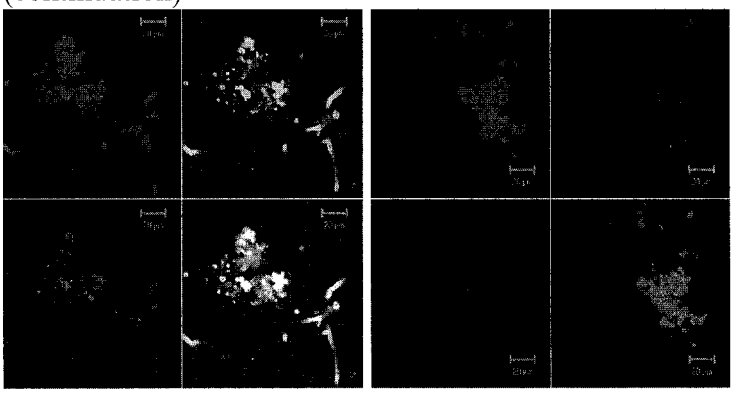

CLSM Projections of flocs during stable system operating conditions

CLSM projections in reflectance and fluorescence mode from day 37 (stable system operating conditions). In the fluorescent images, blue represents ConA-AF633, green represent SBA-AF488, and red represents WGA-tmr. 63x/0.9 W objective;
Scale bar = 20 μm

Reactor 1 (P-rich)

(a) reflectance

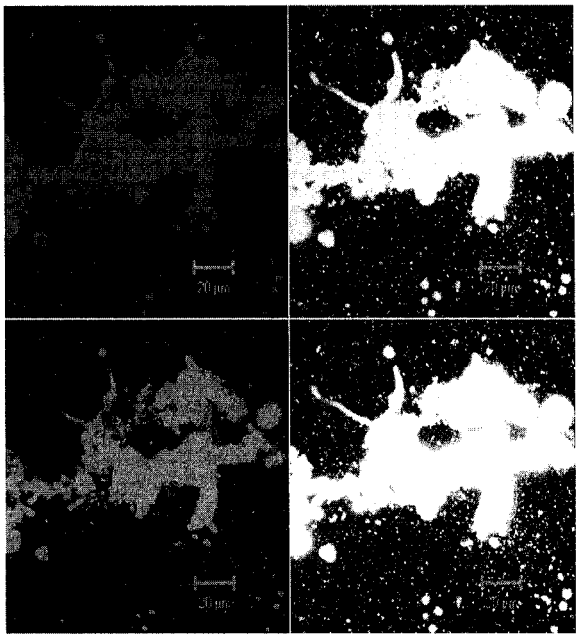

(b) fluorescence

Reactor 2 (P-rich)

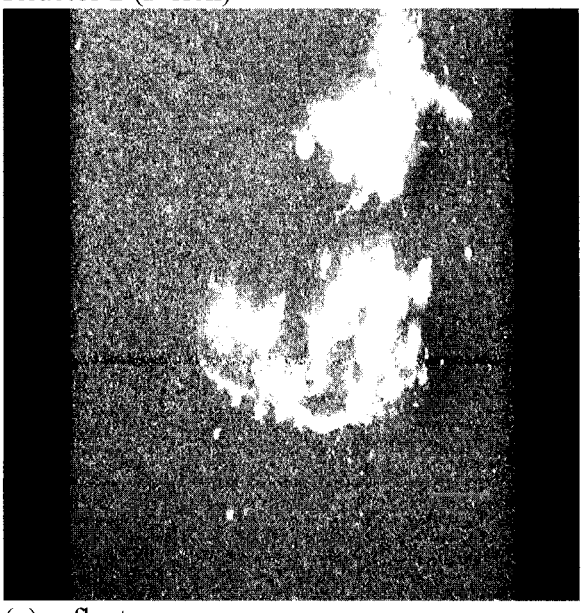

(a) reflectance

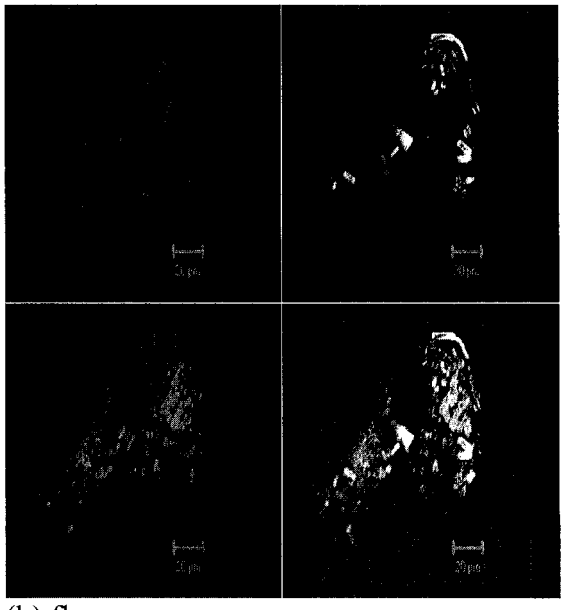

(b) fluorescence

Reactor 3 (P-limited)

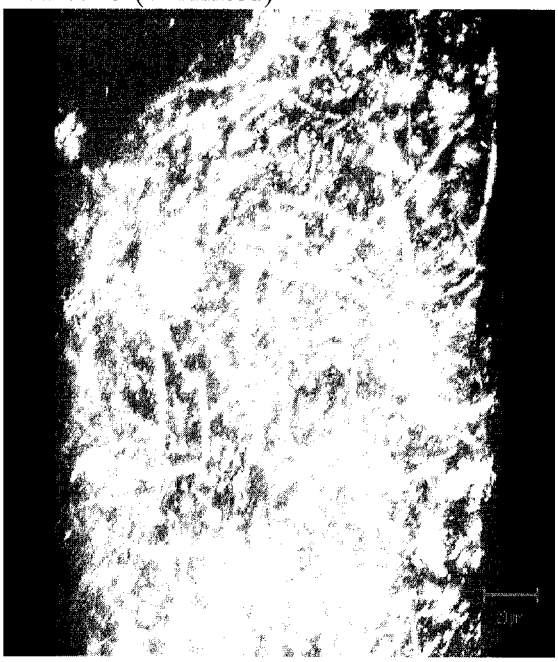

(a) reflectance

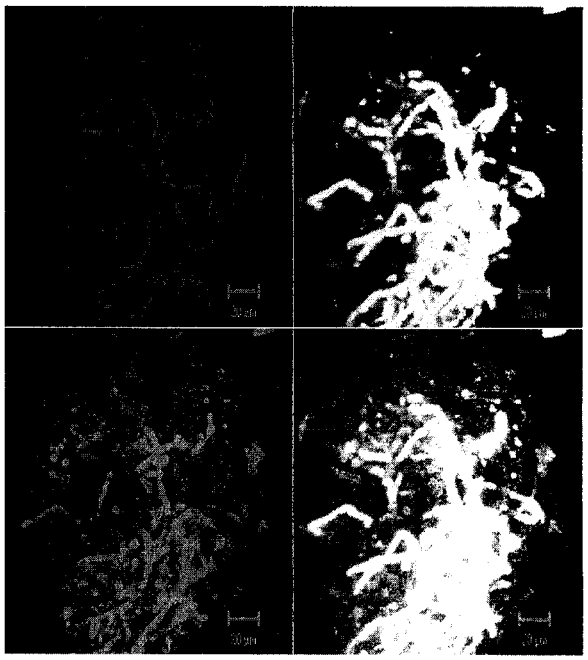

(b) fluorescence

Reactor 4 (P-limited)

(a) reflectance

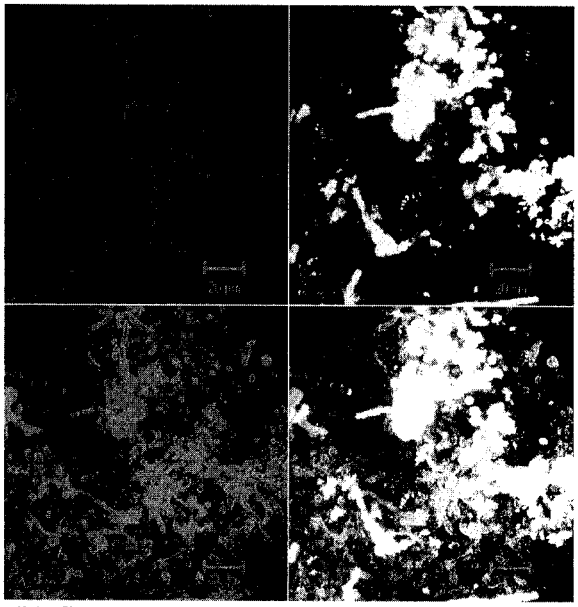

(b) fluorescence

APPENDIX H: Image Analysis Data

ISA 3d Data for Reactor 1

Depth Profile 1:

µm from top	Threshold	Porosity	FD	ADD
1	0.55846213	0.59741512	1.51219502	3.16396135
2	0.5599993	0.58082562	1.55080776	3.03773061
3	0.55432071	0.60397377	1.62073023	2.26179609
4	0.55362486	0.64332562	1.64048027	1.97070714
5	0.54065402	0.65142747	1.69052027	1.62693995
6	0.53753151	0.66608796	1.72692771	1.32640398
7	0.54160221	0.68653549	1.70445715	1.418899
8	0.54883656	0.70871914	1.72550256	1.40894078
9	0.53010201	0.70601852	1.74440817	1.29976203
10	0.52270971	0.70871914	1.7727904	1.33565137
11	0.53761327	0.70698302	1.77467857	1.35762852
12	0.55288458	0.69965278	1.77279295	1.34336739
13	0.55029843	0.68460648	1.76571042	1.43970183
14	0.54826287	0.70466821	1.73496544	1.55366858
15	0.54855864	0.72125772	1.70551423	1.63843472
16	0.52702909	0.74575617	1.69645314	1.40673706
17	0.51371642	0.7658179	1.68988733	1.31960267
18	0.49872369	0.78587963	1.62089896	1.28042032
19	0.49025208	0.80632716	1.58635703	1.30247224
20	0.48029134	0.81577932	1.54316848	1.3368229
21	0.4597917	0.81790123	1.53896466	1.21652714
22	0.43249702	0.82465278	1.56271766	1.22050899
23	0.41707077	0.85706019	1.52727476	1.16054826
24	0.36249086	0.84818673	1.59047927	1.06725584
25	0.30762445	0.82928241	1.65855141	1.07123816
	Average	0.72667438	1.65828935	1.07123816
	Std. deviation	0.08044174	0.08690786	0.53574179

Depth Profile 2:

µm from top	Threshold	Porosity	FD	ADD
1	0.48218093	0.77949011	1.59600562	1.36988882
2	0.3902933	0.92625196	1.36614842	1.25990892
3	0.46773353	0.77719907	1.58553394	1.27498956
4	0.46408182	0.77353395	1.5719651	1.25615736
5	0.46375074	0.76662754	1.59684642	1.24752105
6	0.4796273	0.76832562	1.59837111	1.27203824
7	0.48407166	0.76929012	1.65190592	1.31279118
8	0.48815159	0.77777778	1.67104636	1.23202801

9	0.48273056	0.77218364	1.67757644	1.14785354
10	0.49141211	0.77758488	1.6684787	1.22260333
11	0.50328295	0.7962963	1.65391882	1.23680314
12	0.35334888	0.89390432	1.43066947	1.17189952
13	0.50681759	0.81846635	1.54169789	1.30842482
14	0.45983859	0.81539352	1.61777147	1.16743834
15	0.39324428	0.82458143	1.62504634	1.12396033
16	0.36219199	0.85692542	1.56667677	1.06061268
17	0.33199515	0.85832239	1.57890094	1.05382604
18	0.32029446	0.87404871	1.53373169	1.09690181
19	0.29194871	0.88634585	1.48216258	1.05341498
20	0.28222491	0.85230829	1.5800403	1.09277076
21	0.25352333	0.88368056	1.52078755	1.06297148
22	0.28013807	0.85069444	1.53779191	1.09720337
23	0.29984693	0.85551698	1.53349997	1.09237427
24	0.29232295	0.8422932	1.57146895	1.12184817
25	0.2942436	0.83371914	1.55488396	1.09802414
	Average	0.82523046	1.57251707	1.09802414
	Std. deviation	0.04761274	0.07327075	0.09474478

Depth Profile 3:

µm from top	Threshold	Porosity	FD	ADD
1	0.44357858	0.90354938	1.4314156	1.29508086
2	0.44088039	0.8757716	1.51868739	1.34973146
3	0.48254225	0.84950533	1.542125	1.4847002
4	0.48265063	0.82156636	1.53729425	1.58588186
5	0.43536152	0.81539352	1.57748215	1.31495454
6	0.43690895	0.828125	1.57235996	1.25347481
7	0.44420267	0.8390411	1.57410688	1.21528018
8	0.4480501	0.83024691	1.56453763	1.22735186
9	0.44338886	0.84510031	1.55072852	1.20858248
10	0.43252688	0.84953704	1.5200316	1.20740468
11	0.41342907	0.83980213	1.57660169	1.18121397
12	0.41300705	0.83391204	1.60184874	1.20102212
13	0.41301519	0.84030775	1.56969843	1.16114732
14	0.40186659	0.88040123	1.48439304	1.12631137
15	0.38969701	0.88753858	1.45480353	1.13480566
16	0.39391713	0.88348765	1.43539778	1.16167068
17	0.378458	0.87866512	1.48729329	1.16133242
18	0.32030556	0.86207562	1.54939836	1.08865964
19	0.30027671	0.86709105	1.54342719	1.07943137
20	0.28071616	0.87226135	1.5527156	1.09483048
21	0.26935018	0.88638117	1.52788795	1.08016035
22	0.2807136	0.84953704	1.60801314	1.08533745
23	0.27548517	0.8439429	1.61402927	1.10176007
24	0.26494981	0.8200313	1.69365618	1.0849221
25	0.28860826	0.82600309	1.68797835	1.07737249

Average	0.85317098	1.55103646	1.07737249
Std. deviation	0.02483352	0.0645763	0.12853167

Depth Profile 4:

µm from top	Threshold	Porosity	FD	ADD
1	0.49456211	0.77353395	1.71195335	1.42254478
2	0.50146679	0.75096451	1.68093721	1.36290265
3	0.49556448	0.73148148	1.72768467	1.40660503
4	0.48337163	0.74589202	1.72764456	1.32935803
5	0.49128435	0.7820216	1.69596659	1.24111092
6	0.4913236	0.7820216	1.68544336	1.25145843
7	0.49204284	0.76774691	1.6916001	1.27376664
8	0.48297235	0.75578704	1.70287435	1.18082689
9	0.49196036	0.78317901	1.65227545	1.18779869
10	0.49957223	0.79494599	1.60638716	1.20070727
11	0.4841191	0.80516975	1.53078393	1.28903357
12	0.47529074	0.81057099	1.51912372	1.26772732
13	0.48301859	0.82619599	1.49852944	1.25667413
14	0.47211668	0.81577932	1.50905685	1.25051293
15	0.4725635	0.80844907	1.5051378	1.26857459
16	0.47042972	0.8121142	1.51973252	1.20257375
17	0.46776765	0.82040895	1.50051807	1.22742127
18	0.46065324	0.82589984	1.50328732	1.24859738
19	0.44514164	0.85686728	1.43736402	1.19360035
20	0.38564776	0.85416667	1.46820576	1.19251824
21	0.31472855	0.8563777	1.50694542	1.09635508
22	0.27341576	0.85783179	1.54114331	1.07482606
23	0.25746672	0.86844136	1.52654115	1.09603917
24	0.2690559	0.88013699	1.50032335	1.08954683
25	0.29384903	0.91049383	1.40444513	1.09290381
Average	0.81105911	1.57415618	1.09290381	
Std. deviation	0.04564576	0.10151929	0.09421622	

Depth Profile 5:

µm from top	Threshold	Porosity	FD	ADD
1	0.49186759	0.77816358	1.60861369	1.81172791
2	0.48518209	0.77083333	1.61361927	1.70048332
3	0.48252616	0.76584507	1.55408706	1.8830544
4	0.48355276	0.78530093	1.49449196	1.86685089
5	0.49396051	0.79340278	1.42357756	1.94152038
6	0.45629802	0.79680365	1.47316903	1.6333022
7	0.44524318	0.81631455	1.4903609	1.49321351
8	0.43117718	0.81338028	1.51544151	1.39736226

9	0.45471785	0.83179012	1.42142171	1.39515061
10	0.48193135	0.85388128	1.34658888	1.47211535
11	0.47236574	0.86033951	1.26562467	1.61718814
12	0.48270983	0.87364969	1.21079893	1.82832371
13	0.47184224	0.88136574	1.21115787	1.93271638
14	0.45312259	0.8879108	1.23978242	1.56012689
15	0.44316382	0.88848157	1.24699517	1.64738356
16	0.42920368	0.89236111	1.2690908	1.44480369
17	0.4048286	0.89313272	1.35048187	1.35927688
18	0.4136364	0.90798611	1.33555722	1.38353937
19	0.40160811	0.90030441	1.36804623	1.3606254
20	0.34747256	0.88908179	1.38834869	1.24812469
21	0.31059108	0.87750772	1.40382096	1.20385525
22	0.31228373	0.89197531	1.40000883	1.14712698
23	0.29186345	0.88908179	1.42355845	1.15520252
24	0.28892955	0.8910108	1.43039413	1.11730617
25	0.27773637	0.85358796	1.5305701	1.14944031
	Average	0.8513397	1.40062432	1.14944031
	Std. deviation	0.04694433	0.11806847	0.26654309

ISA 3d Data for Reactor 2

Depth Profile 1:

µm from top	Threshold	Porosity	FD	ADD
1	0.48808346	0.78935185	1.58166496	1.45139132
2	0.49594103	0.77854938	1.54424981	1.52311639
3	0.51523632	0.76678241	1.58906211	1.61519915
4	0.50284767	0.72839506	1.66018569	1.56673232
5	0.5023636	0.71431327	1.71440801	1.41558227
6	0.5014375	0.70621142	1.73289733	1.33014282
7	0.50612054	0.70505401	1.71504499	1.36081363
8	0.50188401	0.69560185	1.75288991	1.22298616
9	0.4920153	0.69810957	1.76282118	1.20336251
10	0.47258561	0.71971451	1.75965402	1.18204226
11	0.47167656	0.75	1.73985458	1.14490414
12	0.46375426	0.77584877	1.72411092	1.12052038
13	0.43962879	0.79494599	1.72484452	1.1052714
14	0.40211589	0.83622685	1.67181158	1.06824666
15	0.39370679	0.8587963	1.57326194	1.10519933
16	0.39247859	0.8591821	1.54055481	1.07460344
17	0.41665534	0.86921296	1.48766947	1.08373841
18	0.42851538	0.86612654	1.4701293	1.1111078
19	0.4241309	0.82947531	1.51862702	1.18541415
20	0.44731822	0.82465278	1.53285111	1.22096788
21	0.46003391	0.81520062	1.54280765	1.28835164
22	0.47843824	0.81616512	1.53335771	1.33527369
23	0.47566714	0.79513889	1.56137121	1.40305234
24	0.49544845	0.80478395	1.56191129	1.35872293
	Average	0.78324331	1.62483505	1.35872293
	Std. deviation	0.05729568	0.09845986	0.16451139

Depth Profile 2:

µm from top	Threshold	Porosity	FD	ADD
1	0.3028492	0.90962441	1.3541711	1.12173795
2	0.29989592	0.91516517	1.30359105	1.11332084
3	0.36271863	0.92770167	1.23215459	1.11945419
4	0.3893885	0.90721451	1.34927903	1.14844513
5	0.39388933	0.8748071	1.41002629	1.15939612
6	0.42159771	0.85798122	1.49644907	1.20108493
7	0.42559376	0.84303653	1.56523745	1.20549928
8	0.44859669	0.83504566	1.60765768	1.29961972
9	0.44334065	0.82658179	1.58930239	1.27809575
10	0.45665665	0.82567086	1.59943471	1.30759883
11	0.46015343	0.81279343	1.58554687	1.25080046
12	0.46058169	0.80555556	1.638991	1.35636189

13	0.45637411	0.81616512	1.59221281	1.25837311
14	0.46305959	0.83912037	1.59705161	1.20663711
15	0.45138148	0.85050154	1.55971159	1.19506445
16	0.42953329	0.8513302	1.56200566	1.2125621
17	0.38095742	0.84383562	1.57832064	1.15363622
18	0.38506302	0.88599537	1.45851019	1.10994488
19	0.33099602	0.8597973	1.55742335	1.10630704
20	0.30436209	0.84018265	1.62825706	1.11799305
21	0.29649472	0.8304071	1.64669767	1.13612993
22	0.30165796	0.82326838	1.68502579	1.07998002
23	0.29429526	0.81925419	1.70124215	1.08630531
24	0.30407446	0.80652006	1.727616	1.0922708
25	0.28383372	0.82133899	1.67368134	1.0743251
	Average	0.84915579	1.54798388	1.0743251
	Std. deviation	0.03541005	0.12850985	0.07970343

Depth Profile 3:

µm from top	Threshold	Porosity	FD	ADD
1	0.44039254	0.85262346	1.45660056	1.24936086
2	0.46042744	0.83159722	1.50576645	1.26132338
3	0.48384279	0.81346451	1.54634149	1.28862126
4	0.49335939	0.77160494	1.62949963	1.28296203
5	0.5092507	0.71759259	1.6588626	1.38117823
6	0.5295295	0.69405864	1.67971363	1.45345503
7	0.52650904	0.69216134	1.6808942	1.47813457
8	0.52905023	0.70679012	1.69295913	1.4897331
9	0.52958588	0.72261346	1.68954247	1.44457097
10	0.51949331	0.73553241	1.70491226	1.39091545
11	0.52511404	0.74080595	1.70474463	1.47729751
12	0.51705418	0.74429224	1.73734275	1.37142698
13	0.5179986	0.7494213	1.71168049	1.33899355
14	0.50281618	0.74556327	1.7031179	1.35990817
15	0.50233704	0.76041667	1.66209521	1.45485853
16	0.49442062	0.78896605	1.63236709	1.37585425
17	0.48326171	0.81114969	1.59528477	1.29790595
18	0.46711422	0.81886574	1.60434017	1.25175614
19	0.43642722	0.80767747	1.6183046	1.26011538
20	0.45202388	0.83815586	1.5782671	1.16481669
21	0.43613073	0.84625772	1.56920585	1.14895002
22	0.44511611	0.86130401	1.48602727	1.18635553
23	0.43307846	0.86516204	1.51257347	1.17494706
24	0.4326125	0.8728482	1.4826267	1.18144835
25	0.38163676	0.8533105	1.54893066	1.15652085
	Average	0.78568942	1.61568004	1.15652085
	Std. deviation	0.05852967	0.08359955	0.11254627

Depth Profile 4:

µm from top	Threshold	Porosity	FD	ADD
1	0.48784328	0.78761574	1.52052741	1.86877228
2	0.50090726	0.79783951	1.52449531	1.99415138
3	0.50647327	0.80111883	1.5326511	1.87516855
4	0.4950656	0.79205247	1.54211713	1.67469425
5	0.48307351	0.80079909	1.58735546	1.51877579
6	0.47211084	0.79301698	1.59560985	1.38473958
7	0.46819807	0.81423611	1.58502231	1.26689487
8	0.45253743	0.80536265	1.52681518	1.32486784
9	0.45518429	0.81674383	1.53919163	1.26920688
10	0.48258071	0.83892747	1.52213919	1.29326664
11	0.48796618	0.82713964	1.54543455	1.37059662
12	0.49372509	0.81944444	1.53020658	1.45323663
13	0.48351481	0.80086072	1.52937372	1.4668528
14	0.48025921	0.78915895	1.51797018	1.41596607
15	0.48351979	0.77992958	1.52733541	1.49941065
16	0.48392277	0.77681327	1.57104971	1.48405604
17	0.4932615	0.77625571	1.59896253	1.4997085
18	0.4752592	0.77102623	1.55628372	1.70559773
19	0.47753034	0.78915895	1.58427434	1.82235437
20	0.4442394	0.78337191	1.67555162	1.66672212
21	0.42150604	0.79571759	1.67690693	1.60470472
22	0.39399914	0.80054012	1.69758204	1.47410777
23	0.38248866	0.80767747	1.65912956	1.42563083
24	0.36681131	0.80111883	1.64529061	1.38970691
25	0.36057868	0.81092032	1.64941742	1.27522641
	Average	0.79907386	1.57762774	1.27522641
	Std. deviation	0.01638886	0.05769442	0.20577867

Depth Profile 5:

µm from top	Threshold	Porosity	FD	ADD
1	0.49573637	0.88580247	1.1799923	2.49162283
2	0.50655	0.82394366	1.46131303	2.20599333
3	0.52145329	0.76060957	1.5887559	1.96458319
4	0.51930865	0.67824074	1.69497569	1.83217947
5	0.53265678	0.60397377	1.741192	1.85980549
6	0.54099488	0.57696759	1.75346512	1.86581164
7	0.55721379	0.54166667	1.72752692	2.03717497
8	0.54973044	0.54433029	1.74853963	1.77641258
9	0.55315443	0.56577932	1.78381091	1.54153113
10	0.54110981	0.58584105	1.77637438	1.47555498
11	0.54068365	0.63541667	1.7623722	1.42167178

12	0.51887614	0.67496142	1.75149459	1.41327653
13	0.50642823	0.72627315	1.68557947	1.32983665
14	0.49538988	0.76349765	1.61483443	1.34675226
15	0.46081678	0.77797068	1.60255693	1.41136157
16	0.46468	0.80844907	1.56211146	1.4403782
17	0.44285743	0.81905864	1.61029846	1.43347683
18	0.41943841	0.82716049	1.49058162	1.48714485
19	0.37093268	0.83805592	1.48524414	1.35832948
20	0.35093741	0.8595679	1.57928215	1.32428609
21	0.33136941	0.87962963	1.46602562	1.2991312
22	0.30031178	0.88271605	1.43611903	1.33914779
23	0.27547423	0.88318113	1.42552047	1.33419175
24	0.29673416	0.87152778	1.48964526	1.2123789
25	0.26111	0.85113459	1.51424173	1.24367425
	Average	0.74663024	1.59727414	1.24367425
	Std. deviation	0.12214706	0.14861438	0.33305662

ISA 3d Data for Reactor 3

Depth Profile 1:

µm from top	Threshold	Porosity	FD	ADD
1	0.50698036	0.81983025	1.48857691	1.42528827
2	0.52092101	0.79591049	1.51670709	1.45672918
3	0.51498466	0.77565586	1.5220028	1.4795454
4	0.50598211	0.77623457	1.54832427	1.47350983
5	0.49769717	0.78125	1.5370152	1.48978672
6	0.47960751	0.82600309	1.45453599	1.32778008
7	0.46442707	0.86400463	1.35225925	1.49724217
8	0.43844386	0.88213735	1.2689197	1.54395879
9	0.45671377	0.90316358	1.21920303	1.53996805
10	0.45289725	0.90104167	1.23446322	1.49598581
11	0.43333534	0.88753858	1.31963907	1.44465271
12	0.43191881	0.88657407	1.29238967	1.32448634
13	0.43966678	0.8746142	1.31070806	1.32655611
14	0.43742673	0.86709105	1.34379853	1.34425782
15	0.42903034	0.85223765	1.40227401	1.30936507
16	0.42496751	0.84799383	1.43751233	1.33995475
17	0.42476643	0.8597608	1.41771845	1.21958877
18	0.42177952	0.86265432	1.42599522	1.27320222
19	0.41772361	0.87789352	1.42950375	1.1824075
20	0.41372251	0.88946759	1.38893229	1.22829518
21	0.42382467	0.89756944	1.32766187	1.22864877
22	0.40397296	0.9054784	1.32571866	1.24969789
23	0.32252332	0.89891975	1.38917455	1.24140602
24	0.27295091	0.87075617	1.47680989	1.22458146
25	0.27935454	0.88020833	1.4632504	1.20845633
	Average	0.85935957	1.39572377	1.20845633
	Std. deviation	0.04077344	0.09410216	0.1181973

Depth Profile 2:

µm from top	Threshold	Porosity	FD	ADD
1	0.54177638	0.69816119	1.58106018	1.94711716
2	0.54225588	0.6711034	1.62244085	1.9593463
3	0.54964209	0.64988426	1.60702017	2.06910009
4	0.54682959	0.65246763	1.61802889	1.98832721
5	0.54217997	0.66358025	1.66920167	1.8024563
6	0.53307105	0.69714506	1.64607155	1.65244236
7	0.49960837	0.76877934	1.58584013	1.41501774
8	0.47197217	0.81468798	1.49280702	1.3362857
9	0.47872588	0.84278549	1.46533763	1.39755291
10	0.46846118	0.84113394	1.51415854	1.31835986
11	0.48236592	0.84115806	1.49939521	1.36057237

12	0.48310128	0.86033951	1.43977065	1.35403786
13	0.47168964	0.85570988	1.45135562	1.32323051
14	0.46083063	0.84972994	1.45082391	1.32326352
15	0.43595837	0.84722222	1.48947756	1.24420469
16	0.42877749	0.84625772	1.49515323	1.16518182
17	0.41392975	0.84017997	1.49524546	1.19304357
18	0.4137157	0.86502347	1.43340646	1.20516062
19	0.43221409	0.88194444	1.38466866	1.27457037
20	0.43346238	0.9039873	1.31078822	1.226226
21	0.39028622	0.90335648	1.30317272	1.17657665
22	0.39656321	0.91975309	1.26238852	1.17040058
23	0.39701226	0.93622848	1.1822427	1.25790868
24	0.4201514	0.95129376	1.18240126	1.35991332
25	0.43326852	0.96420188	1.03633475	1.45019263
	Average	0.82264459	1.44874366	1.45019263
	Std. deviation	0.09670718	0.15997206	0.28530276

Depth Profile 3:

µm from top	Threshold	Porosity	FD	ADD
1	0.44404066	0.91936728	1.26544751	1.28073451
2	0.46003009	0.92399691	1.27479048	1.44250214
3	0.45935456	0.93569254	1.16229516	1.37546988
4	0.43063907	0.91704718	1.24572292	1.48073676
5	0.44504784	0.91571537	1.28392434	1.58289982
6	0.45918785	0.91280864	1.24744844	1.51546961
7	0.47132067	0.8902392	1.22714352	1.50727698
8	0.48422821	0.84143519	1.40976717	1.56479108
9	0.49149821	0.82687793	1.41553343	1.55892679
10	0.49341198	0.81886574	1.43645151	1.4643419
11	0.4819757	0.8279321	1.45068657	1.52675188
12	0.43720382	0.83371914	1.51905908	1.30224404
13	0.40872746	0.83487654	1.49326404	1.26491871
14	0.41776446	0.85127315	1.43240073	1.21950303
15	0.45302464	0.87133488	1.3292608	1.3864725
16	0.48761909	0.87866512	1.27770651	1.6259655
17	0.44772902	0.86554784	1.39517026	1.39838885
18	0.45926594	0.88078704	1.29216926	1.57613866
19	0.4718529	0.8904321	1.23927746	1.77932334
20	0.4364833	0.89041096	1.27895334	1.58842851
21	0.44686874	0.90374228	1.27489773	1.51228612
22	0.41712452	0.89954338	1.31046219	1.47987081
23	0.37350569	0.89564043	1.34296553	1.22624796
24	0.4176012	0.92840376	1.19654905	1.39612588
25	0.46750323	0.9380787	1.10586881	1.87371786
	Average	0.88369734	1.31628863	1.87371786

Std. deviation	0.03721871	0.10420333	0.15821743

Depth Profile 4:

µm from top	Threshold	Porosity	FD	ADD
1	0.39294291	0.96161265	1.11103817	1.20754676
2	0.42433842	0.91248097	1.31349924	1.2707378
3	0.44473364	0.86207562	1.48197925	1.2288502
4	0.48253226	0.8287037	1.50556338	1.41674499
5	0.49594385	0.84384921	1.4659895	1.44873686
6	0.49466692	0.83568075	1.4736775	1.48322672
7	0.50596203	0.78240741	1.58765217	1.54795907
8	0.51727624	0.74885845	1.62910177	1.43535713
9	0.51891136	0.75489045	1.63520412	1.42248256
10	0.52623093	0.76060957	1.5962092	1.45702728
11	0.50114278	0.77621283	1.57837627	1.3594681
12	0.4723028	0.81732253	1.52751166	1.27268129
13	0.42411776	0.85320216	1.496451	1.2126507
14	0.39842456	0.88318113	1.38372555	1.14559883
15	0.43300681	0.90509259	1.33083128	1.30884808
16	0.43668785	0.90625	1.38679924	1.22471695
17	0.41369982	0.89178241	1.47901209	1.20975709
18	0.42852909	0.88108828	1.45933436	1.24057631
19	0.40525283	0.86902006	1.51958552	1.24153986
20	0.3906037	0.87636933	1.50708607	1.25850143
21	0.40056741	0.89853395	1.35828644	1.21696351
22	0.37656591	0.90239198	1.3239127	1.18135467
23	0.32786253	0.89136225	1.34127288	1.27897851
24	0.30017737	0.90354938	1.3401019	1.09691417
25	0.28091388	0.90121283	1.40116811	1.12672256
	Average	0.85790962	1.44933477	1.12672256
	Std. deviation	0.05677737	0.12110653	0.12120096

Depth Profile 5:

µm from top	Threshold	Porosity	FD	ADD
1	0.44724106	0.93816591	1.15679635	1.37603591
2	0.4910622	0.89583333	1.2444599	1.39418228
3	0.50616257	0.8458529	1.3079341	1.56819158
4	0.51766596	0.796875	1.51563712	1.70327045
5	0.50766117	0.77464789	1.51265661	1.7240274
6	0.53474519	0.76195988	1.50410651	1.77545359
7	0.53306946	0.74266975	1.55235487	1.84450998
8	0.52132686	0.73344749	1.61179768	1.65923699
9	0.49464936	0.81462191	1.50058944	1.42256326
10	0.451952	0.86967275	1.42792891	1.26077159

11	0.38944224	0.88425926	1.37358965	1.20877785
12	0.4216178	0.90509259	1.30602405	1.15322061
13	0.42956209	0.92561	1.17881595	1.32707789
14	0.43653848	0.92283951	1.19539921	1.27131094
15	0.39432022	0.91435185	1.26648414	1.21040326
16	0.417232	0.91040689	1.30645802	1.2133294
17	0.41266003	0.91396605	1.3446178	1.17028792
18	0.35078344	0.89486883	1.37705219	1.12190168
19	0.35732877	0.92920525	1.2701655	1.06827512
20	0.32769188	0.93036265	1.2850384	1.14764805
21	0.34890175	0.95563272	1.06198292	1.22351335
22	0.32415878	0.95524691	1.03146885	1.19622585
23	0.38177323	0.9679784	0.95722484	1.26047507
24	0.38644265	0.9783105	0.83654874	1.22638383
25	0.40763539	0.97089041	0.91283606	1.27291424
	Average	0.88531074	1.28151871	1.27291424
	Std. deviation	0.07382531	0.20597579	0.22604504

ISA 3d Data for Reactor 4

Depth Profile 1:

µm from top	Threshold	Porosity	FD	ADD
1	0.5367265	0.80073302	1.47063014	1.57866556
2	0.53882411	0.79166667	1.47314568	1.57124446
3	0.53326096	0.765625	1.4617701	1.81820992
4	0.53726295	0.76909722	1.50019456	1.81447139
5	0.53266287	0.75713735	1.53142936	1.77668971
6	0.52726319	0.7337963	1.57185923	1.57701082
7	0.53034957	0.72395833	1.56411772	1.61151383
8	0.5386291	0.72878086	1.54080861	1.70909585
9	0.52652306	0.71682099	1.61435459	1.54656526
10	0.53443103	0.71315586	1.61010886	1.58046092
11	0.53744267	0.70814043	1.64308085	1.58864214
12	0.53792932	0.70023148	1.64270107	1.52838315
13	0.5458204	0.69174383	1.68348441	1.5410953
14	0.54543148	0.66550926	1.69234977	1.61911038
15	0.55406406	0.63541667	1.6977909	1.68094519
16	0.54948199	0.61863426	1.71792727	1.6249459
17	0.55459907	0.61574074	1.73102377	1.64550245
18	0.55407148	0.63252315	1.69158714	1.69558945
19	0.54898205	0.65914352	1.69677576	1.61850073
20	0.52244048	0.69540895	1.69353218	1.45929243
21	0.49999714	0.74035494	1.6649939	1.46257102
22	0.46761464	0.77951389	1.61299368	1.42275332
23	0.46332129	0.80497685	1.573131	1.33713291
24	0.44111955	0.82619599	1.55724144	1.30827448
25	0.4174766	0.81925154	1.52098558	1.37796056
	Average	0.72374228	1.6063207	1.37796056
	Std. deviation	0.0627096	0.08440844	0.13433825

Depth Profile 2:

µm from top	Threshold	Porosity	FD	ADD
1	0.50367973	0.80692488	1.46709876	1.61206327
2	0.50290862	0.7758216	1.54240608	1.54552441
3	0.52545084	0.73513302	1.61129822	1.52978229
4	0.54271064	0.7195216	1.61325556	1.66946825
5	0.55076511	0.71508488	1.59385217	1.69346438
6	0.55022061	0.67199391	1.63454348	1.76085725
7	0.56465507	0.64699074	1.64304903	1.81833156
8	0.56536511	0.63445216	1.63024004	1.94416836
9	0.55716049	0.64216821	1.6653432	1.76966582
10	0.55132294	0.66457382	1.70275427	1.55344182
11	0.53814719	0.68055556	1.70717417	1.49064409

12	0.53444697	0.68595679	1.72611938	1.4780875
13	0.53352647	0.68557099	1.71894493	1.44745927
14	0.54215391	0.69939117	1.71541474	1.53529103
15	0.54131288	0.68962191	1.73216908	1.59446043
16	0.53868668	0.70422535	1.72985126	1.53094812
17	0.5328861	0.70563272	1.71847262	1.53277257
18	0.51887321	0.72029321	1.71737311	1.42568883
19	0.50329401	0.7345679	1.74062786	1.3100425
20	0.49089894	0.76195988	1.69412087	1.21142857
21	0.4874365	0.76623631	1.68919345	1.21514134
22	0.44522998	0.76986883	1.68836507	1.22547196
23	0.44411743	0.78881279	1.67815683	1.18656434
24	0.44039051	0.81404321	1.65088455	1.17292329
25	0.41259544	0.81318466	1.6381038	1.1993731
	Average	0.72130344	1.6659525	1.1993731
	Std. deviation	0.05382434	0.06548481	0.21567101

Depth Profile 3:

µm from top	Threshold	Porosity	FD	ADD
1	0.49940617	0.79655712	1.55492002	1.40764285
2	0.51942677	0.78375772	1.53448367	1.42445292
3	0.53775788	0.77507716	1.59260808	1.50243914
4	0.54128141	0.74807099	1.58421425	1.66806862
5	0.54797246	0.72241512	1.58921462	1.72670787
6	0.54451961	0.71990741	1.62119331	1.69749136
7	0.54525531	0.69965278	1.64334066	1.59343472
8	0.54217443	0.68132716	1.67203812	1.56867674
9	0.55280552	0.68209877	1.6686055	1.58542091
10	0.557261	0.67484779	1.67194805	1.75412723
11	0.5608026	0.65721451	1.73635539	1.56963019
12	0.55793693	0.63213735	1.72371254	1.63061872
13	0.56958339	0.62287809	1.72341019	1.61970053
14	0.57204383	0.59702932	1.75102024	1.60191999
15	0.56603604	0.58564815	1.76353457	1.60161748
16	0.56628797	0.6101466	1.73479024	1.64901329
17	0.56212214	0.62403549	1.72668761	1.6381987
18	0.56391993	0.64814815	1.71945642	1.64148953
19	0.56137938	0.64332562	1.72784358	1.65184197
20	0.55699273	0.62615741	1.72573444	1.73724696
21	0.54506912	0.61689815	1.73099871	1.70359682
22	0.54573664	0.64390432	1.69080641	1.66379247
23	0.53447986	0.67881944	1.66619399	1.55649502
24	0.52211005	0.71277006	1.61438715	1.60944517
25	0.49993347	0.73591821	1.59315173	1.66728159
	Average	0.67674972	1.67042598	1.66728159

	Std. deviation	0.05992611	0.06754969	0.08523097

Depth Profile 4:

µm from top	Threshold	Porosity	FD	ADD
1	0.50687516	0.82253086	1.41296369	1.52656809
2	0.50201035	0.83333333	1.40710029	1.53593125
3	0.49109974	0.82210807	1.42647549	1.47713782
4	0.50525391	0.82002315	1.42662025	1.41643183
5	0.49457938	0.81346451	1.48416402	1.35824765
6	0.46407767	0.79803241	1.53984637	1.28196526
7	0.4937442	0.80922068	1.54341308	1.24853218
8	0.50973161	0.78973765	1.5402423	1.33988844
9	0.51088577	0.77854938	1.53913135	1.4174917
10	0.52097075	0.78063166	1.543082	1.43343105
11	0.52609977	0.77353395	1.53040749	1.44762055
12	0.52553209	0.75312989	1.56710618	1.5180701
13	0.5225027	0.7507716	1.5816123	1.55057106
14	0.51822834	0.7507716	1.61149867	1.49920542
15	0.52157781	0.76331811	1.56279813	1.54972623
16	0.52545361	0.75636574	1.56229355	1.60518183
17	0.51494186	0.7444825	1.58975631	1.64469214
18	0.51158367	0.75964506	1.54671322	1.64413383
19	0.51072984	0.77893519	1.52161507	1.54569259
20	0.48823068	0.79128086	1.5347011	1.42724938
21	0.48752361	0.82156636	1.45540831	1.36992861
22	0.47620463	0.84047068	1.43055968	1.33445103
23	0.45244256	0.84992284	1.40934634	1.32929095
24	0.43140917	0.85648148	1.39485777	1.28589969
25	0.41370224	0.8685312	1.41296191	1.27469368
	Average	0.79707355	1.50298699	1.27469368
	Std. deviation	0.03663512	0.06874354	0.11776749

Depth Profile 5:

µm from top	Threshold	Porosity	FD	ADD
1	0.4821391	0.88541667	1.24704154	1.55231001
2	0.50237808	0.85146605	1.34524606	1.45848331
3	0.50312223	0.80381944	1.45785732	1.45658745
4	0.51037005	0.77777778	1.56166308	1.44353151
5	0.5186701	0.73401826	1.62158985	1.58978974
6	0.53857895	0.69386574	1.68158514	1.6527177
7	0.54202398	0.65473396	1.74883016	1.48656835
8	0.54925024	0.63213735	1.79874917	1.34528399
9	0.55714862	0.61689815	1.83108369	1.36048149
10	0.5608605	0.60230829	1.85152912	1.2656898

11	0.57379715	0.61786265	1.84104057	1.28370348
12	0.5647967	0.62384259	1.83670419	1.29021847
13	0.56093267	0.63888889	1.82189772	1.29345604
14	0.55061294	0.65046296	1.80531392	1.25300085
15	0.53690562	0.6724537	1.78307496	1.30507156
16	0.53027857	0.69232253	1.75349396	1.32955732
17	0.53047415	0.70109546	1.71755383	1.46159569
18	0.53281635	0.74054784	1.63828893	1.47929875
19	0.51545857	0.77102623	1.62842859	1.37941013
20	0.50766661	0.78877315	1.56259452	1.52619304
21	0.479049	0.79699391	1.57227067	1.32089577
22	0.43744818	0.81404321	1.58536157	1.16594651
23	0.41322007	0.82445988	1.58575797	1.17477649
24	0.39281853	0.82669082	1.58211423	1.12533481
25	0.38668967	0.85719875	1.56584095	1.13663733
	Average	0.73076417	1.65699647	1.13663733
	Std. deviation	0.08840638	0.15786899	0.14250369

APPENDIX I: Porosity and Statistical Analysis

Porosity					
Reactors	Mean 1	Mean 2	Mean 3	Mean 4	Mean 5
R1	0.72667438	0.82523046	0.85317098	0.81105911	0.8513397
R2	0.78324331	0.84915579	0.78568942	0.79907386	0.74663024
R3	0.85935957	0.82264459	0.88369734	0.85790962	0.88531074
R4	0.72374228	0.72130344	0.67674972	0.79707355	0.73076417

Reactor 1 and 2

t-Test: Two-Sample Assuming Unequal Variances

	Variable 1	*Variable 2*
Mean	0.804033733	0.802522
Variance	0.002965865	0.00167
Observations	4	6
Hypothesized Mean Difference	0	
Df	5	
t Stat	0.047338197	
P(T<=t) one-tail	0.482038153	
t Critical one-tail	2.015049176	
P(T<=t) two-tail	0.964076307	
t Critical two-tail	2.570577635	

Reactor 3 and 4

t-Test: Two-Sample Assuming Unequal Variances

	Variable 1	*Variable 2*
Mean	0.861784	0.729927
Variance	0.000647	0.001862
Observations	5	5
Hypothesized Mean Difference	0	
Df	6	
t Stat	5.886188	
P(T<=t) one-tail	0.000533	
t Critical one-tail	1.943181	
P(T<=t) two-tail	0.001066	
t Critical two-tail	2.446914	

COD:N:P	Grouped Porosity				
100/5/1	0.72667438	0.82523046	0.85317098	0.81105911	0.8513397
	0.78324331	0.84915579	0.785689	0.79907386	0.74663
R3	0.85935957	0.82264459	0.88369734	0.85790962	0.88531074
R4	0.72374228	0.72130344	0.67675	0.79707355	0.730764

COD/N/P:100/5/1-100/5/0.1
Grouped R1 and R2 - R3

t-Test: Two-Sample Assuming Unequal Variances

	Variable 1	*Variable 2*
Mean	0.803126725	0.861784372
Variance	0.00191686	0.000646621
Observations	10	5
Hypothesized Mean Difference	0	
df	12	
t Stat	-3.27389854	
P(T<=t) one-tail	0.003327477	
t Critical one-tail	1.782286745	
P(T<=t) two-tail	0.006654955	
t Critical two-tail	2.178812792	

COD/N/P:100/5/1-100/5/0.1
Grouped R1 and R2 - R4

t-Test: Two-Sample Assuming Unequal Variances

	Variable 1	*Variable 2*
Mean	0.803126725	0.729926632
Variance	0.00191686	0.00186245
Observations	10	5
Hypothesized Mean Difference	0	
df	8	
t Stat	3.081799165	
P(T<=t) one-tail	0.007537871	
t Critical one-tail	1.85954832	
P(T<=t) two-tail	0.015075742	
t Critical two-tail	2.306005626	

APPENDIX J: Fractal Dimension and Statistical Analysis

Fractal Dimension					
Reactors	Mean 1	Mean 2	Mean 3	Mean 4	Mean 5
R1	1.658289	1.572517	1.551036	1.574156	1.400624
R2	1.624835	1.547984	1.61568	1.577628	1.597274
R3	1.395724	1.448744	1.316289	1.449335	1.281519
R4	1.606321	1.665953	1.670426	1.502987	1.656996

R1 and R2

t-Test: Two-Sample Assuming Unequal Variances

	Variable 1	*Variable 2*
Mean	1.551325	1.59268
Variance	0.008781	0.000952
Observations	5	5
Hypothesized Mean Difference	0	
Df	5	
t Stat	-0.93735	
P(T<=t) one-tail	0.195806	
t Critical one-tail	2.015049	
P(T<=t) two-tail	0.391612	
t Critical two-tail	2.570578	

R3 and R4

t-Test: Two-Sample Assuming Unequal Variances

	Variable 1	*Variable 2*
Mean	1.378322	1.620537
Variance	0.005881	0.004975
Observations	5	5
Hypothesized Mean Difference	0	
Df	8	
t Stat	-5.19813	
P(T<=t) one-tail	0.000412	
t Critical one-tail	1.859548	
P(T<=t) two-tail	0.000824	
t Critical two-tail	2.306006	

COD : N: P	Grouped Fractal Dimension				
100/5/1	1.658289	1.572517	1.551036	1.574156	1.400624
	1.624835	1.547984	1.61568	1.577628	1.597274
R3	1.395724	1.448744	1.316289	1.449335	1.281519
R4	1.606321	1.665953	1.670426	1.502987	1.656996

COD/N/P:100/5/1-100/5/0.1
Grouped R1 and R2 - R3

t-Test: Two-Sample Assuming Unequal Variances

	Variable 1	*Variable 2*
Mean	1.572002	1.378322
Variance	0.004801	0.005881
Observations	10	5
Hypothesized Mean Difference	0	
df	7	
t Stat	4.759057	
P(T<=t) one-tail	0.001031	
t Critical one-tail	1.894578	
P(T<=t) two-tail	0.002062	
t Critical two-tail	2.364623	

COD/N/P:100/5/1-100/5/0.1
Grouped R1 and R2 - R4

t-Test: Two-Sample Assuming Unequal Variances

	Variable 1	*Variable 2*
Mean	1.572002	1.620537
Variance	0.004801	0.004975
Observations	10	5
Hypothesized Mean Difference	0	
df	8	
t Stat	-1.26367	
P(T<=t) one-tail	0.120963	
t Critical one-tail	1.859548	
P(T<=t) two-tail	0.241927	
t Critical two-tail	2.306006	

APPENDIX K: Average Diffusion Distance and Statistical Analysis

Average Diffusion Distance (μm)					
Reactors	Mean 1	Mean 2	Mean 3	Mean 4	Mean 5
R1	1.071238	1.098024	1.077372	1.092904	1.14944
R2	1.358723	1.074325	1.156521	1.275226	1.243674
R3	1.208456	1.450193	1.873718	1.126723	1.272914
R4	1.377961	1.199373	1.667282	1.274694	1.136637

R1 and R2

t-Test: Two-Sample Assuming Unequal Variances

	Variable 1	*Variable 2*
Mean	1.097796	1.221694
Variance	0.000953	0.012023
Observations	5	5
Hypothesized Mean Difference	0	
Df	5	
t Stat	-2.43208	
P(T<=t) one-tail	0.029614	
t Critical one-tail	2.015049	
P(T<=t) two-tail	0.059229	
t Critical two-tail	2.570578	

R3 and R4

t-Test: Two-Sample Assuming Unequal Variances

	Variable 1	*Variable 2*
Mean	1.386401	1.331189
Variance	0.088381	0.043391
Observations	5	5
Hypothesized Mean Difference	0	
Df	7	
t Stat	0.340097	
P(T<=t) one-tail	0.37188	
t Critical one-tail	1.894578	
P(T<=t) two-tail	0.743761	
t Critical two-tail	2.364623	

COD: N:P	**Grouped Average Diffusion Distance**				
100/5/1	1.071238	1.098024	1.077372	1.092904	1.14944
	1.358723	1.074325	1.156521	1.275226	1.243674
100/5/0.1	1.208456	1.450193	1.873718	1.126723	1.272914
	1.377961	1.199373	1.667282	1.274694	1.136637

COD: N: P 100/5/1 and 100/5/0.1

t-Test: Two – Samples Assuming Unequal Variance

		Variable 1	*Variable 2*
Mean		1.159745	1.358795
Variance		0.010031	0.059412
Observations		10	10
Hypothesized	Mean		
Difference		0	
Df		12	
t Stat		-2.38862	
P(T<=t) one-tail		0.017111	
t Critical one-tail		1.782287	
P(T<=t) two-tail		0.034221	
t Critical two-tail		2.178813	